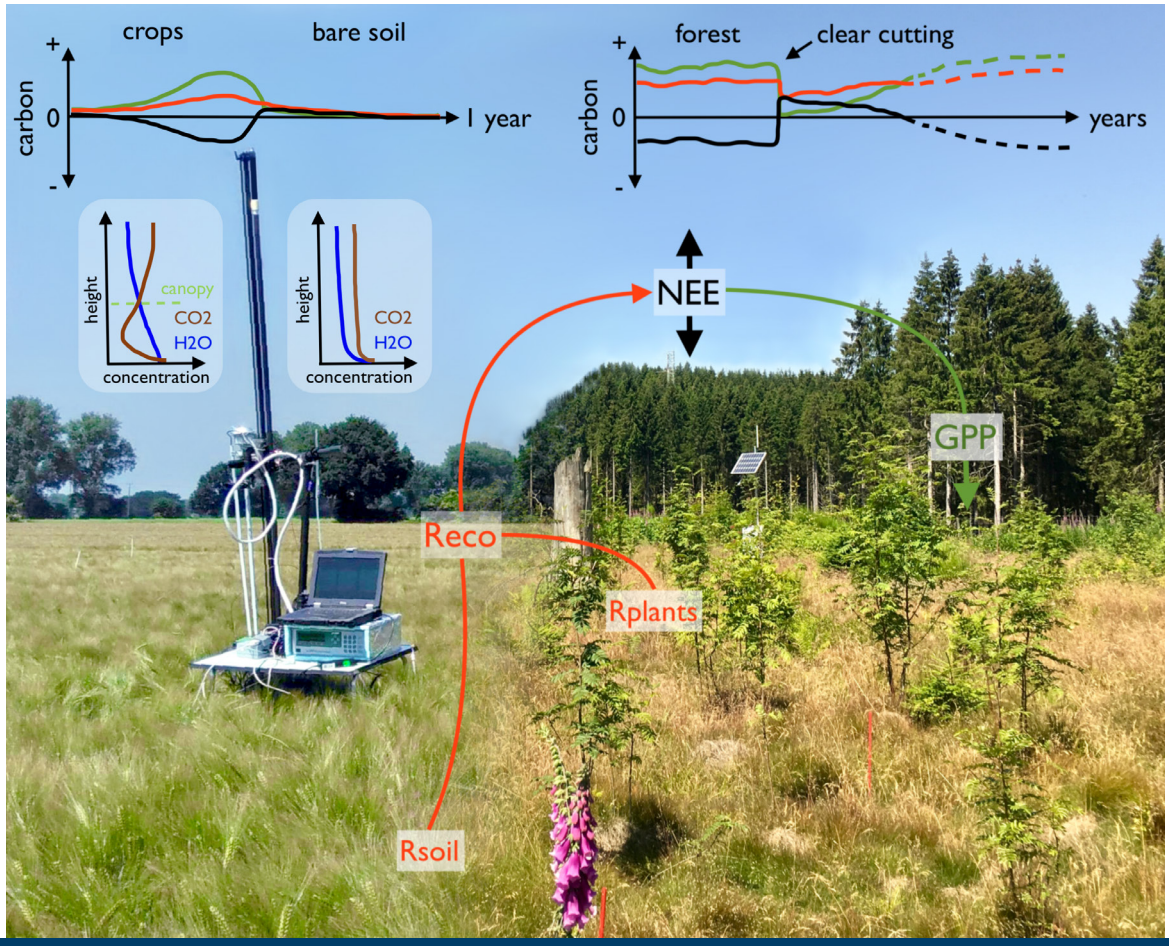

Partitioning of carbon dioxide exchange in rapidly and slowly changing ecosystems

Patrizia Ney

Energie & Umwelt / Energy & Environment
Band / Volume 476
ISBN 978-3-95806-431-7

Mitglied der Helmholtz-Gemeinschaft

JÜLICH
Forschungszentrum

Schriften des Forschungszentrums Jülich
Reihe Energie & Umwelt / Energy & Environment Band / Volume 476

Forschungszentrum Jülich GmbH
Institut für Bio- und Geowissenschaften
Agrosphäre (IBG-3)

Partitioning of carbon dioxide exchange in rapidly and slowly changing ecosystems

Patrizia Ney

Schriften des Forschungszentrums Jülich
Reihe Energie & Umwelt / Energy & Environment Band / Volume 476

ISSN 1866-1793 ISBN 978-3-95806-431-7

Bibliografische Information der Deutschen Nationalbibliothek.
Die Deutsche Nationalbibliothek verzeichnet diese Publikation in der
Deutschen Nationalbibliografie; detaillierte Bibliografische Daten
sind im Internet über http://dnb.d-nb.de abrufbar.

Herausgeber und Vertrieb:	Forschungszentrum Jülich GmbH Zentralbibliothek, Verlag 52425 Jülich Tel.: +49 2461 61-5368 Fax: +49 2461 61-6103 zb-publikation@fz-juelich.de www.fz-juelich.de/zb
Umschlaggestaltung:	Grafische Medien, Forschungszentrum Jülich GmbH
Druck:	Grafische Medien, Forschungszentrum Jülich GmbH
Copyright:	Forschungszentrum Jülich 2019

Schriften des Forschungszentrums Jülich
Reihe Energie & Umwelt / Energy & Environment, Band / Volume 476

D 5 (Diss. Bonn, Univ., 2019)

ISSN 1866-1793
ISBN 978-3-95806-431-7

Vollständig frei verfügbar über das Publikationsportal des Forschungszentrums Jülich (JuSER)
unter www.fz-juelich.de/zb/openaccess.

Abstract

A key question in times of climate change is, how the biosphere responds to global change and the local land use management in regard to its carbon cycle. At the present time, the land surface acts as a sink for anthropogenic carbon dioxide (CO_2) emissions. However, additional CO_2 is released simultaneously by land use change. There is still no clear understanding of the sensitivity of photosynthetic CO_2 uptake and respiratory CO_2 release to environmental parameters. One possible way to disentangle the flux of greenhouse gases is source-partitioning, e.g. into photosynthesis and respiration (CO_2) or into evaporation and transpiration (H_2O). Currently, there are a number of procedures for source-partitioning, however, each method has its disadvantages and allows for extensions and improvements. In this thesis, one instrumental and a data-driven partitioning approaches are taken up and demonstrated by examples of an agro- and forest ecosystem.

First, we present the prototype of a portable elevator based device for measuring temporal and spatial high-resolution profiles of CO_2, H_2O, temperature and wind velocity between the soil surface and the atmospheric surface layer above crop canopies. The vertical distribution of CO_2 and H_2O concentrations can thus be determined qualitatively for dense crop stands. Between spring 2015 and autumn 2016, campaign measurements were carried out in winter wheat, winter barley, and in an intercrop mixture during different plant development stage and at different times of day. A gas analyzer continuously records the concentrations at a frequency of 20 s^{-1} over a 2 m profile height. We present a post-processing technique of the measurements (e.g. the correction of time lags) and show the resulting vertical profiles as 30-minute averages over height steps of 0.025 m. The profiles clearly show the effects of soil respiration and photosynthetic carbon uptake within the plant stand, which vary both during the time of day and during the vegetation period. Using the Monin-Obukhov similarity theory, measurements over bare soil and a short plant canopy were analyzed to check the validity of the elevator measurements and the raw data processing. It was found that the derived fluxes of CO_2, latent and sensible heat, and momentum correlated well with eddy-covariance (EC) measurements.

While the carbon balance of an agricultural area alternates between source and sink during a vegetation period, this process usually requires decades for the management of forest ecosystems. In general, forests in Central Europe assimilate more CO_2 on an annual average than they emit and thus are a sink for atmospheric CO_2. This may change as soon as the forest ecosystem is intervened. An extreme example of such an intervention is clear cutting. After deforestation, the forest changes from a former sink to a source of CO_2.

We present seven years of CO_2 flux measurements over a 70 year old spruce monoculture in the Eifel National Park, from which about 20 % were deforested three-years after beginning of the observation period. An EC system mounted on top of a 37.8 m high tower within the forest, continuously collects fluxes of sensible and latent heat, CO_2 and momentum.

After partial deforestation, a second EC station was installed within the deforested area and was running parallel to the forest station. Complete time series and annual carbon budgets of the net ecosystem exchange (NEE) of CO_2 and its components, gross primary production (GPP) and ecosystem respiration (R_{eco}), were calculated using gap-filling and source-partitioning methods. In addition, local chamber measurements of soil respiration are taken into account and the climatic effects of the changed CO_2 sequestration and the biophysical effect of changed albedo are compared.
In contrast to the deforested area, the annual sums of NEE measured above the forest show a strong carbon sink with low inter-annual variability. One year after deforestation, the vegetation on the deforested area consisted mainly of grasses and shrubs; from the second year onwards, an increased growth of new trees (mainly mountain ash) could be observed. The recovering vegetation is reflected in the annual sums of NEE, which decreased from a carbon source (500 g C m^{-2} y^{-1}) towards neutral over the past four years, due to an increase in the photosynthetic activities.
In the last chapter, the carbon balance of a three-year crop rotation cycle was examined. The study site Selhausen is located in an intensively managed agricultural region within the Lower Rhine Embayment. About 34 % of the area of Germany was covered by agriculture in 2015 (FAO, 2015). The ability of agricultural areas to sequester or also to emit carbon gives them an important role in the local and global carbon cycle. In order to calculate or to model the local carbon balance for an agroecosystem, information about the measured NEE and its components GPP and R_{eco} are needed. The most frequently used partitioning methods in ecosystem studies are the so-called data-based nonlinear regression functions (NLR). NLR describes the nonlinear relationship between the measured NEE and environmental variables, such as air temperature or solar radiation, which are the main drivers of respiration and photosynthetic processes.
The study presented here uses a nighttime (NT) and daytime data based (DT) NLR approach for the partitioning of measured NEE in a 3-year crop rotation cycle, consisting of winter wheat/winter barley/catch-crop and sugar beet. In addition, an own algorithm was developed and implemented that calculates NLR without a previous separation of the dataset into day- and nighttime data. The seasonal and inter-annual fluxes of NEE, GPP and R_{eco} showed typical patterns and orders of magnitude of an agroecosystem within Central Europe. The cumulated daily sums of the NEE varied between +10 and -14 g C m^{-2} d^{-1} depending on the cultivated crop and season. The highest CO_2 uptake took place between May and June in winter wheat. The highest emissions were observed after harvest of winter barley, when crop residues in the soil favoring an increase in soil respiration due to decomposition processes. Over the 3-year crop rotation, the ecosystem acted as a carbon source with a release of 0.7 to 1.0 kg C m^{-2}, depending on the used source-partitioning model.
Comparing the different NLR methods, it became apparent that the NT based application overestimated R_{eco} compared to the other methods, resulting in deviations in NT vs. DT of 16 %, 6 % and 15 % between the cumulated fluxes of NEE, GPP and R_{eco}. The differences between NT and the own method were in general smaller. Other studies also reported discrepancies in the partitioning of NEE using the methods described above. Their and our work shows that there is still a need for further investigation regarding source-partitioning strategies.

Zusammenfassung

Im Hinblick auf den aktuellen Klimawandel besteht die Frage, wie die Biosphäre auf den Globalen Wandel und die daraus hervorgehende lokale Landnutzungsänderung bezüglich ihres Kohlenstoffkreislaufes reagiert. Die Landoberfläche ist zum gegenwärtigen Zeitpunkt eine Senke für anthropogene Emissionen von Kohlenstoffdioxid (CO_2), jedoch wird gleichzeitig durch Landnutzungsänderungen zusätzliches CO_2 freigesetzt. Nach wie vor ist nicht eindeutig geklärt, wie sensitiv die photosynthetische CO_2-Aufnahme und die atmungsbedingte CO_2-Freisetzung eines Ökosystems gegenüber Umweltparametern reagieren. Eine Möglichkeit, den vertikalen Fluss der Treibhausgase in ihre Quellen und Senken aufzuspalten, bietet das sogenannte Source-Partitioning. Hierbei werden z. B. vertikale CO_2-Flüsse in Photosynthese und Respiration oder im Fall von Wasserdampfflüssen (H_2O) in Evaporation und Transpiration aufgetrennt. Derzeitig existieren mehrere Ansätze und Verfahren für das Source-Partitioning, jedoch besitzt jede Methode auch gewisse Nachteile und läßt Raum für Erweiterungen und Verbesserungen. In dieser Arbeit wird zum einen ein Ansatz getestet, der sogenannte Zusatzmessungen benötigt und zum anderen eine analytische Partitionierungsmethode aufgegriffen. Beide Ansätze werden anhand von Fallbeispielen in Agrar- und Waldökosystemen demonstriert und untersucht.

Zuerst wird der Prototyp einer mobilen Liftanlage präsentiert, mit der zeitlich sowie räumlich hochaufgelöste Messung von CO_2-, H_2O-, Temperatur- und Windgeschwindigkeitsprofilen zwischen der Bodenoberfläche und der erdnahen atmosphärischen Grenzschicht über der Pflanzenoberfläche eines Ackers durchgeführt wurden. Die vertikale Verteilung der Konzentrationen von CO_2 und H_2O kann somit qualitativ für einen dichten Pflanzenbestand bestimmt werden. Dafür wurden zwischen Frühjahr 2015 und Herbst 2016 Kampagnenmessungen in Winterweizen, Wintergerste und einer Zwischenfruchtmischung während verschiedenen Stadien der Pflanzenentwicklung und zu unterschiedlichen Tageszeiten durchgeführt. Mit Hilfe eines Gasanalysators wurden kontinuierlich über eine Profilhöhe von 2 m die Konzentrationen mit einer Frequenz von 20 s^{-1} aufgezeichnet. Wir demonstrieren die Nachbearbeitung der Messungen (z. B. die Korrektur von Zeitverzögerungen) und zeigen die resultierenden vertikalen Profile als 30-minütige Mittel mit einer Auflösung von 0.025 m. Die Profile zeigen innerhalb des Planzenbestandes deutlich die Effekte der Bodenatmung und der photosynthetischen Kohlenstoffaufnahme, die sowohl innerhalb der Tageszeiten als auch während der Vegetationsperiode variieren. Mit Hilfe der Monin-Obukhov'schen Ähnlichkeitstheorie wurden Messungen über unbewachsenem Boden und einer niedrigen Pflanzendecke analysiert, um die Validität der Profilmessungen und der Rohdatenverarbeitung zu überprüfen. Die abgeleiteten Flüsse von CO_2, latente und sensible Wärme und Impuls zeigen eine gute Übereinstimmung zu den parallel durchgeführten Eddy-Kovarianz-Messungen.

Während die Kohlenstoffbilanz einer Ackerfläche im Laufe einer Vegetationsperiode zwischen Quelle und Senke wechselt, dauert dieser Prozess in bewirtschafteten Waldökosyste-

men meist Jahrzehnte. Im Allgemeinen nehmen Wälder in Mitteleuropa im Jahresmittel mehr CO_2 auf, als sie abgeben und stellen somit eine Senke für atmosphärisches CO_2 dar. Diese Situation kann sich ändern, sobald ein Eingriff in das Waldökosystem stattfindet. Ein Extrembeispiel eines solchen Eingriffs sind flächenhafte Kahlschläge, die den Wald nach der Abholzung von einer ehemaligen Senke zu einer Quelle für CO_2 umwandeln.
In dieser Arbeit präsentiert werden sieben Jahre CO_2-Flussmessungen über einer rund 70 Jahre alten Fichten-Monokulturfläche im Nationalpark Eifel, von der rund 20 % drei Jahre nach Beginn der Messung abgeholzt wurden. Ein Eddy-Kovarianz-System, das auf einem 37.8 m hohen Turm innerhalb des Waldes montiert wurde, erfasste kontinuierlich Flüsse sensibler und latenter Wärme, CO_2 und Impuls. Nach der teilweisen Entfichtung wurde eine zweite EC-Station innerhalb der Entfichtungsfläche installiert und parallel zur Waldstation betrieben. Komplette Zeitreihen und jährliche Kohlenstoffbilanzen des Netto-Ökosystemaustauschs von CO_2 (NEE) und seiner Komponenten Brutto-Primärproduktion (GPP) und Ökosystematmung (R_{eco}) wurden mit Hilfe von Gapfilling- und Source-Partitioning Methoden berechnet. Daneben wird die gemessene Bodenatmung berücksichtigt und dich sich gegenüberstehenden Klimaeffekte der durch die Entfichtung veränderten CO_2-Sequestrierung und dem biophysikalischen Effekt der geänderten Albedo betrachtet.
Im Gegensatz zur abgeholzten Fläche zeigten die über dem Wald gemessenen jährlichen NEE-Summen eine starke Kohlenstoffsenke mit geringer zwischenjährlicher Variabilität. Ein Jahr nach der Entfichtung bestand die Vegetation auf der abgeholzten Fläche hauptsächlich aus Gräsern und Sträuchern; ab dem zweiten Jahr konnte ein vermehrter Zuwachs neuer Bäume (vorwiegend Eberesche) beobachtet werden. Die wiederaufkommende Vegetation spiegelte sich in den jährlichen Summen des NEE wieder, so entwickelte sich die Entfichtungsfläche von einer Kohlenstoffquelle (ca. 500 g C m^{-2} y^{-1}) innerhalb der betrachteten vier Jahre aufgrund der Zunahme photosynthetischer Aktivitäten zunehmend zu einem CO_2 neutralen Zustand.
Im anschließenden Kapitel wird die Kohlenstoffbilanz eines Ackers über eine drei Jahre andauernde Fruchtwechselfolge untersucht. Der Versuchsstandort Selhausen befindet sich in einer landwirtschaftlich intensiv genutzen Region innerhalb der Niederrheinischen Bucht. Rund 34 % der Fläche Deutschlands war im Jahr 2015 durch Landwirtschaft genutzt (FAO, 2015). Die Fähigkeit von landwirtschaftlichen Flächen Kohlenstoff zu binden, aber auch zu emittieren, ist von großer Bedeutung für den lokalen und globalen Kohlenstoffkreislauf. Um eine lokale Kohlenstoffbilanz für ein Agrarökosystem aufstellen und modellieren zu können, benötigt man neben dem gemessenen vertikalen Netto-Ökosystemaustausch zusätzliche Informationen bezüglich seiner Zusammensetzung aus Brutto-Primärproduktion und Ökosystematmung. Die in Ökosystemstudien am häufigsten genutzten Partitionierung-Methoden sind die sogenannten datenbasierenden nichtlinearen Funktionen (NLR). Sie beschreiben den nichtlinearen Zusammenhang zwischen dem gemessenen NEE und Umgebungsvariablen wie Lufttemperatur oder solare Strahlung, die maßgeblich Atmungs- und Photosyntheseprozesse steuern. In der hier vorgestellten Studie wird für die Aufteilung der gemessenen NEE über einer 3-jährigen Fruchtwechselfolge, bestehend aus Winterweizen / Wintergerste / Zwischenfrucht und Zuckerrübe, der Ansatz einer reinen Nacht- (NT) und einer größtenteils Tagdaten (DT) basierenden NLR benutzt. Zusätzlich wurde ein eigener Algorithmus entwickelt und implementiert, der NLR ohne eine vorangehende Aufteilung in Tag- und Nachtdaten berechnet. Der Verlauf der saisonalen und zwischenjährlichen Flüsse von NEE, GPP und R_{eco} zeigten typische Muster und Größenordnungen einer landwirtschaftlich genutzen

Fläche innerhalb Mitteleuropas. Die kumulierten Tagessummen der NEE variierten je nach angebauter Frucht und Jahreszeit zwischen +10 und -14 g C m^{-2} d^{-1}. Die höchste CO_2-Aufnahme fand zwischen Mai und Juni im Winterweizen statt. Die höchsten Emissionen wurden nach der Ernte von Wintergerste beobachtet, wobei vermutlich untergepflügte Erntereste im Boden einen Anstieg der Bodenatmung durch Dekompositionsvorgänge begünstigt haben. Über die komplette Fruchtwechselfolge und bei reiner Betrachtung des vertikalen CO_2-Flusses zeigte das Ökosystem, je nach verwendetem Partitionierungsmodell, eine Netto-CO_2-Aufnahme von -1.3 bis -1,6 kg C m^{-2} und stellte somit eine Senke für Kohlenstoff dar. Werden zusätzlich zum NEE der Kohlenstoffeintrag und -austrag durch Sähen und Ernte, sowie die Emissionen aus Feldbewirtschaftungsmaßnahmen in der Kohlenstoffbilanzierung berücksichtigt, wird der Acker eine Kohlenstoffquelle (0.7 bis 1.0 kg C m^{-2}).
Beim Vergleich der unterschiedlichen NLR fiel auf, dass die Anwendung, die ausschließlich auf Nachtdaten basiert, grundsätzlich höhere Werte der Ökosystematmung ermittelt, als die anderen verwendeten Methoden. So kam es in den kummulierten Flüssen zu Abweichungen von 16 %, 6 % und 15 % zwischen NEE, GPP und R_{eco} im Vergleich zwischen NT und DT. Geringer fielen die Unterschiede zwischen NT und der eigenen Methode aus. Auch andere Studien berichten von Diskrepanzen in der Partitionierung von NEE bei der Verwendung der oben beschriebenen Methoden. Diese und auch unsere Arbeit zeigen, dass weiterhin Forschungsbedarf hinsichtlich der Anwendung von Source-Partitioning besteht.

Contents

List of Figures

List of Tables

List of Abbreviations

a.s.l.	above sea level
a.g.l.	above ground level
BMBF	Bundesministerium für Bildung und Forschung (Federal Ministry of Education and Research)
C_{exp}	carbon import
C_{imp}	carbon import
DT	daytime
DFG	Deutsche Forschungsgemeinschaft (German Research Foundation)
DEC	disjunct-eddy-covariance
DM	dry matter
DWD	Deutscher Wetterdienst (German Weather Service)
EBC	energy balance closure
EC	eddy-covariance
EFO	emissions from field operations
GHG	greenhouse gas
GHGB	greenhouse gas budget
GPP	gross primary production
IDAS-GHG	instrumental and data-driven approaches to source-partitioning of greenhouse gas fluxes
ICOS	integrated carbon observation system
LRC	light response curve
IRGA	infrared gas analyzer
MAD	mean absolute deviation
MSL	mean sea level
MOST	Monin–Obukhov similarity theory
NECB	net ecosystem carbon budget
NEE	net ecosystem exchange
NEP	net ecosystem production
NPP	net primary production
NT	nighttime
NLR	non-linear regression
PE	polyethylene
PVC	polyvinyl chloride
RMA	reduced major axis
REA	relaxed-eddy-accumulation
RMSE	root mean square error

SHF	soil heat flux
SWC	soil water content
TERENO	terrestrial environmental observatories
USDA	united states department of agriculture
UTC	universal time coordinated
VPD	vapour pressure deficit

List of Symbols

Symbol	Name of Symbol	Dimension
A_{site}	surface area	m^{-2}
B	ground heat flux	W m^{-2}
C	confidence interval	
c_p	specific heat at constant pressure	J kg^{-1} K^{-1}
d	displacement height	m
E	evapotranspiration	mm
E_0	activation energy	K
ET	evapotranspiration	mm
f	frequency	1 s^{-1}
F_c	CO_2 flux	µmol m^{-2} s^{-1}
F_s	CO_2 storage flux	µmol m^{-2} s^{-1}
g	acceleration due to gravity	m s^{-2}
GAI	green area index	m^2 m^{-2}
GPP	gross primary production	µmol m^{-2} s^{-1}
GPP_{sat}	maximum CO_2 uptake rate at light saturation	µmol m^{-2} s^{-1}
H	sensible heat flux	W m^{-2}
h	height	m
h	height bin	
L	Obukhov length	
M	number of individual measurements	
M_a	molar mass of air	Kg mol^{-1}
m_a	mass of the atmosphere	Kg
M_c	molar masses of carbon	Kg mol^{-1}
M_{ind}	number of statistically independent measurements	
N	number of height bins	
NEE	net ecosystem exchange	µmol m^{-2} s^{-1}
p	pressure	kPa
P	precipitation	mm
PAI	plant area index	m^2 m^{-2}
PAR	photosynthetically active radiation	W m^{-2}
Q	net radiation	W m-1
R_{auto}	autotrophic respiration	µmol m^{-2} s^{-1}
R_{eco}	total ecosystem respiration	µmol m^{-2} s^{-1}
R_{hetero}	heterotrophic respiration	µmol m^{-2} s^{-1}

R_s	soil respiration	μmol m^{-2} s^{-1}
RF_{NEE}	radiative forcing of CO_2	W m^{-2} m^{-2}
RF_α	radiative forcing of albedo	W m^{-2} m^{-2}
RH	relative humidity	%
$S\downarrow$	global radiation	W m^{-2}
T	temperature	°C / K
T	transpiration	mm
t	time	s
T_0	activation temperature	°C/K
T_{air}	air temperature	°C/K
T_{ref}	reference temperature	°C/K
T_s	soil temperature	°C/K
u	lateral wind velocity	m s^{-1}
u_*	friction velocity	m s^{-1}
w	vertical wind velocity	m s^{-1}
z	height	m
z_0	aerodynamic roughness length	m
z_{0J}	scalar roughness length	m
α	light utilization efficiency	
α	albedo	
α_0	coefficient	
β	airborne fraction	
Δh	height bin size	m
Δt	time shift	s
Δt_{opt}	optimal time lag	s
θ	potential temperature	°C/K
θ_*	scaling parameter for temperature	°C/K
θ_0	scaling parameter for temperature	°C/K
κ	von Karman constant	
λE	latent heat flux	W m^{-2}
ρ_{air}	density of air	kg m^{-3}
σ	standard deviation	*
φ_h	universal functions for heat	
φ_m	universal functions for momentum	
χ_{CO_2}	CO_2 mole fraction	μmol mol^{-1}
χ_{H_2O}	H_2O mole fraction	mmol mol^{-1}
X	scalar	*
$X*$	scaling parameter for scalar X	*
ψ_h	stability corrections for exchange of sensible heat	
ψ_m	stability corrections for momentum exchange	

Note

* dimension according to the use of quantity

1 Introduction

1.1 Motivation

With the industrial revolution in the 18th century, a major human intervention in the Earth's ecosystem began. Burning fossil fuels, deforestation and changes in land use have led to an increasing concentration of carbon dioxide (CO_2) in the atmosphere. The trace gas CO_2 plays a significant role in affecting the Earth's climate. Its concentration increased from 280 parts per million (ppm) before the industrial revolution to 400 ppm in August 2018 and lead to a global warming of 0.65 to 1.0 °C (North et al., 2014). Land use change and the anthropogenic climate change influence each other and are summarized under the term "global change".

The three major reservoirs in the global carbon cycle are the oceans, terrestrial biosphere and atmosphere. Over 90 % of the carbon is located in oceans and the smallest part is in the atmosphere (North et al., 2014). Although oceans form the largest reservoirs of CO_2, the Earth's biosphere is subject to direct anthropogenic intervention and responds to it more rapidly. Terrestrial ecosystems take up CO_2 through photosynthesis, convert it into organic carbon compounds and fix it in form of plant material or plant residues above and below the soil surface. At the same time, CO_2 is released by plant respiration and decomposition of plant material. These adverse fluxes, the assimilation and respiration of CO_2, react directly to changes into the global carbon cycle and are the focus of this thesis.

The increased global atmospheric CO_2 concentration leads to an increased photosynthesis rate, because plants can assimilate CO_2 more effectively. As a result, increasing CO_2 concentrations influence plant growth to a non-negligible extent. This effect is called "CO_2 fertilization effect" and depends further on the plant species and other environmental conditions, such as temperature, soil type, nutrient and water availability (Kimball et al., 1993; Allen Jr and Amthor, 1995). The CO_2 fertilization effect is responsible for the fact that a considerable part of the anthropogenic CO_2 emissions can be fixed in the biomass (Keenan et al., 2016). A higher rate of photosynthesis, however, leads to an increase in plant and soil respiration, in which respiration increases exponentially with increasing temperature. In addition, changes in land use, such as deforestation for agricultural purposes, affect carbon loss from the terrestrial ecosystem. The land surface currently absorbs approximately one third of CO_2 from combustion of fossil fuels. Additionally, up to 14 % of CO_2 releases are caused from land use changes. It is noteworthy that the changes in photosynthetic uptake as well as the CO_2 emissions from respiratory processes and land use change are in the same order of magnitude as direct emissions from fossil fuels (Stocker et al., 2013).

Another main greenhouse gas is water vapour (H_2O). It has a major global warming reinforcing feedback factor (Dessler and Sherwood, 2009). Temperature rise caused by climate change increases the evaporation rate and thus the H_2O content in the atmosphere. The

increased water vapour concentration absorbs a greater amount of longwave radiation, resulting in a further increase in temperature.
Vertical fluxes of CO_2 and H_2O between an ecosystem and the atmosphere can be measured directly using the well established eddy-covariance (EC) technique. Today, more than 500 flux measurement sites are operating world wide and gather long time series of trace gases (e.g. CO_2, H_2O, methane, nitrous oxides) and energy fluxes (impulse, latent and sensible heat) between different terrestrial ecosystems and the atmosphere. The goal is to study ecosystem-atmosphere interactions and acquire new knowledge about the global carbon cycle (Baldocchi, 2014). However, the method has a disadvantage, because it only determines the vertical net exchange between the terrestrial surface and the atmosphere. To quantify the effects described above, knowledge about the individual components of the net exchange are needed, which can only be estimated indirectly from the EC method with so called source-partitioning approaches (Aubinet et al., 2012). The strategies for source-partitioning are described in Section 1.2.

1.2 Partitioning of net fluxes of CO_2 and H_2O

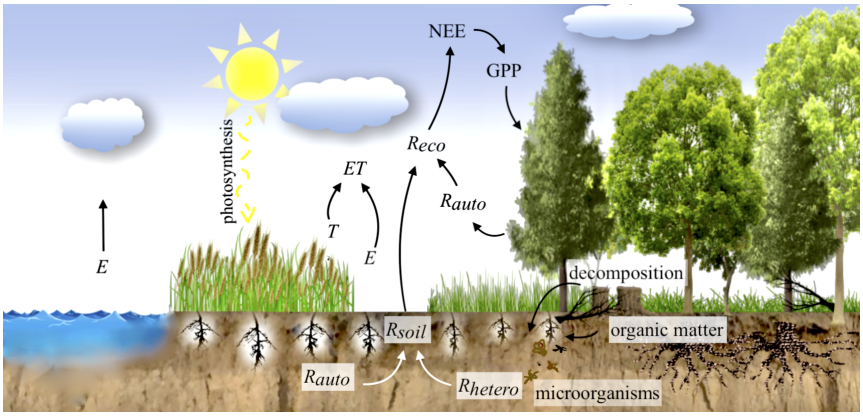

Figure 1.2.1: *Net fluxes of CO_2 and H_2O partitioned into their individual components for terrestrial ecosystems.*

To understand the exchange processes involved in an ecosystem, additional information on the composition of the net fluxes is required. The individual components of the net CO_2 and H_2O fluxes of terrestrial ecosystems are shown schematically in Figure 1.2.1. The net CO_2 flux (or net ecosystem exchange, NEE) is divided into two opposing processes of photosynthesis-induced uptake (gross primary production, GPP) and respiration-induced CO_2 release (ecosystem respiration, R_{eco}). The general meteorological convention implies that fluxes from the atmosphere to the biosphere have a negative sign and vice versa. However, in many scientific articles a positive sign is often used for the representation of GPP. Consequently, the following definition of net ecosystem exchange is given for this thesis:

$$NEE = R_{eco} - GPP, \tag{1.2.1}$$

In some studies, instead of NEE the terminology net ecosystem CO_2 uptake is used, also

known as net ecosystem productivity (NEP, where NEP=−NEE).

R_{eco} comprises all breathing components of an ecosystem and can be divided into autotrophic (R_{auto}) and heterotrophic respiration (R_{hetero}). The former mainly includes plants that gain their energy from solar radiation, the latter includes organisms that need parts of other organisms to gain energy through metabolic processes. Furthermore, respiration can be divided into above- and below-ground respiration (R_{above}, R_s). R_{above} contains all plants above the earth's surface as well as all other living organisms. Below-ground processes are mostly assigned to soil respiration (R_s), which encompasses the respiration of roots, microorganisms, and the release of CO_2 by inorganic processes.

Net fluxes of H_2O are defined as:

$$ET = E + T, \tag{1.2.2}$$

where ET is evapotranspiration, which results from the sum of plant transpiration T and evaporation E from the soil surface and of intercepted water. Again the convention that fluxes directed from the soil surface towards the atmosphere have a positive sign, and vice versa (Aubinet et al., 2012).

To separate NEE into GPP and R_{eco} (as well R_s, R_{auto} and R_{hetero}) or ET into its components T and E, so called flux partitioning strategies are required. Existing applications can generally be divided into data-driven and instrumental approaches.

Data-driven methods mainly include applications that use empirical relationships between measured EC net CO_2 fluxes to other environmental variables like temperature and incoming radiation. The most widely used (e.g., in the global network FLUXNET (Aubinet et al., 2012)) standard flux partitioning approaches are non linear regression (NLR) analyses after Reichstein et al. (2005) and Lasslop et al. (2010). The former use only nighttime NEE data, which are equivalent to R_{eco}. The assumption that respiration is temperature controlled allows to model R_{eco} empirically, using Arrhenius types equations. In the latter method, data is fitted to daytime NEE using light response curves. Both NLR methods are discussed comprehensively in Chapter 4 (see Section 4.2.6).

A further data driven approach, which is still in the experimental phase, uses purely raw data from high-frequency EC measurements of NEE and latent heat for source-partitioning. Sources of CO_2 can be partitioned into respiratory above- and below-canopy components by relating turbulent events with simultaneous CO_2 and H_2O release to transport from below the plant canopy using a conditional sampling method (Thomas et al., 2008). Scanlon and Sahu (2008) and Scanlon and Kustas (2010) developed a partitioning method using high-resolution data to separate fluxes into those originating from stomatal processes (NPP and transpiration) and non-stomatal processes (R_s and evaporation). In a next step, the flux-variance similarity was used to formulate an analytical expression based on the water use efficiency (Aubinet et al., 2012).

Instrumental approaches include the use of supplementary measurements. These comprise chamber-based approaches that provide additional information on leaf, stem and soil fluxes. The latter is measured with soil CO_2 efflux chambers (see Chapter 3) and can be further partitioned into heterotrophic and autotrophic components by root extraction. Further to be mentioned are profile measurements (see Chapter 2) for estimating vertical sink and source strength inside plant canopies (Raupach, 1989a,b; Ney et al., 2017). Still rarely studied and practiced is flux partitioning of EC-measured NEE and latent heat (ET) using tracers

like stable isotopes of CO_2 and H_2O, which, e.g., contains information about the isotopic signature ($^{18/16}O$ ratio) of different ecosystem components and the atmosphere (Bowling et al., 2001; Yakir and da Silveira Lobo Sternberg, 2000).
Some source-partitioning methods are used less frequently, as they are in principle a side-product of modelled terrestrial ecosystem processes or flux gap-filling applications. One of these are inversions of biophysical soil-vegetation-atmosphere-transport ecosystem models (e.g. agroecosystem model AgroC in Klosterhalfen et al., 2017) or biosphere energy-transfer hydrology model BETHY (Knorr and Kattge, 2005), which are driven by observations of meteorological data and various ecosystem parameters. Other less frequently used methods are primarily alternative statistical techniques like Kalman filter (Gove and Hollinger, 2006), look-up tables (Falge et al., 2001a), marginal distribution sampling (Reichstein et al., 2005), semi-parametric model technique (Stauch and Jarvis, 2006), and artificial neural network (Papale and Valentini, 2003; Braswell et al., 2005; Moffat et al., 2010; Evrendilek, 2013). Desai et al. (2008) presented a detailed comparison of these methods for the NEE partitioning into GPP and R_{eco}.

1.3 Thesis objectives

This dissertation was written as a part of the project IDAS-GHG (FKZ 01LN1313A: Instrumental and Data-driven Approaches to Source-Partitioning of Greenhouse Gas Fluxes: Comparison, Combination and Advancement) funded by the German Federal Ministry of Education and Research (BMBF), which aims to systematically compare and improve existing methods for partitioning measurements of the net greenhouse gas exchange over agricultural land, forests and other ecosystems into their respective source and sink components. Especially for agricultural ecosystems or managed forests, a profound knowledge of the exchange of carbon (C) at ecosystem level is of high importance for the development of mitigation strategies, in particular for adaptation and reduction of the impacts of climate change (Houghton et al., 2000).
The separation of net fluxes measured by the EC method, e.g., into assimilation and respiration as described in Section 1.2, does not provide any detailed knowledge for the exact localization of the source and sink distribution between soil and vegetation. For this reason supplementary measurements with additional measurement systems are necessary. Such an additional system, which identifies the distribution of source and sink areas, is described in Chapter 2. This is a prototype of an elevator system specifically developed within the framework of this project. The instrument setup is based on the profile measurement method already established in micrometeorology, with which fluxes, concentrations, temperature or wind speeds can be measured from the soil surface to a few meters above the ground/plant canopy at levels of five to seven height levels. In contrast to the already established profile measurements, the system presented in Chapter 2 is able to provide continuous measurements of concentrations (as mole fractions) of CO_2, H_2O, temperature and wind speed from the soil surface to approximately 2 m a.g.l. The temporal and / or spatial resolution can be adjusted at any time during post-processing. A further advantage of the measurement system is that the profiles are measured with the same sensors. Thus, uncertainties that can arise when using several instruments at different height levels do not arise.
The profile system (see Fig. 1.3.1) was tested in different crop types, different stages of

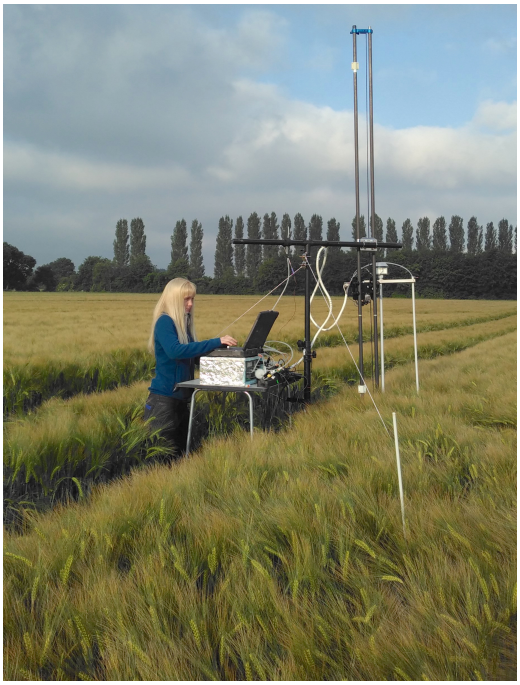

Figure 1.3.1: *The author of this thesis working on the profile measurement set-up in a winter barley field in Selhausen, Germany.*

plant development (different seasons) and over bare soil. It provides a detailed insight into the distribution of photosynthetic carbon assimilation and soil respiration within the plant layer and thus delivers qualitative information of sources and sinks. With additional consideration of vertical humidity, temperature and wind distributions, biophysical processes can be identified.

In agroecosystems the change from a bare, CO_2-emitting soil surface to a CO_2-assimilating vegetation cover occurs over relatively small time scales (usually once or twice within a year). Additionally, applied management strategies are also reflected rapidly in the local carbon budget. In contrast, these processes will last considerably longer in forest ecosystems (up to several decades, see Fig. 1.3.2). Mid-latitude forests sequester large amounts of atmospheric CO_2 (Valentini et al., 2000) and play an important role in the global carbon cycle, particularly in the context of climate change. The study site I used to examine these processes, presented in Chapter 3, offers the possibility to monitor the change from a spruce monoculture to a natural deciduous forest and to analyze the corresponding effects to the local carbon cycle during the succession process. The most important questions to answer here are, how long it will take for a disturbed forest area to absorb more CO_2 than it releases (compensation point) and how long it will take to fix as much CO_2 as it has emitted due to the disturbance (payback period) (Aguilos et al., 2014).

The focus of this study is the quantification of the magnitude of the initial sink and source strength change and the pace of vegetation recovery in the first four years after the partial deforestation. EC measured net fluxes of CO_2 between the ecosystem and atmosphere were

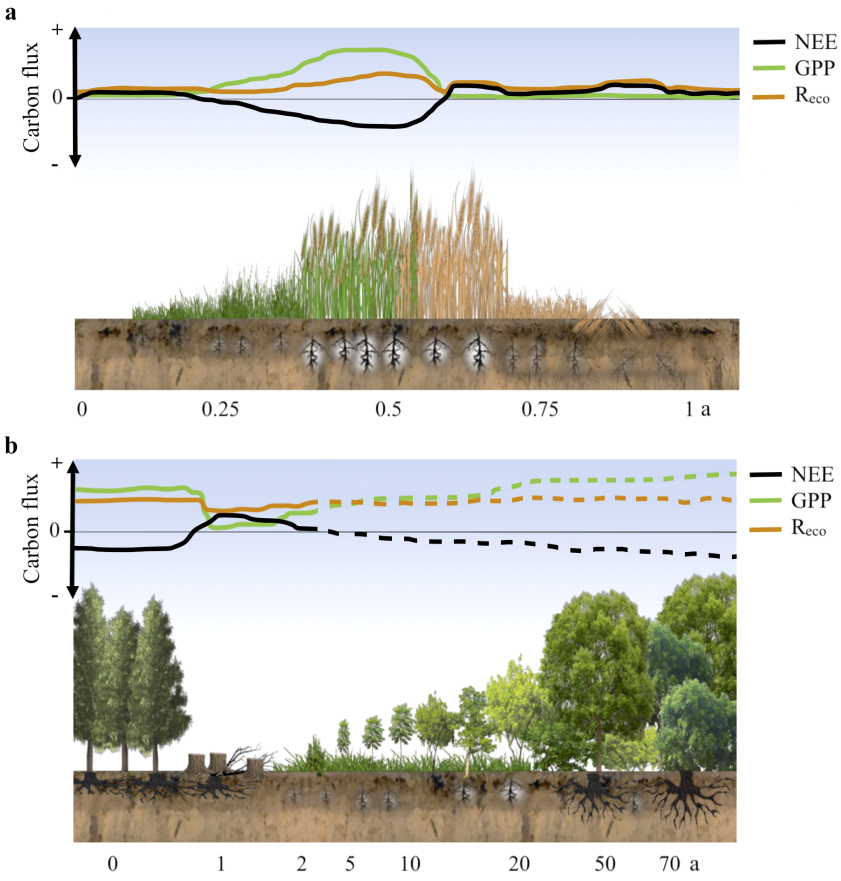

Figure 1.3.2: *Carbon fluxes as net ecosystem exchange (NEE), gross primary production (GPP) and ecosystem respiration (R_{eco}) in two types of ecosystems. a) full crop vegetation cycle and b) forest succession towards deciduous forest. Solid lines show performed measurements and dashed lines indicate the expected course of carbon fluxes.*

partitioned into GPP and R_{eco} using a data-driven non linear regression model after Lasslop et al. (2010). Additional measurements with soil CO_2 efflux chambers were carried out to allow a finer partitioning of R_{eco} into above- and below-ground (R_s) fractions.

With regard to the carbon balance, there are only few studies that have investigated a natural succession within the same forest ecosystem after partial deforestation that provide information about the duration until the disturbed ecosystem returns to a CO_2 sink. An advantage of the Wüstebach study site (see Fig. 1.3.3), presented here, over previous study sites is that reference measurements over adjacent undisturbed forest were carried out before as well as after the clearcut.

In the last Chapter we return to the agroecosystem already introduced in Chapter 2. Long term measurements of CO_2 fluxes over agriculturally managed land are important to improve our knowledge and understanding of the climate and management effects on the local and global carbon cycle (Béziat et al., 2009). Furthermore, agroecosystems have a large potential

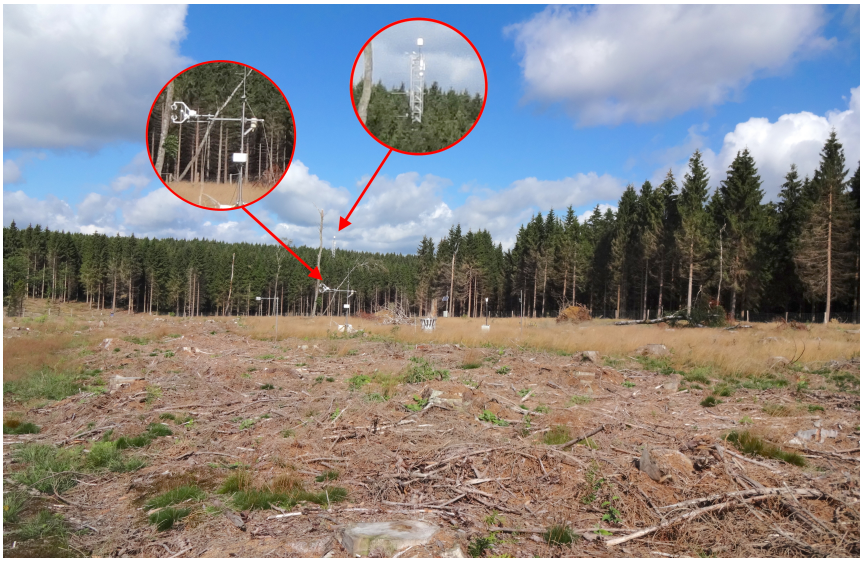

Figure 1.3.3: *Photograph of the Wüstebach catchment in August 2014, one year after deforestation, facing west. The 37 m high meteorological tower with the flux measurements is situated in the spruce forest (background). A second EC station is located in the middle of the picture inside the clearcut area.*

for the mitigation of climate change (Ravindranath and Ostwald, 2008). Today, many agricultural sites are monitored using the EC method. In order to investigate the CO_2 exchange of a crop land, information on photosynthetic and respiratory processes of the arable land are required. The most frequently used method for source-partitioning in field studies is the data-based non-linear regression approach. It can be implemented quickly and easily because different software packages are already available. In this context, the method already applied in Chapter 3 is taken up again in the fourth Chapter and different variants of these flux-partitioning method are compared and analyzed for a 3-year crop rotation cycle. Some studies have shown that differences between the methods can occur by extrapolating determined parameters of NLR, for example, from nighttime data to day time fluxes and vice versa. In order to minimize those effects, an own source-partitioning algorithm was developed, which uses a full NEE data set without a separation between day- and nighttime for parameterizing NLR functions. Beside the consideration of the partitioned CO_2 fluxes for the 3-year crop rotation, the total greenhouse carbon budget (including carbon import and export through seeding and harvesting, as well as emissions from field management) were calculated and analyzed.

2 High-resolution vertical profile measurements for carbon dioxide and water vapour concentrations within and above crop canopies[†]

2.1 Introduction

Surface-layer gradients or profiles of temperature, wind speed, humidity and trace gases have traditionally been used to determine the land surface-atmosphere fluxes of momentum, sensible and latent heat, before the eddy-covariance method became feasible on a large scale. Today, they are used to determine storage terms and advection (Aubinet et al., 2005; Montagnani et al., 2009), inform or validate models (Sogachev et al., 2005; Haverd et al., 2011), partition vertically displaced sinks and sources (Raupach, 1989b; Leuning, 2000; Santos et al., 2011) and characterize microclimatic conditions in plant canopies. As with other flux determination methods, such as the relaxed-eddy-accumulation (REA) method (Businger and Oncley, 1990; Fotiadi et al., 2005a,b) and the disjunct-eddy-covariance (DEC) method (Rinne et al., 2001; Baghi et al., 2012), profile measurements are also used in conditions, or for scalars, not suitable for eddy-covariance measurements, e.g., because rapid-response sensors are unavailable. For sensor-based measurements, the costs increase proportionally with the number of measurement levels, and care must be taken to calibrate sensors against each other since any systematic deviation will affect the apparent profile. For trace gases and humidity, this can be avoided by multiplexer systems, and for temperature and partly also humidity, distributed temperature sensing has recently been suggested (Thomas et al., 2012; Euser et al., 2014). Another means of obtaining data from an arbitrary number of measurement heights consists of sounding, i.e. moving the same sensor or trace-gas analyzer inlet vertically. This is frequently done on a large scale with radiosondes, tethersondes and aircraft (Lothon et al., 2014), but has received comparatively little attention in surface-layer (Brosy et al., 2017) or canopy studies.

Accurate micrometeorological measurements in low and dense plant stands are particularly challenging. Instruments must not affect plant activity or structure, and dense canopies lack the large volumes of air to which most conventional instruments are adapted. Only few studies have been done with elevator systems for measuring vertical profiles, and most of them were preconfigured to stop at a finite number of levels. Noone et al. (2013) used an elevator system at a 300-m high research tower to obtain H_2O and CO_2 mixing ratios every few tens of metres, with a sounding time of 9 min for one ascent/descent. Mayer et al. (2009, 2011) tested an existing service elevator on a 99-m tower to measure profiles of

[†]this chapter has been published as: Ney, P. and Graf, A. (2018): High-resolution vertical profile measurements for carbon dioxide and water vapour concentrations within and above crop canopies. Boundary-Layer Meteorology 166, 449–473, https://doi.org/10.1007/s10546-017-0316-4.

temperature, relative humidity and mixing ratios of CO_2, H_2O and O_3 in continuous mode, moving up and down once every 10 min. A smaller elevator was used by Jäggi et al. (2006) to measures ozone profiles with a total vertical distance of 1.5 m, which moved alternately to seven levels and remained at each for at least 100 s. Drüe (1996) designed a 1.2-m high elevator, which moves at 30-s intervals to a specified height to measure temperature and radiation for 20 s. Gradients of water vapour and CO_2 concentrations within and above different plant populations have mostly been obtained using multiport systems, which are controlled by solenoid valves, sampling air sequentially at five to eight levels, taking from 1 min (Al-Saidi et al., 2009; Xu et al., 1999) to 10-20 min (Ahonen et al., 1997; Brooks et al., 1997; Buchmann and Ehleringer, 1998) or 30 min (Leuning, 2000; Miyata et al., 2000) for one cycle (profile).

Here, we introduce a technique to obtain vertical profiles of CO_2 and H_2O (as mole fractions χ_{CO_2} and χ_{H_2O}), as well as temperature and wind speed within and above crop canopies and bare soil, as an amendment to existing eddy-covariance measurements. An elevator continuously moves up and down (taking approximately 36 s for one ascent/descent) between the soil surface and 2.1 m a.g.l. with an ascent speed around 0.06 m s^{-1}, collecting about 25 profiles each in upward and downward mode over 30 min at a logging frequency of 20 s^{-1}. The system was installed and operated on selected measurement days to act as a mobile campaign solution and as a prototype for a long-term installation, which requires additional protection against heavy rain and windy conditions. While the actual vertical and temporal resolution can be configured during data processing, we here mostly present 30-min mean profiles of 0.025-m thick layer averages as a basis for checking the plausibility of the measurement and raw-data-processing approach. For those measurements that were made over bare soil and short canopies, flux-profile relationships are well established and a particularly rigid plausibility test can be performed by comparing fluxes derived from these profiles to eddy-covariance measurements. Such a comparison is given below.

2.2 Methods

2.2.1 Test site

The tests were carried out at the TERENO research site Selhausen (ICOS site code DE-RuS). The test site is situated in the southern part of the Lower Rhine Embayment in the river Rur catchment (50°52'09"N, 06°27'01"E, 104.5 m a.s.l., Fig.2.2.1) in Germany.

The device was placed and operated in a test field with a size of 9.8 ha, cultivated with a rotation of crops, during selected periods of the growing season of winter wheat (*Triticum aestivum L.*) and after harvest in the year 2015, the growing season of winter barley (*Hordeum vulgare L.*) in spring 2016 and a catch-crop mixture (*Vicia sativa L., Pisum sativum L., Avena strigosa Schreb., Raphanus sativus L., Trifolium alexandrinum L., Phacelia tanacetifolia Benth., Guizotia abyssinica (L.f.) Cass.*) in autumn 2016.

The annual mean air temperature is 9.9 °C and the annual precipitation sum is 698 mm (Graf et al. 2012). The maximum crop height ranged from 0.7 to 0.8 m in winter wheat and 0.95 to 1.05 m in winter barley. The soil is an Orthic Luvisol and the texture is silt loam according to the USDA classification (Graf et al. 2008). Table 2.2.1 gives an overview of the test days and the associated summary of the measurement properties and weather conditions.

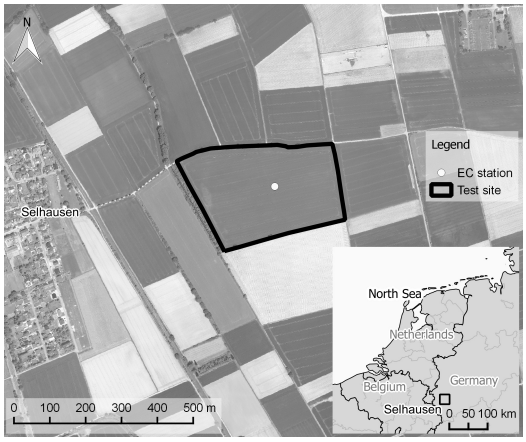

Figure 2.2.1: *Overview of the test site Selhausen.*

2.2.2 Eddy-covariance and other continuous measurements

Reference values of sensible heat flux (H) and latent heat flux (λE), friction velocity (u_*) and CO_2 flux (F_C) were calculated from measurements by a permanently-running eddy-covariance station at the Selhausen site. It operates with a three-dimensional sonic anemometer (Model CSAT-3, Campbell Scientific Inc., Logan, Utah, USA) to measure the wind vector and the sonic temperature. An open path infrared gas analyzer (Model LI- 7500, Li-Cor Inc. Biosciences, Lincoln, Nebraska, USA) measured the CO_2 concentration and the absolute humidity 2.5 m above the surface, with a fetch of at least 120 m and up to 210 m in the prevailing west-south-west wind direction. The measurement frequency was 20 s^{-1}. Turbulent fluxes were calculated as 30-min averages using the 'TK3.11' software package, which includes rigorous quality control and correction procedures (Mauder and Foken 2011, Mauder et al. 2013). Here, only data of the highest quality (flag 0) was used. Gaps in the eddy-covariance data set were filled with the REddyProc package after Reichstein et al. (2005).

Energy balance quantities were measured with a net radiometer (NR01, Hukseflux, Delft, the Netherlands), up to four self-calibrating soil heat-flux plates (HFP01SC, same manufacturer), and soil water content and temperature measurements in the layer above the heat flux plate for surface soil heat flux calculation following the calorimetric method (Appendix A1). Photosynthetically active radiation (PAR) was measured with a quantum sensor (Li190, LI-COR, Lincoln, Nebraska, USA). Both radiation instruments were mounted at a height of 2.5 m.

An automated soil CO_2 efflux chamber system (Li-8100, Li-Cor Inc. Biosciences, Lincoln, Nebraska, USA) was operated with at least three and up to four long-term chambers. The chambers were placed on PVC soil collars of 0.2 m in diameter and a height of 0.07 m, which were inserted 0.05 m into the soil. The closing interval for each chamber was 30 min, and it was closed for 90 s for each flux measurement. CO_2 and water vapour concentration as well as chamber headspace temperature were measured every second. The CO_2 concentration was corrected for changes in air density and water vapour dilution. The soil respiration (R_s) was calculated by fitting a linear regression to the corrected CO_2 concentrations from 30 s

Table 2.2.1: *Profile measurements: measuring periods (number of 30-min mean profiles within the measurement period in brackets), measured variables (χ_{CO_2} and χ_{H_2O} are mole fractions of CO_2 and H_2O, u is wind speed and T is temperature), weather condition (cloud amount in okta and wind speed in Beaufort number), canopy and profile height.*

date	time UTC	variables	weather condition	canopy height m	profile height m
winter wheat					
14 April 2015	1515-1545	χ_{CO_2}, χ_{H_2O}	1, 2-3	0.20	1.85
20 Mai 2015	0850-0920	χ_{CO_2}, χ_{H_2O}, u, (T)	4, 2	0.70	1.90
1 June 2015	1630-1700	χ_{CO_2}, χ_{H_2O}, u, (T)	3, 1	0.80	2.10
7 June 2015	1530-1600	χ_{CO_2}, χ_{H_2O}, u	1, 2	0.80	2.10
8 June 2015	0630-1830 (10)	χ_{CO_2}, χ_{H_2O}, u	1, 2-3	0.80	2.10
30 June 2015	1100-1130	χ_{CO_2}, χ_{H_2O}, u, (T)	0, 1	0.80	2.10
17 July 2015	1230-1300	χ_{CO_2}, χ_{H_2O}, u, (T)	0, 2	0.80	2.10
bare soil					
13 August 2015	1030-1100	χ_{CO_2}, χ_{H_2O}, u, (T)	0, 2	-	2.10
10 September 2015	1500-1530	χ_{CO_2},χ_{H_2O}, u, (T)	2, 3	-	2.10
winter barley					
31 Mai 2016	1230-1300	χ_{CO_2}, χ_{H_2O}, u, (T)	6-7, 2	1.10	2.10
6 June 2016	0730-1240 (5)	χ_{CO_2}, χ_{H_2O}, u, T	0, 0-1	0.95	2.10
9 June 2016	0400-2300 (20)	χ_{CO_2}, χ_{H_2O}, u, T	0-1, 0-2	0.95	2.10
10 June 2016	0000-1100 (12)	χ_{CO_2}, χ_{H_2O}, u, T	1-2, 0-1	0.95	2.10
bare soil					
18 July 2016	1400-2200 (9)	χ_{CO_2}, $\chi_{H_2O}{}^{+}$, u, T	0-2, 0-1	-	2.10
intercrop					
23 September 2016	0930 -1200 (4)	χ_{CO_2}, $\chi_{H_2O}{}^{+}$, u, T	1-5, 2-3	0.22	2.10
23 November 2016	1100-1330 (5)	χ_{CO_2}, $\chi_{H_2O}{}^{+}$, u, T	7, 2	0.45	2.10
24 November 2016	1400-2300 (12)	χ_{CO_2}, $\chi_{H_2O}{}^{+}$, u, T	1, 3-4	0.45	2.10
25 November 2016	0000-1530 (25)	χ_{CO_2}, $\chi_{H_2O}{}^{+}$, u, T	1,1-2	0.45	2.10
16 December 2016	1000-1330 (8)	χ_{CO_2}, $\chi_{H_2O}{}^{+}$, u, T	1,2-3	0.35	2.00

(T) Temperature measurements with limited usability.
$^{+}$ Insulated, heatable χ_{CO_2} and χ_{H_2O} sampling tubes connected to the gas analyzer.

after closing until reopening.
Information about the leaf and plant area index (PAI) and green area index (GAI) over the whole plant growing seasons were collected in intervals of four weeks in field with a LAI-2200 plant canopy analyzer (Li-Cor Inc. Biosciences, Lincoln, Nebraska, USA) and with a destructive method (LI-3100C area meter, Li-Cor Inc. Biosciences, Lincoln, Nebraska, USA). On dates where optical and destructive measurements of PAI were taken, both methods compared well, such that uncorrected optical PAI values are reported for days where no destructive measurements were available. In June and November 2016, vertical profiles of PAI were measured manually in winter barley and catch-crop from the soil surface up to the canopy top every 0.05 m with a SunScan-System SS1 (Delta-T devices, Cambridge, UK).
On profile measurement days (see Table 2.2.1), the elevator system was placed at a distance of 15 - 30 m from the eddy-covariance station at a day-dependent direction to prevent both installations from obstructing the fetch of each other.

2.2.3 Profile measurement set-up

The system measures mole fractions (amount of substance per mole of moist air) of CO_2 (χ_{CO_2}) and water vapour (χ_{H_2O}) with a resolution of 20 s^{-1} between the soil surface, the

plant canopy and the atmosphere while continuously moving the intake of a sampling tube between the ground surface and a maximum height, which was around 2 m in our case. The measurement system was continuously improved, such that the schematic illustration in Fig. 2.2.2 represents the device version in the last measuring period starting in July 2016 (see Table 2.2.1 and Appendix A1). The elevator consists of a camera tracking slide (c) for moving time-lapse photography (Dynamic Perception LLC, Ann Abor, Minnesota, USA) mounted vertically to a tripod (b). A motor is mounted on the carriage (slider) (f) which drives up and down on a toothed drive belt (d). Two cuffs (e) are attached to the frame at the upper and lower end position, which trigger reversion of the sense of motion on contact. The time of these events is logged to a text file on a computer. A rotation sensor on the slider, using the same toothed belt, provides position data with a nominal resolution of approximately 0.003 m, which are logged as counted steps to the same text file at intervals of 0.17 s.

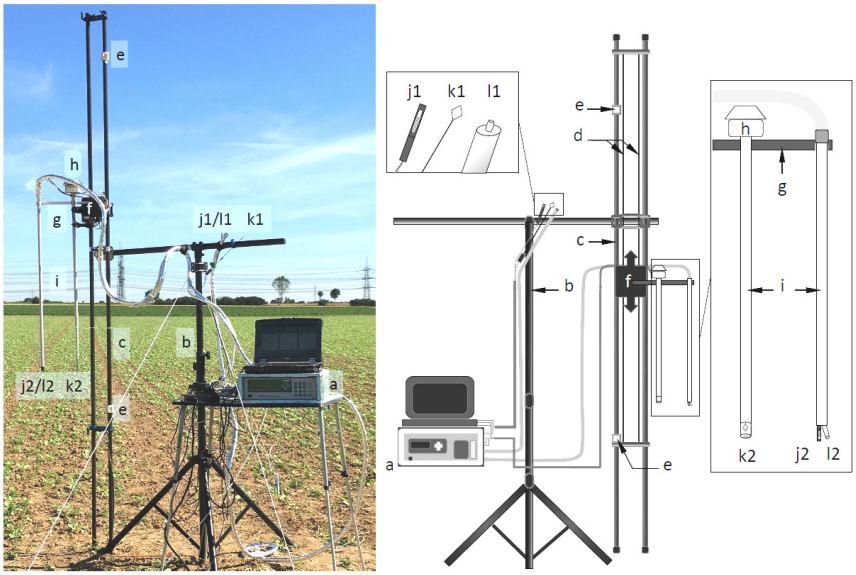

Figure 2.2.2: *The profile-measurement set-up in the field (left) and as a schematic diagram (right). (a) gas analyzer, (b) tripod, (c) tracking slide, (d) toothed drive belt, (e) upper and lower limiting ring (cuff), (f) carriage, (g) extension arm, (h) thermocouple ventilation unit, (i) conduit, (j) fixed-height (1) and moving (2) hot-wire anemometer, (k) fixed-height (1) and moving (2) thermocouple and (l) fixed-height (1) and moving (2) inlet tubes from gas analyzer.*

χ_{CO_2} and χ_{H_2O} were measured by a closed-path, differential infrared absorption gas analyzer (LI7000, Li-Cor Inc. Biosciences, Lincoln, Nebraska, USA) (a). Each of the two cells of the analyzer was connected through a 1 µm filter to a polyethylene tube of 0.0035 m inner diameter. The outlets of the cells were connected to the internal pump of the LI7000, which was run at maximum speed, leading to a flow rate of about 30 l h^{-1} through each tube. χ_{CO_2} and χ_{H_2O} in both cells and diagnostic variables of the LI7000 were logged at intervals of 0.05 s (20 s^{-1}). While the end of one tube (l1) was attached to the tripod at a fixed height of approximately 2 m, the other one was attached to an extension (g) on the carriage (Fig. 2.2.2f). Tube length, heating and insulation changed over time as indicated in Table 2.2.1

and described in Appendix 1A.
Wind speed was measured using two hot-wire anemometers (8455- 075-1, TSI, Shoreview, Minnesota, USA) (j), one of which was fixed at approximately 2 m (j1), while the other (j2) was attached near the tip of the conduit, such that the sensor was level with the tube intake (l2) and about 0.02 m away from it. Temperature was measured by two fine-wire thermocouples (FW3, Campbell Scientific, Logan, Utah, USA) (k), one of which was fixed at approximately 2 m (k1), while the other one (k2) was attached to a second conduit, the junction tip level with the other moving measurements and 0.2 m away from them. While the fixed-height thermocouple was operated unshielded, the moving thermocouple was shielded against direct contact with plants or soil by an empty conduit with a diameter of 0.015 m, with a fine fiberglass mesh at the tip and a ventilation unit (h) at the other end of the conduit, which produced a flow rate at the tip of 3.7 m s^{-1}. This final wind and temperature set-up was the result of stepwise improvements described in Appendix A1.

2.2.4 Profile data processing

While the continuously moving set-up allows us to chose the temporal and vertical resolution of mean profiles during data processing, we consistently use time-averaging blocks of 30 min. For each such block, the logged slider position data in steps was assembled to the height by scaling the minimum step number to 0 m and the maximum step number to the topmost measuring height during the respective measuring period (approximately 2 m, for details see Table 2.2.1). Values missing after adding the position dataset (0.17-s resolution) to the gas concentration, temperature and wind speed data (0.05-s resolution) via the nearest time stamp, were filled using linear interpolation.
Physically unrealistic values were filtered out before the calculation of mean profiles by a plausibility screening and a spike detection algorithm based on median absolute deviation (MAD) limits, similar to the one described in Mauder et al. (2013). However, the chosen limits were extended to accommodate the larger variability of the moving sensor data (Table 2.2.2).

Table 2.2.2: *Thresholds used for plausibility tests, spike detection tolerances and shift limits (in s) for lag removal. Spike tolerances are given in equivalent standard deviations, i.e., in the median absolute deviation (MAD) divided by 0.6745, which matches one standard deviation in normal distributions but is less outlier-sensitive otherwise (see Mauder et al. 2013).*

variable	consistency limits	spike tolerance	shift limits (s)
$\chi_{CO_2 fix}$	200 to 900 µmol mol^{-1}	9 σ_{eq}	-30 to 0
$\chi_{CO_2 var}$	200 to 900 µmol mol^{-1}	20 σ_{eq}	-30 to 0
$\chi_{H_2O fix}$	0 to 50 mmol mol^{-1}	9 σ_{eq}	-30 to 0
$\chi_{H_2O var}$	0 to 50 mmol mol^{-1}	20 σ_{eq}	-30 to 0
u_{fix}	0 to 10 m s^{-1}	9 σ_{eq}	-10 to 10
u_{var}	0 to 10 m s^{-1}	20 σ_{eq}	-10 to 10
T_{fix}	0 to 40 °C	9 σ_{eq}	-20 to 10
T_{var}	0 to 40 °C	20 σ_{eq}	-20 to 10
p	70 to 110 kPa	9 σ_{eq}	-
elevator speed	-0.2 to 0.2 m s^{-1}	-	-

The response times of the wind and temperature sensors, electronic delays, and tube transport of the gas samples can lead to delays in each variable with respect to the position data. Different delays for CO_2 and H_2O, in spite of the common tube and analyzer system, are

well-known from closed-path eddy-covariance measurements due to the higher adhesivity of water vapour to tube walls (Ibrom et al. 2007). These delays are determined empirically by a hysteresis minimization algorithm. Within possible shift limits (see Table 2.2.2), the variables are shifted with respect to the position data in 0.05-s steps, and for each candidate delay and variable a preliminary vertical profile is computed, including the profile of the standard deviation of the variable

$$\sigma_{x,h}(\Delta t) = \sqrt{\frac{1}{M(h)} \sum_{i=1}^{M(h)} [x(h,i,\Delta t) - \bar{x}(h,\Delta t)]^2}, \tag{2.2.1}$$

where x is the variable of interest, Δt the shift backwards in time according to the respective candidate delay, and M the number of individual 0.05-s measurements i available in the respective height bin after shifting x by Δt with respect to the position data. Here, the height bins are 0.025 m high. The final delay for each variable is the one that minimizes the average of this standard deviation over all heights,

$$\bar{\sigma}_x(\Delta t) = \sqrt{\frac{1}{N} \sum_{h=1}^{N} \sigma^2{}_{x,h}(\Delta t)}, \tag{2.2.2}$$

where N is the number of height bins h, and the overbar denotes averaging. Required time shifts determined this way for the moving sensors were assumed to be equally applicable to the respective fixed-height sensor, due to the identical measurement systems and tube lengths. Delay correction of the fixed-height measurements is not of importance here, but might be relevant when analyzing e.g. fast fluctuations of moving sensor signals in comparison to those of fixed-height measurements.

After determining the optimal time lag Δt_{opt}, Eq. 2.2.1 can also be used to determine the uncertainty (stochastic error) of the final profile of x at each height separately. To provide the uncertainty as a 95 % confidence interval, we use the equation,

$$C_{0.95,x,h} = 1.96 \frac{\sigma_{x,h}(\Delta t_{opt})}{\sqrt{M_{ind}}}, \tag{2.2.3}$$

where M_{ind} is the number of statistically independent samples per height bin, which may be smaller than M due to oversampling of an autocorrelated time series, a problem for which different strategies exist in the framework of eddy-covariance data processing (Lenschow et al., 1994; Finkelstein and Sims, 2001; Moene and Michels, 2002; Van Dijk et al., 2004; Graf et al., 2010; Billesbach, 2011; Mauder et al., 2013). In our dataset, the samples contributing to $\bar{x}_h$ have a clustered temporal structure, with $M = M_1 \cdot M_2$, M_1 being the number of passes through a height bin during the averaging interval (approximately 50 in 30 min) and M_2 the average number of samples recorded during a single pass (8 in the time of approximately 0.4 s needed to pass each height bin). The integral time scale of atmospheric turbulence for our variables of interest in the atmospheric boundary layer is typically between 0.4 and 6 s (Lenschow et al., 1994; Finkelstein and Sims, 2001). A worst-case assumption that the M_2 consecutive samples during a single pass of a height bin do not notably contribute to a reduction in uncertainty leads to a conservative estimate $M_{ind} \approx M_1$. This assumption will be revisited in the results, Sect. 2.3.1, in an analysis with synthetically-reduced raw data acquisition frequency.

Profile measurements are frequently used to estimate the contribution of storage changes below the eddy-covariance measurement level to possible differences between the measured turbulent flux and surface exchange, particularly in case of CO_2. To receive a storage term estimate that is in phase with the flux time series and does not suffer from additional methodological low-pass filtering, we averaged three consecutive ascents and descents at the beginning and at the end of each 30-min time block to yield near-instantaneous χ_{CO_2} profiles representing approximately the first and last 3.5 min. After conversion to units of µmol m^{-3} using the according temperature profile and average pressure, the height-integrated concentration differences and exact time spans between consecutive near-instantaneous profiles were used to estimate the average storage change in µmol m^{-2} s^{-1} for each 30-min profile measurement, but also for each 30-min break in the case of hourly repeated profile measurements on 9-10 June 2016 and 18 July 2016 (see Table 2.2.1 and Sect. 2.3.3).

2.2.5 Profile shape validation and flux determination using Monin-Obukhov similarity theory

During the post-harvest measurements above bare soil and short catch-crop canopy (canopy height $\leq$ 0.22 m), a large portion of the total profile should follow surface-layer scaling. Therefore, we analyzed those measurements in the framework of Monin-Obukhov similarity theory to check the validity of the measurement and raw-data processing approach, derive CO_2, sensible and latent heat fluxes, and compare them to eddy-covariance and chamber measurements.

Flux derivation from surface-layer profiles is based on the integrated flux-profile relations for momentum, heat and mass as described in Appendix A2. Based on these equations (Eq. 5.0.1 to 5.0.6) the friction velocity u_* and the flux of sensible heat or other scalars can be calculated from the slope of a linear regression between logarithmized height $\ln(z)$ and wind speed u, respectively $\ln(z)$ and potential temperature θ or another scalar X (Arya, 2001; Foken, 2006):

$$\ln z - \psi_m \left(\frac{z-d}{L} \right) = \frac{\kappa}{u_*} u + \ln z_0, \tag{2.2.4}$$

$$\ln z - \psi_h \left(\frac{z-d}{L} \right) = \frac{\alpha_0 \kappa}{\theta_*} \theta - \frac{\alpha_0 \kappa}{\theta_*} \theta_0 + \ln z_{0\theta}, \tag{2.2.5}$$

where ψ_m and ψ_h are the stability corrections for momentum exchange and exchange of sensible heat, z_0 and d are the aerodynamic roughness length and displacement height, $z_{0\theta}$ is the scalar roughness length, L is the Obukhov length, κ is the von Karman constant, the coefficient $\alpha_0 = 1.25$, θ is the potential temperature, θ_0 is the potential temperature at $z - d = z_{0\theta}$, and θ_* is the scaling parameter for temperature according to Eq. 5.0.5 (Appendix A2). Apart from the measured profiles, z_0 and d are needed as well as an initial estimate of L, which can then be improved by iteration. To estimate stability values from the measured vertical profiles only, u_* and the sensible heat H were replaced in Eq. 5.0.4 (Appendix A2) by the surface-layer gradient equations (Foken, 2006):

$$u_* = \sqrt{-\overline{u'w'}} = \frac{\kappa}{\varphi_m \left(\frac{z-d}{L} \right)} \frac{\partial u}{\partial \ln(z-d)}, \tag{2.2.6}$$

$$\overline{w'\theta'} = -\frac{\alpha_0 \kappa u_*}{\varphi_h\left(\frac{z-d}{L}\right)} \frac{\partial\theta}{\partial \ln(z-d)}, \tag{2.2.7}$$

where φ_m and φ_h are the universal functions for momentum and heat. Thus we achieve the Obukhov length in the form

$$L = \frac{\theta}{g\,\alpha_0} \frac{1}{\partial\theta} \frac{\partial u^2}{\partial \ln(z-d)} \frac{\varphi_{m^2}}{\varphi_h}, \tag{2.2.8}$$

where g is the acceleration due to gravity, and the gradients in the term $\frac{1}{\partial\theta} \frac{\partial u^2}{\partial \ln(z-d)}$ were estimated from the vertical profiles of wind and potential temperature by two linear regressions of θ and $\ln(z)$, respectively, against u. For the regression of each variable we used an algorithm, which iteratively omitted data points at one or both ends of the profile until the p-value of the regression was optimized, for example, to prevent the influence of profile values measured below the surface layer. The universal function for momentum φ_m and heat φ_h is in the unstable case $\varphi_m^2 \approx \varphi_h$ (Foken, 2006) and thus neglected in the first estimate of L. The roughness length z_0 was computed from the offset of the regression of $\ln(z)$ against u. To account for a possible displacement height d, the whole procedure was repeated for all d values between zero and the canopy height, until the R^2 value of $\ln(z)$ against u is maximized.

Now, with d and z known and a first estimate of L and z_0 available, we can compute first momentum and heat flux estimates with Eq. 2.2.4 and 2.2.5. After that, a second and third estimate of the stability was performed by calculating a new L with the resulting heat and momentum flux and the original definition (Eq. 5.0.4). After that, the flux of the other scalars (H_2O and CO_2) was estimated in analogy to Eq. 2.2.5. For diagnostic purposes, the model profiles consistent with the estimated fluxes and aerodynamic parameters can be derived by applying the basic equations 5.0.1 to 5.0.3 in forward mode again, and compared to the measured profiles.

2.3 Results and discussion

2.3.1 Raw data processing diagnostics

An example is given in Fig.2.3.1 to demonstrate the effect of profile data processing described in Sect. 2.2.4. Figure 2.3.1a shows a raw data time series of χ_{CO_2} from the moving and the fixed height sensor for an interval of 30 min measured in winter barley. The high and low peaks of χ_{CO_2} reflect the source at the soil surface and the mid canopy sink, respectively. Both time series coincide when the moving sensor was at the approximate height of the fixed one. Figure 2.3.1b and Fig. 2.3.1c show the same data for every ascent and descent as a function of moving sensor position before and after lag removal. Averaged mean profiles before and after lag removal are displayed in Fig. 2.3.1c. Before lag determination, the standard deviation and resulting uncertainty (see Eq. 2.2.1 and 2.2.3) is larger than with the applied final delay. The final delay was calculated by Eq. 2.2.1 and is highlighted in development of $\bar{\sigma}_x$ (Eq. 2.2.2) as a function of the delay in Fig. 2.3.1, in this case raw data were lagged by 11 s.

Figure 2.3.2 demonstrates that the estimated lag time for χ_{H_2O} is longer than for χ_{CO_2} (a), and increases with relative humidity (b). During the first 24-h measurement in June

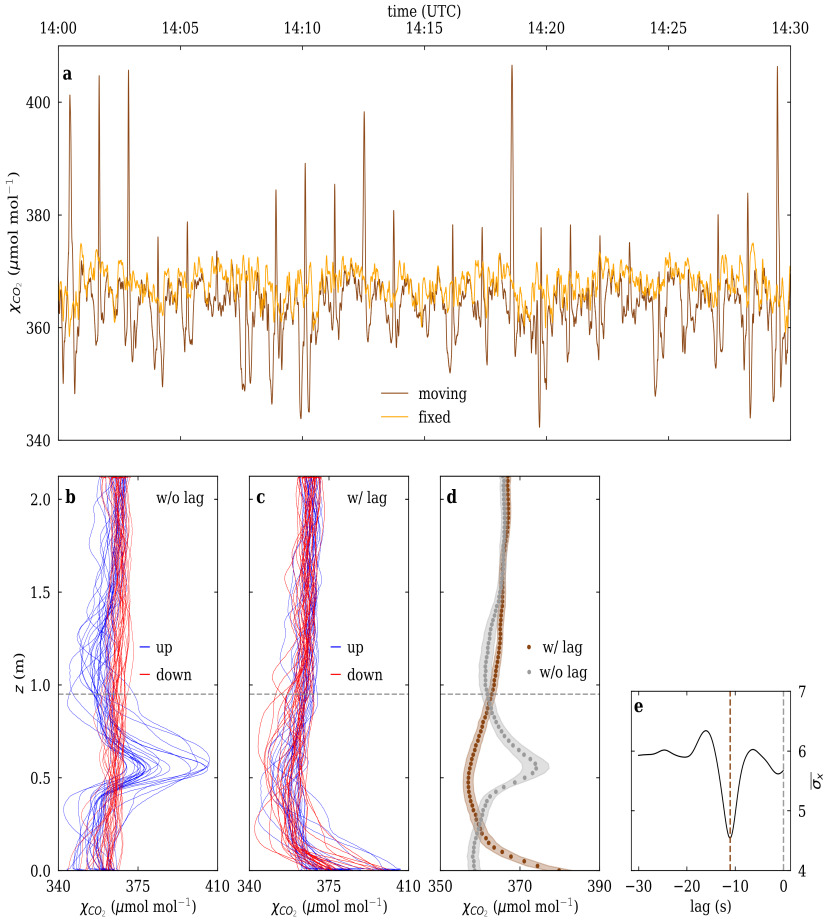

Figure 2.3.1: *a) Raw data time series of χ_{CO_2} for the moving and the fixed height sensor from 9 June 2016 from 1400 to 1430 UTC. b) Vertical profile of χ_{CO_2} vs. height z (m, a.g.l) at 9 June 2016 from 1400 to 1430 UTC with all upward and downward soundings before lag removal procedure (w/o lag) and c) after lag removal procedure (w/ lag). d) 30-min mean profile of χ_{CO_2} averaged over all profiles before and after lag removal, shaded areas indicate the 95 % confidence interval resulting from the standard deviation between individual samples and e) development of $\bar{\sigma}_x$ as a function of the lag. Dashed lines in b, c and d declare the canopy height.*

2016 (Sect. 2.3.3), we found that in conditions with high air humidity (mostly nocturnal situations) the determination of the lag for χ_{H_2O} failed. Lags in the signal of closed-path analyzers can be subject to adsorption of water vapour to the inner tube walls. The extent of condensation is related to the relative air humidity, but also to the wall material (Bloom et al., 1980), its age, and to the presence of aerosols (Mammarella et al., 2009; Nordbo et al., 2013). Humidity also has an effect on the lag of the measured χ_{CO_2}, although in an attenuated form, due to solubility in water. We minimized this problem in the following observation periods by heating and insulating the sampling tube (Appendix A1). A linear humidity-lag relation might be fitted to each of the sub-datasets (3-m tube length, 4.5 m,

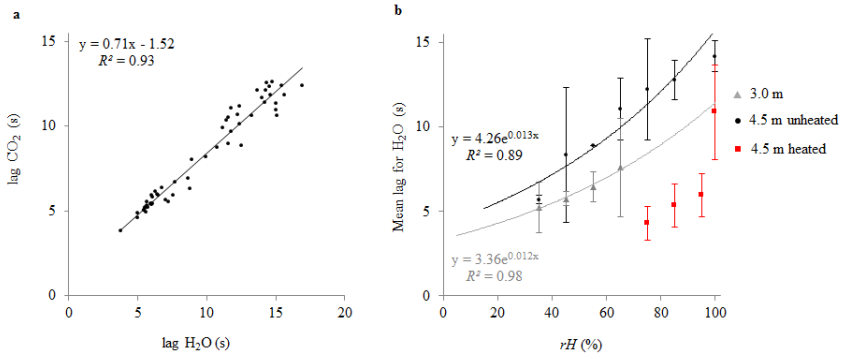

Figure 2.3.2: *a) Linear dependence between the determined lag time (s) of χ_{H_2O} and χ_{CO_2}. b) Lag (s) of χ_{H_2O} averaged over humidity classes with error bars indicating one standard deviation from the mean, plotted against relative humidity (RH). Lag times for tube length of 3 m (triangles) and 4.5 m unheated (dots) and 4.5 m heated (square).*

4.5 m heated) shown in Fig. 2.3.2. However, consideration of all sub-datasets across the larger humidity range and literature (Mammarella et al., 2009) suggest a progressive relationship. The axis intercepts of empirical exponential fits to the unheated datasets with different tube lengths have a ratio of 1.3, which roughly reflects the length change (factor 1.5) and thus suggests a proportionality between tube length and lag time. The dataset with activated tube heating does not allow for a robust intercept estimation due to missing low humidity situations, but clearly shows an accelerating effect on lag time. A sharp increase above 90 % suggests that the heating power may be insufficient to optimally handle fully saturated conditions.

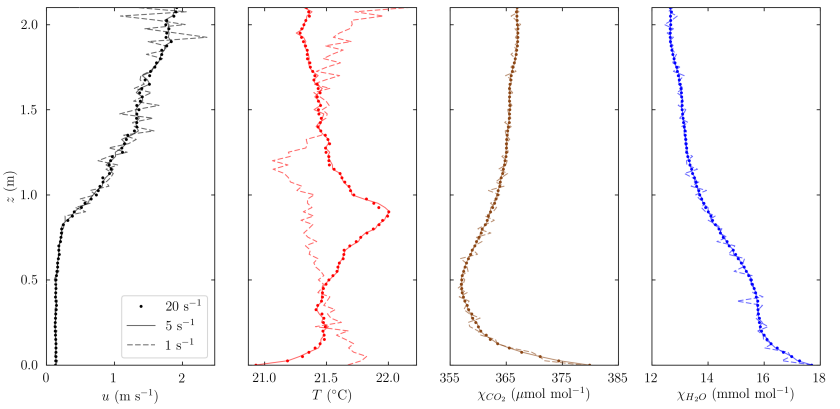

Figure 2.3.3: *30-min mean profiles of wind speed u, temperature T, χ_{CO_2} and χ_{H_2O} at 2016-06-09 1400-1430 UTC based on the original raw data acquisition frequency of 20 s^{-1} (dots) and simulated lower resolutions of 5 s^{-1} (lines) and 1 s^{-1} (dashed lines).*

Figure 2.3.3 shows the effect of a simulated lower data acquisition frequency on the resulting

time-averaged profiles. A decrease from 20 s^{-1} to 10 s^{-1} yields hardly visible effects (not shown). For the variables χ_{CO_2} and χ_{H_2O} almost the same is true for 5 s^{-1}, indicating that the physical low-pass filtering properties of the closed-path system are on the same order of magnitude. At 1 s^{-1}, scatter considerably increases for all variables, and the temperature profile is subject to a failure of lag determination. In this case, the target vertical resolution (0.025 m) and given elevator speed (0.06 m s^{-1}) do not ensure any more that the raw values contributing to a single profile height stem from all of the approximately 50 soundings per 30 min. To avoid this, the measurement frequency should be at least 5 s^{-1} with the given speed and target resolution. The increase in scatter visible in Fig. 2.3.3 largely confirms the assumption made in Sect. 2.2.4 that measurement uncertainty of the final profiles is mostly determined by the number of elevator passes through a height bin during which at least one raw record was sampled, and less by the number of such raw records during an individual pass.

2.3.2 Profiles of CO_2 and H_2O over a winter wheat plant growing season

In 2015, profile measurements were carried out during chosen growth stages of winter wheat as well as after harvest and cultivation. The profiles shown in Fig. 2.3.4 were collected during different hours of the day (0850-1630 UTC, see Table 2.2.1), but care was taken to have at least one pair of measurements under comparable weather conditions during the different growth stages and we generally avoided rainy and overcast conditions (maximal amount of cloud about 4 oktas), while covering a large range of wind-speed conditions (30-min averages between 0.3 - 5 m s^{-1}).

Figure 2.3.4 shows the mean profiles of χ_{CO_2} in µmol mol^{-1} and χ_{H_2O} in mmol mol^{-1} (amount of substance per mole of moist air) versus height (z) above ground level (a.g.l.) in the growing season of winter wheat 2015. In the middle of April (Fig. 2.3.4a), when the plants were in an early vegetative stage, there was only a small reduction in χ_{CO_2} in the plant stand with a low χ_{CO_2} accumulation near the soil surface. From the middle of May until end of June (Fig. 2.3.4b-e), the crops reached their highest growth rate and GAI, with high gradients of χ_{CO_2} between the soil surface (415 µmol mol^{-1}) and the mid canopy space (365 µmol mol^{-1}) on 07 June. At the same time, F_C reached its highest negative daily means, which underpins the CO_2 uptake by the plants.

χ_{H_2O} usually decreased with height in agreement with the fact that during the day there are only sources and no sinks, both at the ground surface (evaporation) and in the canopy (transpiration). However, on 1, 7 and 30 June a zone of stagnation can be seen between both sources. Later in summer (Fig. 2.3.4f), when grains were formed and leaves turned yellow, the GAI began to decline, until photosynthesis finally ceased. On 17 July, two weeks before harvest, the profiles of χ_{CO_2} and χ_{H_2O} showed only a source at the surface due to soil respiration and evaporation, indicating no significant transpiration and respiration in the plant canopy. After harvesting, both profiles measured over bare soil (Fig. 2.3.4g and h) depicted a similar logarithmic pattern, but differ in the absolute value. We suppose that the large differences in χ_{CO_2} and χ_{H_2O} covered by the profiles between these two dates are a product of different source strengths on the one hand and different turbulent exchange on the other. The measurement on 13 August took place between 1030 and 1100 UTC, thus earlier than most other measurements within the growing season of winter wheat. Remaining

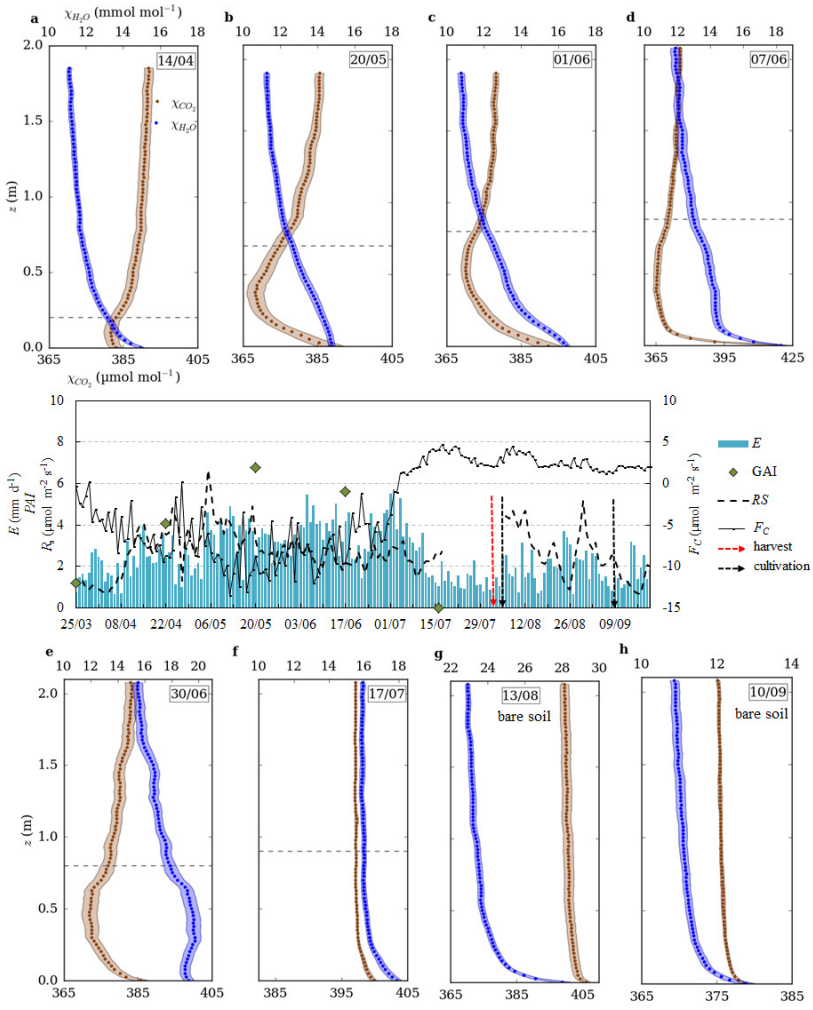

Figure 2.3.4: *30-min mean profiles of χ_{CO_2} and χ_{H_2O} vs. height z (m, a.g.l.) during selected periods of the growing season and after harvest (bare soil) of winter wheat. Dashed lines declare the plant height. Daily means and sums of CO_2 flux F_C and evapotranspiration E, the PAI and daily means of soil respiration R_s. No soil respiration data were available from 17 July until 6 August 2015 because of instrumental removal due to harvest and cultivation.*

CO_2 enrichment from the nocturnal boundary layer in the surrounding atmosphere may have led to a higher χ_{CO2} level. Furthermore, the different weather conditions might have had an influence. The measurement on 13 August was characterized by 10 °C higher air and soil temperature (thus enhancing respiration, as seen in the soil respiration and F_C measurements), and by a 1.5 m s^{-1} lower wind speed and at the particular time of day also a higher evapotranspiration (E) compared to the measurement on 10 September. In general, concentration gradients, including those in plant canopies, are determined by the interplay between source strength, mixing intensity and the background concentration in the surrounding boundary layer.

2.3.3 Diurnal cycle of profiles of CO_2, H_2O, temperature and wind speed over winter barley and bare soil

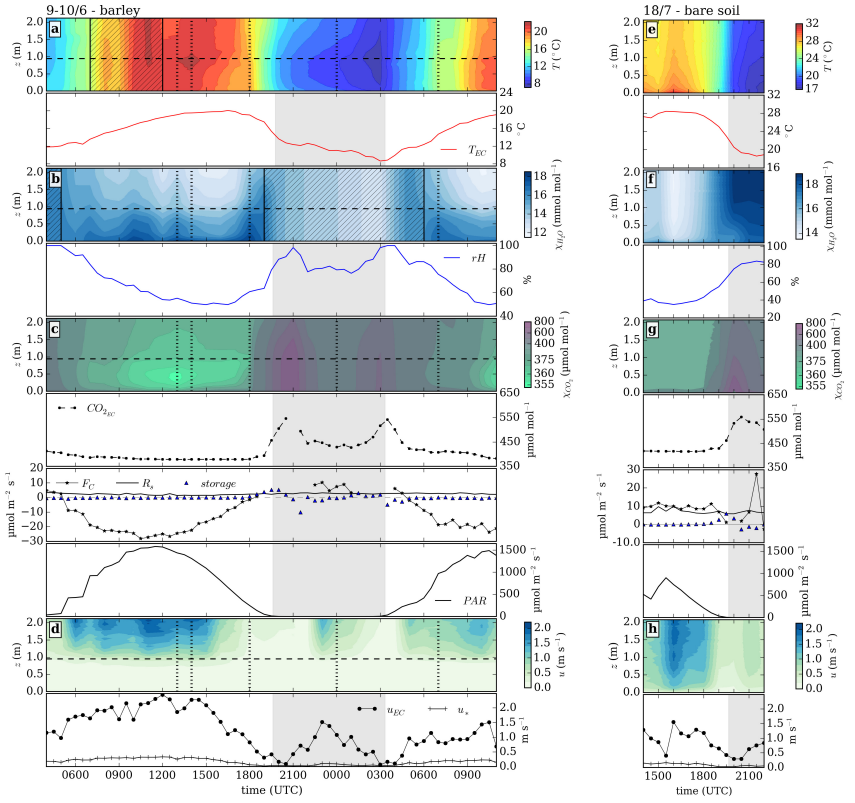

Figure 2.3.5: *Time height sections and time series measured in a barley field (left) and bare soil (right). a) temperature T and T_{EC}, b) χ_{H_2O} and relative humidity (RH), c) χ_{CO_2}, CO_2 flux F_C (not gap filled), $CO_{2\,EC}$ and the soil respiration R_s, the photosynthetically active radiation PAR and d) wind speed u_{EC} and friction velocity u_*. The ordinate is the height z (m, a.g.l.). Black dashed lines show the plant height (0.95 m). Time series of temperature T_{EC}, relative humidity RH, F_C, $CO_{2\,EC}$, u_{EC} and u_* are measured at 2.5 m above ground from the nearby eddy-covariance station. Solar noon corresponds to approximately 1130 UTC. Hatched areas refer to questionable data due to failure of thermocouple ventilation (T) and missing tube heating (χ_{H_2O}) and grey shaded areas mark the nighttime. Vertical dotted lines in the figure on the left side mark selected 30-min mean profiles showed in Fig. 2.3.6*

Longer measurements covering day and night conditions (cf. Tab. 2.2.1) were performed to find out how the profiles change over the day in different vegetation covers. As an example, we present here a 30-h measurement in winter barley on 9–10 June 2016 and an 8-h measurement after the harvesting of barley over cultivated bare soil (rough surface with soil aggregates and remaining stubble) on 18 July 2016 (Fig. 2.3.5). Measurements for one mean profile were performed during the first 30 min of every full hour. The mean height of barley was about 0.95-1.0 m and the entire height of the profile was 2.1 m. The cumulative PAI of the barley canopy was 6.3, of which 83 % were approximately homogeneously distributed between the canopy top and 0.3 m a.g.l., corresponding to 6.5 m^2 m^{-3}. In the lowermost

0.3 m, density was lower with 3.7 m^2 m^{-3}.

The measurement in barley was one of the first dates with a shielded, ventilated thermocouple (see Sect. 2.2.3), but from 0700 to 1200 UTC the ventilation was interrupted due to a power cable failure (hatched area in Fig. 2.3.5a). χ_{H_2O} profiles were not evaluable on 9–10 June from 0400 to 0500 UTC and between 1900 and 0600 UTC (marked by hatched areas in Fig. 2.3.5d) due to water condensation in the inner tube walls during situations with high air humidity and radiative cooling of the tubes (see Sect. 2.3.1). Before the bare soil measurement period, tube insulation and heating was installed (see Appendix A1).

The χ_{CO_2} measured in barley (Fig. 2.3.5c) decreased from 0400 UTC to 1200 UTC by more than 50 µmol mol^{-1} in the mid canopy. The lowest values were about 12 µmol mol^{-1} lower than those at 2.1 m a.g.l, occurring in the mid canopy during mid-day simultaneously to the highest PAR values. This drawdown due to plant uptake is connected with high transpiration. Consequently, χ_{H_2O} in the canopy space was higher than in the air above the canopy. The highest values were found directly above the soil surface, due to evaporation, and in the mid canopy in the midday hours. High χ_{H_2O} near the soil surface below the barley canopy during the day is due to soil respiration, lower light intensity caused by shadowing, a low quantity of photosynthetic organs of the stems and poor mixing (Al-Saidi et al., 2009). Mixing near the soil surface was impeded by a locally-stable temperature stratification, which prevailed during the day below the barley canopy (Fig. 2.3.6f, g, j). The highest temperatures appeared near the canopy top two hours after solar noon (Fig. 2.3.5a). An individual profile near this time (Fig. 2.3.6f) demonstrates that similarly high temperatures prevailed throughout most of the canopy. Between 1400 and 1630 UTC, however, the temperature reached a distinct maximum closely below the canopy top (Fig. 2.3.5a and Fig. 2.3.6g), a phenomenon that could also be observed after sunrise in the next morning. We hypothesize that the solar incident angle had an influence on the shape of the within-canopy temperature profile. Around noon, solar radiation penetrated deeper into the canopy. A decreasing angle of incidence in the afternoon limited the heating to an area just below the canopy surface. The presence or absence of such a distinct temperature maximum increases thermal stability, and thus impedes the turbulent vertical exchange of sensible heat, below it. Therefore, it may be self-reinforcing to some degree. We assume that in such a dense canopy the sensible heat flux was largely determined by the canopy. Similarly, the effect of low solar elevation angles was discussed by Gryning et al. (2001) for a coniferous high-latitude forest. This effect can also be found in the vertical χ_{CO_2} profiles: solar radiation at a low incident angle reached only the upper part of the plants, which is indicated in Fig. 2.3.5c and Fig. 2.3.6c at 1800 UTC by a χ_{CO_2} minimum just below the canopy surface, while the concentration in the deeper area already increased. The vertical wind profile showed consistently low wind speeds within the canopy (< 0.8 m s^{-1}) throughout the observation period. Above the canopy layer and bare soil, the wind speed increased in a log-like profile.

In the late afternoon, cooling expanded upwards from the soil surface and continued in the night with the cooling surface shifted from the soil surface towards the canopy top. At this time, the soil surface was the warmest location within the canopy (Fig. 2.3.6i). Consequently the sign of stability differed between the canopy and the air above, which confirms findings reported by Maitani and Seo (1986) and Jacobs et al. (1994). The lowest temperatures occurred in a wide region above and below the canopy top layer just before dawn at 0300 UTC. Over bare soil, the temperature profiles showed the expected logarithmic form with maximum values in the daytime, and minimum values in the nighttime near the soil

surface. Isothermal conditions were crossed around one hour before sunset, with the sign change of net radiation (not shown here).

During the night, in particular in cases of calm conditions and low turbulence (u_* near zero), a large amount of CO_2 (χ_{CO_2} up to 700 µmol mol^{-1}) accumulated over the whole profile height in barley (Fig. 2.3.5c) as well over bare soil (Fig. 2.3.5g). Matching high concentrations were also observed by the open-path sensor of the eddy-covariance station at 2.5 m above ground. We conclude that the high air humidity and the missing tube heating on 9–10 June did not affect the χ_{CO_2} profile measurements to such a large extent as the χ_{H_2O} profile measurements.

At night during calm conditions, the wind-speed gradient was small over the whole profile (Fig. 2.3.5d, 2000 UTC an Fig. 2.3.6h) and the shape of the wind profile was approximately linear. Increasing wind speed led to a decrease of χ_{CO_2} (Fig. 2.3.5c 2100 and 0300 UTC and Fig. 2.3.5g 2100 UTC). We found positive gradients of χ_{H_2O} above bare soil from 0.1 m upwards, possibly indicating dewfall. However, the gradients slightly increased towards the surface in the lowest 0.1 m. Due to the rough and heterogeneous surface of the field mentioned above, as well as its heterogeneous surrounding (green sugar beet fields and tree rows vs. mature and harvested cereal fields), the sign of the latent heat flux may have varied in space.

The magnitude of the storage term (below Fig. 2.3.5 c and g) was < 1 µmol m^{-2} s^{-1} and < 1 % of the eddy-covariance flux during daytime, but reached more than 10 % of it and occasionally the same order of magnitude during evening, morning and part of the night. The events of ephemeral χ_{CO_2} buildup during periods of low turbulence (two on 9–10 June and one on 18 July 2016) were each reflected by a large oscillation of consecutive positive and negative storage terms. For the largest storage terms, no reliable eddy-covariance fluxes are available for comparison, due to the effects of low friction velocities on quality control and of condensation on the open-path analyzer.

2.3.4 Comparison of profile-derived and eddy-covariance fluxes

Figure 2.3.7 shows an example of theoretical profiles fitted according to Sect. 2.2.5 to 30-min mean profiles of potential temperature, wind speed, χ_{CO_2} and χ_{H_2O}, measured over bare soil.

Lines show the modelled profiles after fitting u_*, z_0, scalar fluxes, scalar surface values at $z_{0\theta}$ (assuming $z_{0\theta} = 0.1\, z_0$) and the Obukhov length L, such that the root-mean-square difference between measured and modelled profile was minimal. The coefficient of determination for the profiles is higher than 0.94 for all four variables, which underlines that the measured profiles match well with MOST.

This was repeated for all measurements with a canopy height ≤ 0.22 m, where the surface layer could be expected to cover a sufficiently large portion of the profile. Situations with a higher canopy are excluded here since the flux-gradient approach is only valid as long the eddy size is lower than the transport scale, which is not always the case in real canopies (Denmead and Bradley, 1985). For each profile, z_0 and d were estimated as described in Sect. 2.2.4. The resulting roughness length z_0 values were 0.01 ± 0.004 m for bare soil and 0.06 ± 0.01 m over the 0.22 m height catch-crop canopy, where the calculated d was 0.15 ± 0.03 m. The empirical algorithm removing data points from the bottom of the profile (see Sect. 2.4) omitted between none and three (corresponding to the lowermost

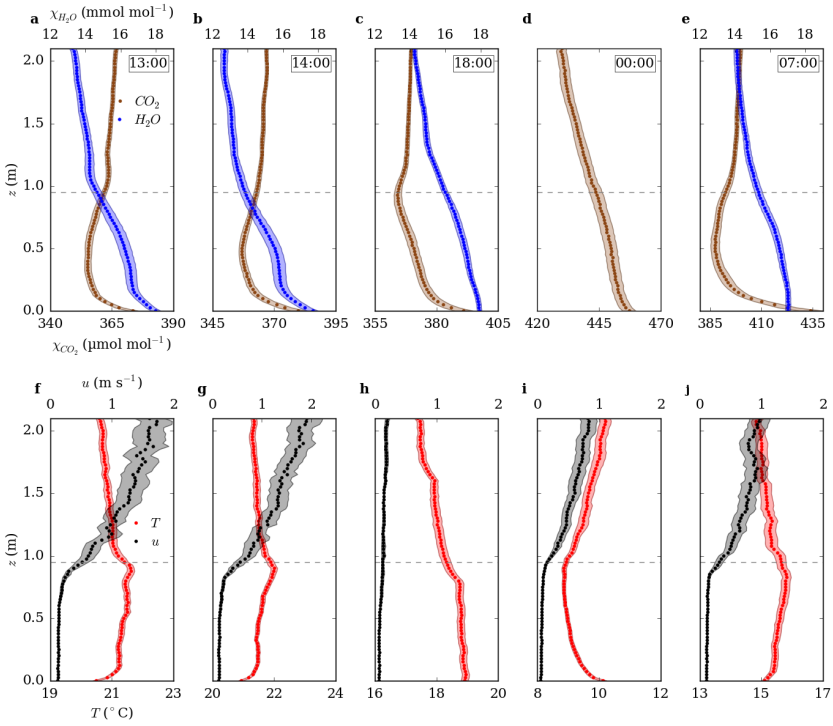

Figure 2.3.6: *Selected 30-min mean profiles of χ_{CO_2}, χ_{H_2O}, wind speed u and temperature T from Fig. 2.3.5*

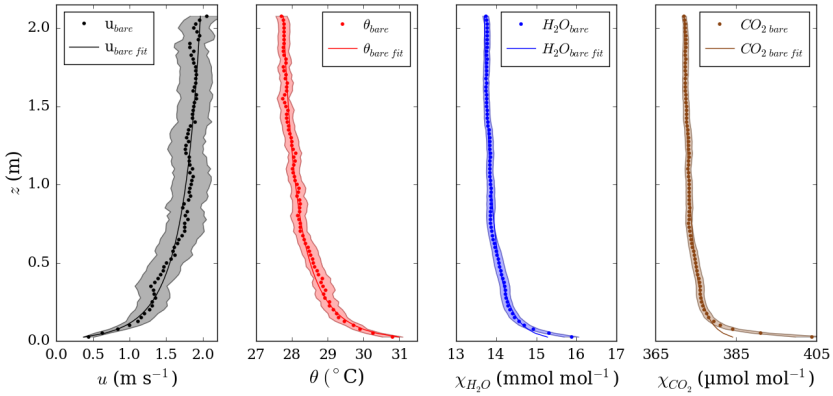

Figure 2.3.7: *Profiles on 18 July 2016 1600 UTC (bare) for wind speed u, potential temperature θ, χ_{CO_2} and χ_{H_2O} vs. height z (m, a.g.l.). Lines indicate model profiles after fitting u_*, z_0, scalar fluxes, scalar surface values at $z_{0\theta}$ (assuming $z_{0\theta} = 0.1\,z_0$) and the Obukhov length L, such that the root mean square difference between measured and modelled profile was minimal.*

0.08 m) data points over bare soil, but on average 0.4 ± 0.13 m on the day with the highest canopy (0.22 m). This automatic deletion is in fair agreement with common assumptions on the height at which surface-layer scaling is approximately valid. For example, the rule $z > d + 4(h_c - d)$ (Munger et al., 2012) yields 0.35 to 0.5 m with the above displacement heights and 0.44 with $d = 2/3h_c$, where h_c is the canopy height.
The resulting fluxes of sensible and latent heat, H_{PR} and λE_{PR} respectively, and u_{*PR} were compared with those determined from the eddy-covariance approach (Fig. 2.3.8). The sample size is 15 for the heat fluxes, 14 for F_C and 13 for u_*, depending on available reference data of the eddy-covariance station. The bi-variate statistic in Tab. 2.3.1 indicates a good overall agreement, particularly for the latent heat flux and F_C (both R^2 = 0.91). The bias was smallest, with less than 1 % for F_C, and largest for u_* (7.3 %, R^2 = 0.73). The coefficients of determination and bias indicate that the profile measurement and raw-data processing approach are suitable to determine vertical profiles, in particular for χ_{CO_2} and χ_{H_2O}. During the potential dew night of 18 July 2016 discussed at the end of Sect. 2.3.3, the profile method yielded slightly negative latent heat fluxes between zero and -0.2 W m^{-2}, while the eddy-covariance station yielded one positive and three negative 30-min fluxes between +9 W m^{-2} and -4 W m^{-2}. Such differences are well inside the uncertainty range of eddy-covariance measurements (Kessomkiat et al., 2013; Mauder et al., 2013).

Table 2.3.1: *Bi-variate statistics of the profile-derived vs. eddy-covariance dataset shown in Fig. 2.3.8, RMA = reduced major axis.*

Quantity	Latent heat flux	CO_2 flux	Sensible heat flux	u_*
Bias	7.9 W m^{-2} (6.9 %)	0.7 µmol m^{-2} s^{-1} (0.7 %)	7.8 W m^{-2} (6.8 %)	0.02 m s^{-1} (7.6 %)
RMSE	22.3 W m^{-2}	3.7 µmol m^{-2} s^{-1}	17.7 W m^{-2}	0.05 m s^{-1}
MAD	8.8 W m^{-2}	3.0 µmol m^{-2} s^{-1}	10.6 W m^{-2}	0.04 m s^{-1}
R^2	0.91	0.91	0.89	0.73
RMA slope	0.9	1.0	1.0	1.1
RMA offset	1.7 W m^{-2}	-0.7 µmol m^{-2} s^{-1}	-6.5 W m^{-2}	-0.01 m s^{-1}

Apart from evaluation against eddy-covariance measurements, fluxes from profiles can also be directly assessed in terms of energy balance closure. On a long-term basis, the eddy-covariance measurements at the site exhibited a closure of 0.85 (Eder et al., 2015). For the 30-min with profile-based estimates of both turbulent heat fluxes, however, the energy balance ratio (Wilson et al., 2002) was 1.07. This may in part be due to too high soil heat flux estimates obtained in unmanaged soil in July 2016 (see Sect. 2.2.2). Without this date, the ratio is 0.82. The respective energy balance ratios of the profile-derived fluxes were 0.97 and 0.80, respectively.

2.4 Conclusion and outlook

We described a high-resolution profile measurement technique based on an elevator system to obtain vertical profiles of CO_2 and H_2O mole fractions, temperature and wind speed. Compared to most other existing systems, the elevator moves continuously. The resulting high vertical resolution may provide a more detailed insight into sources, sinks and processes within a short plant canopy than systems with a finite number of measurement heights.
Measurements during two years within and above crop canopies were largely consistent with profiles found in textbooks based on earlier finite-level measurements and assumptions (Wa-

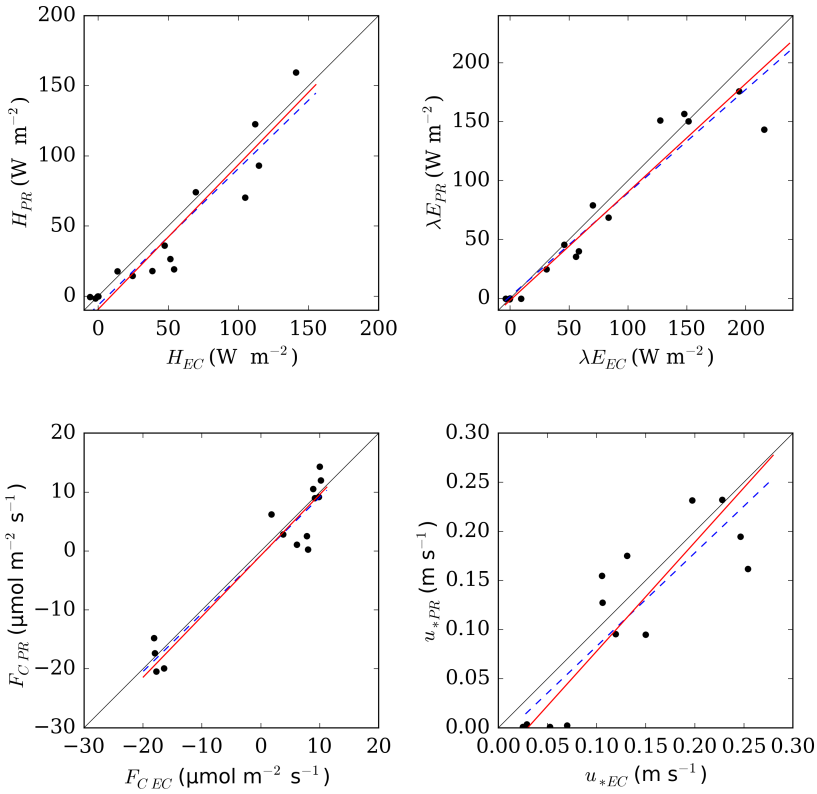

Figure 2.3.8: *Comparison of profile-derived measured profiles over bare soil (6 data points) and low canopy height (≤ 0.22 m) (9 data points) vs. observed sensible heat flux H and latent heat flux λE, F_C and u_* from the eddy-covariance station. The solid black line is the 1:1 line, the red line is the reduced major axis (Webster, 1997) and the blue dashed lines are the least square regression line.*

terhouse, 1955; Kaimal and Finnigan, 1994; Monteith and Unsworth, 2013), but revealed several interesting details concerning the location of scalar minima and maxima within the canopy and close to the surface, and their evolution during the day.

We tested the validity of the measurements by comparing fluxes derived during situations with a single sink or source at or near the soil surface to those determined with a nearby eddy-covariance station. Results were promising particularly for CO_2 and H_2O. This suggests that the profiles determined in canopies with vertically displaced sources can be used in future studies for other tasks, such as validating soil-vegetation-atmosphere models that depend on accurate estimates of CO_2 and H_2O concentrations near the stomata. Inverting concentration profiles within the canopy has been suggested as a way of inferring the vertical scalar source and sink processes. Previous attempts with Lagrangian dispersion analysis used a limited number of measurement heights and were mostly performed in high canopies such as maize and forest (Raupach, 1989b; Leuning, 2000; Santos et al., 2011). The use of concentrations with high vertical resolution may improve their applicability and robustness

especially in low, dense canopies.
Since source attribution is of interest in tall canopies like forests as well, and other motivations for profile measurements, such as computing storage terms, are of particular interest in such ecosystems, it is interesting to note the limitations of the current design when varying the profile height. Apart from required technical adaptations, the current elevator speed would result in a low number of repetitions per averaging time, with unwanted effects on the profile uncertainty. The discussion of the effects of a synthetically reduced raw data acquisition frequency in Sect. 2.3.1 indicated that a large number of repetitions is crucial, while consecutive repetitions during a single pass of a target height bin add little to uncertainty reduction. This means that the elevator speed can be increased, as long as it is matched by the physical response time of the sensors. For CO_2 and H_2O, this would require either a stronger pump or an open-path analyzer. It should be noted, however, that the same measures might be counterproductive for short, dense canopies, in which it is more important than in forests to keep the sensor size and sample air volume small. Also, in forests, a lower vertical resolution (larger height bin size) can be afforded, further increasing the possible elevator speed. In general a system of the type described here should strive to retain a high number of soundings M_1 by adjusting the parameters in $M_1 = tv/h$ while satisfying the condition $min(f_1, f_2) \geq v/\Delta h$, where t is the target averaging time block length, v is the elevator speed, h is the profile height, Δh is the height bin size, f_1 is the raw data acquisition frequency and f_2 is the response frequency of the sensors including effects such as tube damping. If the motivation of performing profile measurements is unavailability of eddy-covariance type fast response sensors for the variable of interest, these two frequencies can limit applicability of the system to tall profiles; otherwise more technical limitations to v such as security issues or avoiding additional turbulence creation will become determining. For a profile of 40 m height, 60-min averaging and 0.33 m vertical resolution, however, an elevator speed of 0.33 m s^{-1} and frequencies $\geq$1 s^{-1} would still be sufficient.

3 CO_2 fluxes before and after partial deforestation of a Central European spruce forest[‡]

3.1 Introduction

Forest ecosystems in the northern mid-latitudes typically act as a sink for atmospheric carbon dioxide (various authors after Lindauer et al., 2014) and hence play an important role in the global carbon cycle. Disturbances in such ecosystems lead to changes in their carbon balance. Carbon dioxide (CO_2) exchange of a forest ecosystem with the atmosphere is the result of photosynthesis (gross primary production, GPP) and ecosystem respiration (R_{eco}). After a disturbance has occurred, the duration of altered exchange rates depends on the type of disturbance, vegetation species, climate conditions and the post-disturbance land management (Luyssaert et al., 2008; Erb et al., 2018).

Many studies examined forest disturbances like clearcut and stand-replacement (Rannik et al., 2002; Kowalski et al., 2003, 2004; Humphreys et al., 2005; Takagi et al., 2009; Grant et al., 2010; Aguilos et al., 2014; Paul-Limoges et al., 2015) with different stand ages (chronosequence studies Kolari et al., 2004; Clark et al., 2004; Humphreys et al., 2006; Gough et al., 2007; Amiro et al., 2010; Grant et al., 2010; Paul-Limoges et al., 2015), fire (Dore et al., 2012; Amiro et al., 2006), insect outbreaks (Seidl et al., 2008) and wind-throws (Knohl et al., 2002; Yamanoi et al., 2015; Liu et al., 2016). Some studies focused on Central European forests; e. g., after wind-throw in a mountain forest in the Alps (Matthews et al., 2017), a mixed forest in Sweden (Lindroth et al., 2009) or an upland spruce forest in Germany (Lindauer et al., 2014). Kowalski et al. (2004) examined the effect of harvest on carbon exchange for four different European forest ecosystems by using eddy covariance (EC) measurements and empirical modeling. One main finding of these studies is that the above-mentioned interventions transformed forests from a carbon absorbing to a carbon emitting ecosystem.

The primary purpose of these studies was to determine to what extent an intervention in forest ecosystems changes their carbon balance and influences the global carbon cycle on the larger scale. Crucial questions, among others, are whether the disturbance turns a prior sink becomes a source and if so, when it becomes a sink again, i.e. when the ecosystem carbon compensation point is reached. As a second important, even later point, a payback period can be defined (Aguilos et al., 2014). To date, only few analyses provide an answer to the duration of forest regeneration up to the compensation point based on observation data

[‡]this chapter is based on the publication: Ney, P., Graf, A., Bogena, H., Diekkrüger, B., Drüe, C., Esser, O., Heinemann, G., Klosterhalfen, A., Pick, K., Pütz, T., Schmidt, M., Valler, V. and Vereecken, H. (2019): CO_2 fluxes before and after partial deforestation of a Central European spruce forest. Agricultural and Forest Meteorology 274, 61–74, https://doi.org/10.1016/j.agrformet.2019.04.009.

(Aguilos et al., 2014), because most observations stopped a few years after the intervention (Lindauer et al., 2014; Kowalski et al., 2003, 2004), or including non-continuous time series (Matthews et al., 2017). Information on the payback time could only be provided by studies that used modeled time series (Aguilos et al., 2014) or by assumptions based on chronosequence studies (Noormets et al., 2007; Wang et al., 2014). To our knowledge, there are no studies in which reference measurements in a remaining stand of the same forest ecosystem were collected and evaluated before and after the disturbance.
The study site investigated in this paper is part of the TERENO (Terrestrial Environmental Observatories) network in Germany. The study area consists of a spruce monoculture (originally intended for wood production), which was partially deforested within a re-naturalization project initiated by the management of the Eifel National Park. This opportunity allowed to examine changes in individual ecosystem components and to compare them with the data of a nearby reference area where the spruce forest remained. In recent years, the study area has been intensively examined, particularly with regard to its hydrological (Rosenbaum et al., 2012; Graf et al., 2014; Baatz et al., 2015; Wiekenkamp et al., 2016a,b) and biochemical (Gottselig et al., 2017; Wu et al., 2017) properties.
Here, we compare a seven year EC dataset of the forest, including three years before and four years after the deforestation, and a four year EC dataset from the deforested site (clearcut), to quantify the magnitude of the initial sink-source strength change and the pace of recovery during the first years. In addition to the net ecosystem exchange of CO_2 (NEE) and its data-driven partitioning into GPP and R_{eco}, we consider measured soil respiration (R_s), and compare the climate effect due to changing CO_2 sequestration to the biophysical one due to changed albedo.

3.2 Material and Methods

3.2.1 Test site and forest management

The Wüstebach research site, named after the Wüstebach stream and its catchment, is located in the Eifel National Park (50°30'N, 6°19'E) within the Eifel low mountain range in Western Germany and is part of the Lower Rhine Valley / Eifel Observatory in the TERENO network (Zacharias et al., 2011). The catchment covers an area of 38.5 ha (Fig. 3.2.1) with an elevation ranging from 595 to 630 m. The slope within the catchment area is 3.6 % on average. Its soils are dominated by Cambisols and Planosols on hill slopes and Gleysols and Histosols in the riparian zone. The main soil texture is silty clay loam with sandstone inclusions (Bogena et al., 2010).
Forestry has dominated the area since the 19th century. Due to a complete deforestation during world war II and reforestation directly thereafter, the predominant vegetation before the clearcut in 2013 was a 70-year-old spruce stock (Norway spruce, *Picea abies L.*) with an area coverage of 90 %. Tree density was 370 trees/ha and tree height 25 m on average (Etmann, 2009). Small parts in the northern part of the study area, particularly along the Wüstebach stream, were covered with meadow (6 %) and the central part of the catchment was covered by peat bog and half-bog with an alder stock near the stream (Lehmkuhl et al., 2010). By using allometric biomass functions, a dry biomass of about 310.5 t ha^{-1} was calculated for the forest area two years before CO_2 flux measurements started, including above and below ground living biomass and deadwood (8.1 t ha^{-1}, Etmann, 2009).

Information about the leaf area index was collected with a SunScan-System SS1 (Delta-T devices, Cambridge, UK) from April 2016 until July 2017 at least once per month in the clearcut and during five dates in the forest in a plot of 10 different locations for the clearcut and 60 for the forest. The mean LAI between the years 2016 and 2017 was 4.2 ($\pm$0.3) and 2.0 ($\pm$0.4) in the forested and deforested area, respectively.

Since 2007, the Wüstebach site has been instrumented with a large variety of measurement equipment to obtain information about hydrological, chemical and meteorological states and fluxes (Bogena et al., 2015). In 2010, a 37.8 m high tower was erected, which hosts an EC station and meteorological measurements.

In September 2013, 8.6 ha of the spruce monoculture forest was deforested. The clearcut area is located in the north-east part of the catchment and was allowed to regenerate naturally towards near natural mixed beech forest. A cut-to-length logging method was applied, where only 3 % of the original biomass was left on-site (Baatz et al., 2015). In the first year after deforestation, the area grew mainly with grasses (e.g.: *Deschampsia flexuosa (L.) Trin.*, *Luzula luzuloides (Lam) Dandy & Wilmott* , *Galium saxatile L.*), red foxglove (*Digitalis purpurea L.*) and fireweed (*Epilobium angustifolium (L.) Holub*). In the following years, new trees appeared, among them in large parts rowan (*Sorbus aucuparia L.*), but also spruce (*Picea abies L.*), birch (*Betula L.*), aspen (*Populus tremula L.*) and elder (*Sambucus L.*). Shrub vegetation spread extensively and comprised broom (*Cytisus scoparius (L.) Link*), heather *(Calluna vulgaris (L.) Hull)* and European blueberry *(Vaccinium myrtillus L.*). Bulrushes (*Juncus effusus L.*) grew in the wet areas mainly at the edge of the stream.

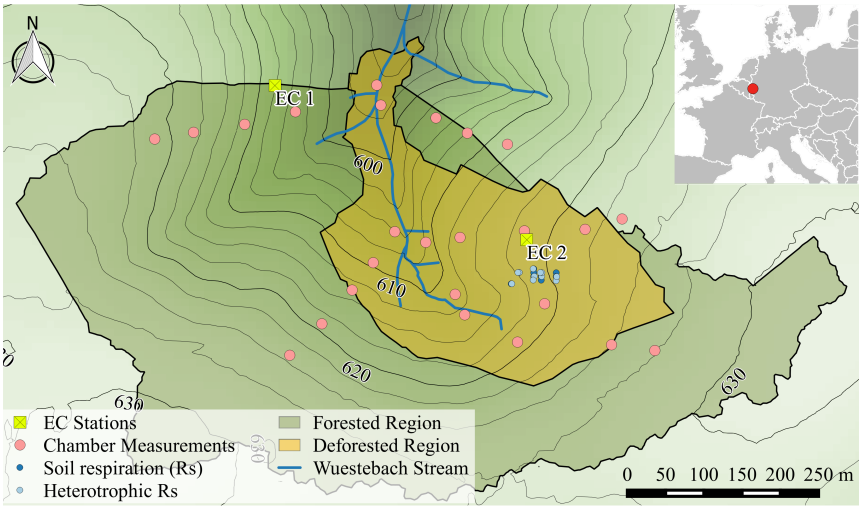

Figure 3.2.1: *Overview of the study area Wüstebach and locations of the measurements after partial deforestation in September 2013. Chamber measurements marked by blue colored dots were performed before deforestation in order to obtain information about the heterotrophic and autotrophic proportion of soil respiration (R_s).*

3.2.2 Eddy-covariance measurements and quality control

Turbulent fluxes of CO_2 (F_{CO_2}), water vapor (λE) and sensible heat (H) were measured by two continuously operating EC stations in the forested area since June 2010 and in the

deforested area since September 2013. Both stations comprised a three-dimensional sonic anemometer (CSAT-3, Campbell Scientific, Inc., Logan, Utah, USA) and an open-path infrared gas analyzer (IRGA, LI-7500, Li-Cor, Inc., Biosciences, Lincoln, Nebraska, USA), whereby the latter were installed with an inclination of 45°. The sensor separation between the sonic anemometer and the IRGA was 0.15 m for the forest EC station and 0.22 m for the clearcut EC station. Both analyzers were calibrated every three months. The forest EC system was mounted on top of a tower at 37.8 m a.g.l., located in the western part of the forested catchment. The second EC station was placed in the deforested area. Its measuring height of initially 2.5 m a.g.l. was changed in June 2017 to 3 m due to vegetation growth. The measurement frequency for both stations was 20 Hz. Turbulent fluxes were calculated as 30-min averages using the TK3.11 software package, which includes rigorous correction procedures and quality control (Mauder and Foken, 2011; Mauder et al., 2013). Additional to the WPL density-flux correction (Webb (1982), implemented in TK3.11) we also considered the correction for self-heating of open-path IRGA after Burba et al. (2008), using site-specific non-gap-filled meteorological data. Since correction terms in Burba et al. (2008) are generally performed for vertically adjusted sensors and our analyzers were mounted inclined to reduce the influence of self-induced heat fluxes, we used a modified form of the correction with a scaling parameter to account only a fraction of the additional heat flux (Järvi et al., 2009; Kittler et al., 2017). Since there is no general consensus on the application of the correction, we decide to show both variants of the resulting CO_2 fluxes, the uncorrected and the self-heating corrected. The corrected flux was calculated considering a scaling factor to reduce the fraction of the additional heat flux for sensors installed with inclination (as described above). The scaling factor used in the literature was determined for an inclination of 15°, much less than at our case. Consequently, we assume that the corrected data indicate the values for the most unfavorable case and that real CO_2 fluxes lie between these and the values without correction. For clarity, the following figures and calculations are based on the uncorrected fluxes, only for the cumulated fluxes both variants are given, whereby the corrected quantities are indicated with CB and values within the text are given in brackets. As a result of the TK3.11 processing, flux data were assigned to three quality classes (good, moderate, bad). For this study, data of good and moderate quality were used.

For measurements above tall canopies, NEE is composed of F_{CO_2} and the CO_2 storage flux (F_s) in the air column below the EC measurement height. However, CO_2 profile measurements were not existing at the study site and F_s was estimated from a single point CO_2 measurement as suggested by Hollinger et al. (2004).

In the first six months of the measuring period, no internal diagnostic flag of the IRGA was logged, which is essential for qualitiy checking prior to flux calculations. Therefore, a subsequent quality check was performed by comparing the absolute humidity measured with the IRGA against the absolute humidity calculated from on-site low frequency measurements. Measured IRGA values were excluded if the absolute humidity differed more than 2 g m^{-3}.

An additional method to check the plausibility of the EC measurements is the comparison between measured latent and sensible heat fluxes, measured net radiation and ground heat flux (e. g., Wilson et al., 2002) . The energy balance equation is:

$$Q - B = H + \lambda E + Res \tag{3.2.1}$$

where Q is net radiation, B is ground heat flux (the storage term of soil heat flux SHF was calculated according to Campbell Scientific (2003) and added to measured SHF), H and λE are eddy covariance fluxes for sensible and latent heat, respectively. Res includes all fluxes, which are not detected by the EC stations (i.e. advection terms, canopy heat storage and others). The energy balance closure (EBC) was calculated using a linear regression between the available energy ($Q-B$) and the energy fluxes ($H+\lambda E$). The residual term Res considered the heat storage of the vegetation and the heat storage caused by temperature and latent heat changes in the canopy air. The storage terms were calculated according the procedure and equations given in Moderow et al. (2009). The canopy heat storage between the ground and the measuring height was determined from the temperature profile (six levels) at the forest tower. The storage change of latent heat in the canopy air was calculated using the humidity measured from the gas analyzer. Biomass temperature was assumed to be equal to the mean surface temperature of the stems. Wet biomass was estimated as 37.7 kg m^{-2} (2009, Etmann, 2009). For canopy specific heat capacity a value of 2.958 J kg^{-1} K^{-1} was used (Moderow et al., 2009). Res was neglected for the clearcut EC station.

The footprint of the observed F_{CO_2} was determined using an analytical footprint model included in the software package TK.311, which was developed according to Kormann and Meixner (2001). We evaluated the cumulative footprint every 30 min for the forest and clearcut EC station up to a distance of 3 km and 1 km, respectively. Target areas were set to calculate the flux contribution originating from the area of interest. Subsequently, all 30-min NEE fluxes with less than 70 % contribution from the target area (i.e., spruce forest and deforested area, respectively) were rejected.

3.2.3 Measurements of meteorological parameters

The meteorological tower at the forest site is equipped with a net radiometer (NR01, Hukseflux Thermal Sensors, Delft, Netherlands) and a photosynthetically active radiation (PAR) quantum sensor (SKP 215, Skye Instruments Ltd, Llandrindod Wells, UK), which were installed on a 5 m long extension arm at 34 m a.g.l.. Air temperature was measured at levels of 38, 31, 27, 24, 16 and 8 m by ventilated and radiation shielded PT-1000 (CS240, Campbell Scientific, Inc., Logan, Utah, USA). Three infrared remote temperature sensors (IR120, Campbell Scientific, Inc., Logan, Utah, USA) were mounted 2 m a.g.l. and sampled surface temperatures of the soil surface, undergrowth and trunk space. In the immediate vicinity of the tower, the soil temperature T_s (thermistor type 107, Campbell Scientific, Inc., Logan, Utah, USA) and soil water content SWC (CS616, same manufacturer) were measured with three sensors each at 0.02, 0.05, 0.1, 0.2, 0.5 and 0.8 m depth. Three heat flux plates (HFP01, Hukseflux Thermal Sensors, Delft, Netherlands) measured the SHF at 0.05 m depth. All micrometeorological parameters were sampled continuously in 10-min intervals.

The EC station at the deforested area was additionally equipped with sensors for air temperature and relative humidity (HMP45C, Vaisala Inc., Helsinki, Finland), radiation quantities (NR01, Hukseflux Thermal Sensors, Delft, Netherlands) and PAR (Li190, LI-COR, Lincoln, Nebraska, USA). Precipitation P (pluviometer Pluvio^2, OTT Hydromet, Kempten, Germany) was sampled at a separate weather station close to the EC station. Furthermore, SHF was measured using three soil heat flux plates (HFP01, Hukseflux Thermal Sensors,

Delft, Netherlands), two deployed in a depth of 0.02 m and one in 0.08 m. T_s (0.01, 0.04 and 0.05 m) and SWC (0.025 m) were measured using thermocouple probes (TCAV, Campbell Scientific, Inc., Logan, Utah, USA) and two water reflectometers (CS616, same manufacturer).
Meteorological parameters which were not available at the Wüstebach site but used in this work for gap-filling came from the TERENO research site Schöneseiffen (50°30'N, 6°22'E, 610 m a.s.l., multi-sensor WXT510, Vaisala Inc, Helsinki, Finland). This station is located about 3 km northeast on an open meadow area.

3.2.4 Chamber measurements

Soil respiration (R_s) measurements with two portable chambers (survey system LI-8100, Li-Cor Inc., Lincoln, Nebraska, USA) started in October 2013, shortly after the clear-cutting. Three polyvinyl chloride (PVC) collars were installed at each of 25 measuring locations (75 measurements in total), which were arranged in transects through the forest (twelve locations) and clearcut (thirteen locations, Fig. 3.2.1). The collars had a diameter of 0.2 m and a height of 0.07 m and were installed such that they protruded 0.02 m above the soil surface. They were left in place during the entire measurement period with occasional re-fitting, if required. Vegetation inside the collars was not removed completely, as it would have affected the soil structure, but kept short by clipping preferably after measurements. On measurement days with a partial or complete snow cover (December 2014, January, March and November 2015, January and November 2016), the columns were carefully cleared from the snow prior to the measurement where necessary. The chamber was placed once on each collar and CO_2 as well as water vapor concentration and chamber headspace temperature were logged every second. The chamber was closed for 90 sec in total, while only the last 60 sec were used for flux calculation by fitting a linear regression to CO_2 concentrations. Fluxes were subsequently corrected for changes in air density and water vapor dilution. Chamber measurements were performed monthly at the same time of the day around noon. Between January and September 2016, measurements were taken every two months.
For calculating the R_s/R_{eco} fraction, a mean was computed for all measured transect R_s values (36 in the forest and 39 in the deforested area) for every measurement day. Half-hourly R_{eco}, calculated after Lasslop et al. (2010) (see Section 3.2.5), were paired with corresponding R_s measurements to calculate a ratio.
In order to obtain information regarding the proportion of heterotrophic and autotrophic respiration to R_s, an additional dataset (April 2011 to March 2014) was evaluated. The installation of the measurement grid is described in Dwersteg (2012) and comprised eleven measuring points with root exclusion, two of which were treated with the method of root elimination, and nine with the method of root trenching. Steel (for trenching) and plastic collars were used with the usual diameter of 0.2 m, but a a length of 0.4 m to avoid re-invasion by roots. The grid was located about 150 m south of the clearcut EC station inside the spruce forest before deforestation. Here, R_s was measured on a weekly basis with the same chamber system and procedure as described above. Autotrophic respiration was calculated by subtracting measured heterotrophic respiration (measurement points with root exclusion) from R_s measured at the corresponding control points.
In an effort to prepare future long-term measurements and to test the relevance of a possible confounding effect of manual measurements at a fixed daytime Keane and Ineson, 2017, for

more information see Appendix B) for our site, we installed one automated chamber near the forest and one near the clearcut EC station in May 2017. The system (Li-8100, Li-Cor Inc. Biosciences, Lincoln, Nebraska, USA), collar size, closure time and analysis strategy were the same as with the manual measurements, while the closure interval was 30 min. Results of these measurements are shown in Appendix B.
On the same day when the monthly R_s measurement were carried out, a transparent chamber was operated inside the cleacut area to sample daytime values of NEE and evapotranspiration. The minimum disturbance chamber has a rectangular tunnel shape with a surface area of 1.6 m^2 and is passively ventilated through the in- and outlet of the tunnel. Due to the passive ventilation principle of the system, measurements had to be excluded when the wind was weak or the wind direction changed within one measuring day. A detailed description of the system and the validation against EC measurements in homogeneous ecosystems is given in Graf et al. (2013). The location of the chamber was changed frequently within the clearcut area and included grass locations as well as bog vegetation. In the context of this study, we focus on these chamber measurements as an additional check on the magnitude of EC fluxes measured on the clearcut (Sect. 3.3.2).

3.2.5 Gap-filling and source-partitioning

Data gaps in meteorological variables of air temperature, humidity and global radiation ($S\downarrow$) were filled with a variant of the data interpolating empirical orthogonal functions (DINEOF) method (Beckers and Rixen, 2003; Graf, 2017), using linear relations to the same variables measured by up to 19 other TERENO stations in a radius of 50 km.
The R package REddyProc (REddyProc Team, 2014), which follows mostly the standardized FLUXNET gap-filling procedure, was used to fill gaps in half-hourly EC data. This method uses marginal distribution sampling or look-up table similar to Falge et al. (2001a) with additional consideration of co-variation of fluxes with meteorological variables and temporal auto-correlation of fluxes described in Reichstein et al. (2005).
Before gap-filling, friction velocity (u_*) filtering was applied to remove NEE data measured under conditions with insufficient turbulence. To identify the u_*-threshold we used a change point detection method described in Barr et al. (2013) (implemented in REddyProc) and was applied to annual subsets of the data. For the forest and clearcut EC stations, thresholds were estimated by 0.35±0.05 m s^{-1} and 0.13±0.01 m s^{-1}, respectively.
The most common method to disentangle GPP and R_{eco} from directly measured NEE is the nonlinear regression method (NLR) based on parameterized non-linear functions, which express semi-empirical relationships between net ecosystem flux and environmental variables, commonly temperature and $S\downarrow$. Many different versions have been implemented (Falge et al., 2001a; Hollinger et al., 2004; Barr et al., 2004; Desai et al., 2005; Richardson and Hollinger, 2007; Noormets et al., 2007). Here, we used a daytime data-based flux-partitioning algorithm after Lasslop et al. (2010), implemented in REddyProc. NEE was modeled using a rectangular hyperbolic light-response curve, taking into account the temperature dependency of respiration and vapor pressure deficit limitation of photosynthesis.
To avoid discontinuities and minimize extrapolation, the datasets were not generally split into e.g. annual subsets before gap-filling and source-partitioning. However, the forest dataset had to be split in the center of one particularly long data gap, which occurred from mid-December 2016 to early March 2017.

3.2.6 Assessment of albedo effect

Afforestation and deforestation affect local and global climate through a multitude of pathways. Beside the net CO_2 exchange, which typically dominates the biogeochemical feedback, changed albedo (α) is often considered an important factor. This biophysical effect can override biogeochemical ones (Betts, 2000), especially during the first years after a land use change, because its radiative fording is immediate as opposed to the slow, continuous accumulation of forcing by a CO_2 source or sink. If the effects of α and NEE are opposite and steady in time, these different temporal dynamics of both result in a compensation time after which the cumulating CO_2 forcing overrides the steady albedo forcing again. According to Rotenberg and Yakir (2010) the compensation time can be on the order of tens of years. On the temporal scale of our study, the short-term dynamics of both NEE and α on the clearcut cannot be ignored, and estimation of a compensation time from both changing quantities might be premature. We used the same basic equations as Rotenberg and Yakir (2010), but rather than solving for compensation time, we explicitly computed radiative forcing of both the (instantaneous) albedo effect and (cumulative) NEE effect for the end of each year after clear-cutting. The global increase in atmospheric CO_2 dry mole fraction due to a local sink or source is

$$\Delta\chi_{CO2} = \frac{\beta \cdot NEE \cdot t \cdot A_{site} \cdot M_a}{m_a \cdot M_c} \tag{3.2.2}$$

(compare Betts, 2000), where t is time, A_{site} is the surface area of the ecosystem, m_a is the mass of the atmosphere ($5.15{\cdot}10^{21}$ g), M_a and M_c are the molar masses of air and carbon required if NEE is given in g C per area and time ($M_a/M_c = 2.414$), and β is an estimate of the airborne fraction (0.5). The resulting radiative forcing

$$RF_{NEE} = 5.35 \cdot \ln(1 + \frac{\Delta\chi_{CO2}}{\chi_{0,CO2}}) \tag{3.2.3}$$

(Myhre et al., 1998), where 5.35 is an empirical value in W m^{-2} and $\chi_{0,CO2}$ is the base concentration to which the change is applied (~ 400 ppm in our case), can be linearized for $\Delta\chi_{CO2} \ll \chi_{0,CO2}$ to yield $RF_{NEE} \approx 5.35 \cdot \Delta\chi_{CO2}\,\chi_{0,CO2}^{-1}$. The global radiative forcing of a local surface albedo change, neglecting any net side effect on the long-wave radiation budget, is

$$\Delta RF_\alpha = \overline{S\downarrow} \cdot \Delta\alpha \, \frac{A_{site}}{A_E}, \tag{3.2.4}$$

where $\overline{S\downarrow}$ is the mean incoming short-wave radiation, $\Delta\alpha$ is the difference in albedo between two land surfaces or between before and after change, and A_E is the surface area of the earth ($5.1{\cdot}10^{14}$ m^2). Here, we used only high-quality local measurements of radiation at each of both sites (Sect. 3.2.3) to determine its α as the ratio between the annual sums of jointly available outgoing and incoming shortwave radiation values. To remove any effect of small interannual fluctuations of annual $S\downarrow$ on the analysis, and accommodate longer data gaps in forest tower radiation, we used for all four years after the deforestation a constant $S\downarrow$ computed as the average of the gap-filled (Sect. 3.2.5) $S\downarrow$ at the clearcut site over the whole period, and a constant forest α based on the study year 2013-2014. The clearcut α, in contrast, was updated for each study year to accommodate for changes resulting from vegetation regrowth. Due to the linearization of RF_{NEE} we can drop A_{site} from both

equations 3.2.2 and 3.2.4 (thus reporting the global effect of each square meter of treated land surface), compute ΔRF_{NEE} between both surfaces directly as a function of their NEE difference ΔNEE, and cumulate it over years. Hence, the combined radiative forcing from both NEE and α is

$$\frac{RF_y}{A_{site}} = \frac{\overline{S\downarrow} \cdot \Delta\alpha_y}{A_E} + \sum_{i=1}^{y} \frac{5.35 \cdot \beta \cdot \Delta NEE_i \cdot M_a}{\chi_{0,CO2} \cdot m_a \cdot M_c}, \tag{3.2.5}$$

where the indices y and i indicate the study year (year after deforestation) under consideration. It has already been clarified by Rotenberg and Yakir (2010) that such a radiative forcing-based comparison is only a rough, convenient way to compare the magnitude of the two presumably most important, often opposite warming and cooling effects of land use change. In the context of our study it is used to demonstrate how CO_2 budget changes, which remain the focus of this paper, can be offset by biogeophysical effects.

3.3 Results and Discussion

3.3.1 Meteorological conditions during the observation period

The climate at the study site is influenced by the Atlantic Ocean with relatively high rainfall. The long-term mean annual temperature is 7 °C and the mean annual precipitation is 1332 mm (reference period 1981-2010, temperature data are taken from the DWD station Schneifelforsthaus and precipitation from Kalterherberg). Winters are moderately cold with periods of snow. Annual average snow duration (snow coverage $\geq$ 50 %) was 50 days with a mean snow depth of 13 cm (1981-2010). Summers are often characterized by relatively humid and cool conditions. The prevailing wind direction is south-west. Figure 3.3.1 shows the meteorological conditions from 1 January 2011 until 30 September 2017. Within the considered time-frame, annual mean air temperature (T) at the research site ranged between 7.1 °C (year 2013) and 8.9 °C (year 2014) with an annual average of 8.2 °C for the entire measurement period (Tab. 3.3.1). Annual sums of P ranged between 990 mm (year 2013) and 1373 mm (year 2012). The observed mean annual precipitation sum was 1160 mm during the observation. The monthly mean T were mostly positive and slightly negative in winter months, except in 2014 and 2016. The coldest winter period was from January until March 2013, the warmest from December 2013 until March 2014, while the summer months of 2015 and 2016 were warmer than average. P is distributed evenly over the whole year, partly with very high P sums in the winter and summer months, due to fronts and convective weather phenomena. Heavy precipitation events took place in January 2012, late summer 2014 and in the summer months 2016. During the observation period (2010-2017), snow duration was in average 44 days with a mean snow depth of 13 cm.

Table 3.3.1: *Annual means of air temperature (T), photosynthetically active radiation (PAR) and annual sums of precipitation (P) for the years 2011-2016 for the Wüstebach catchment.*

year	2011	2012	2013	2014	2015	2016
T (°C)	8.7	7.7	7.1	8.9	8.0	8.5
PAR (µmol m^{-2} s^{-1})	242	224	227	250	269	253
P (mm)	1109	1358	990	1183	1175	1159

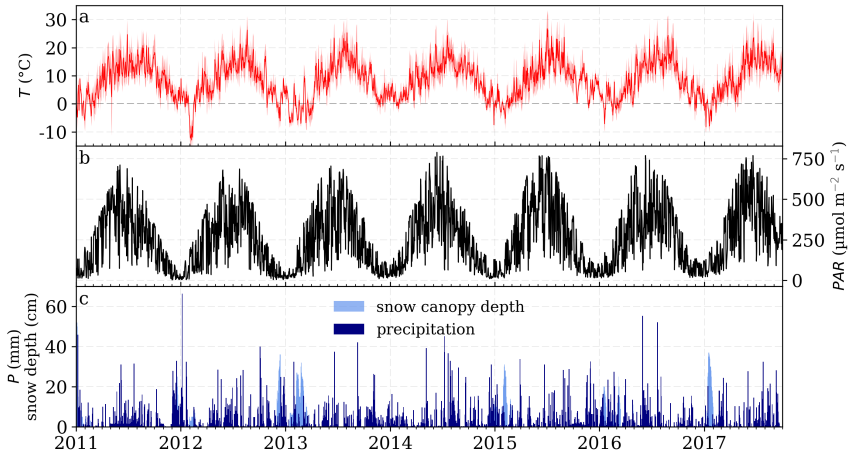

Figure 3.3.1: *Meteorological overview from 1 January 2011 until 30 September 2017 for the Wüstebach catchment. a) Daily mean air temperature (T). Shaded line marks the daily minimum and maximum values. b) daily means of photosynthetically active radiation (PAR) and c) daily sums of precipitation (P) and daily snow depth. Information about the snow depth were taken from the DWD (German Weather Service) station Kalterherberg (535 m a.s.l.), at a distance of 8.4 km to the study area.*

3.3.2 Analyses of flux quality and flux dynamics

After applying quality control in the post processing and u* filtering analysis to all records of measured NEE, only a total data coverage of 52 % and 60 % remained for the EC station in the forest and deforested area, respectively.

The test for energy balance closure on the forest site shows a coefficient of determination (R^2) of 0.85 and a closure of 85 % (year 2013). The deforested EC-station reached a closure of 83 % with a R^2 of 0.87 (year 2014 to 2016). An imbalance around 20 % is well known even under otherwise ideal conditions for using the EC method (Wilson et al., 2002).

The footprint analysis in Figure 3.3.2 shows that 50 % of the cumulative footprint of the forest EC station originated inside the forested region regardless of the wind direction. The 90 % footprint isoline covered most of the catchment as well as surrounding areas, which consisted mainly of spruce monocultures of the same age and height. With easterly and south-easterly winds, the station was influenced by the deforested area. Therefore, fluxes measured from a wind-direction sector between 63°to 135°were removed in addition to the 70 % criterion described in Section 3.2.2. This reduced the evaluable EC data for the forest station to 43 %. The extension of the 90 % footprint isoline was approximate 1000 m, which was primarily caused by the height of the measuring tower and measurements during stable stratification (mostly during the night). The footprint of the EC station in the deforested area was much smaller and its shape reflected a channeling effect of the clearcut on the wind direction at this measurement height (2.5 to 3 m a.g.l.). The 90 %-isoline had a maximum extension of 200 m, which is located almost completely within the limits of the deforested area.

As many studies have shown, clearcuts within ecosystems with tall canopies have an im-

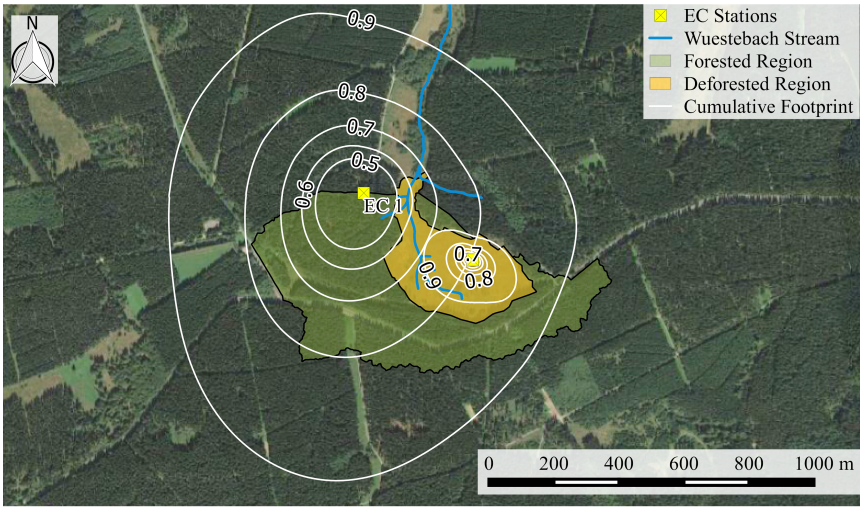

Figure 3.3.2: *Cumulative footprint analysis for the forest EC station (EC 1) and the EC station at the deforested area for the year 2016.*

pact on wind and turbulence regimes within the atmospheric surface layer (Sogachev et al., 2005; Wang and Davis, 2008; Zhang et al., 2007), as for instance recirculation could lead to downwind of the forest edge, which probably bias EC flux measurements. The size of the recirculation area is dependent on the opening size within the canopy and its height (h_c), and can be expressed as a factor of the same (Aubinet et al., 2012). A recirculation area distance of 2 to 5 h_c as formulated in Detto et al. (2008) implies that recirculation may occur within a distance of 50 to 12 m (with h_c = 25 m) between the forest edge and clearcut at our site. This estimated distance did not affect 80 % of the cumulative flux footprint and we assume that the influence of the forest edge on the flux measurements of the clearcut is rather small.

NEE estimated from roving, manual measurements with a transparent minimum disturbance chamber (end of Sect. 3.2.4) was compared with those measured by the clearcut EC station (Fig. 3.3.3). NEE values sampled during the growing season from April to October 2016 and 2017 were excluded from the analysis in order to preclude an influence of regrowing trees, which were not included in the chamber measurement. According to this criterion and wind speed and direction (Sect. 3.2.4), 21 out of a total of 34 measurement days remained evaluable. Given the small (1.7 m^2) and changing footprint of the chamber measurements, the regression in Figure 3.3.3 shows a fairly good agreement between the chamber and EC measurements with a R^2 of 0.75. This result supports our assumption that recirculation did not largely or systematically affect clearcut EC measurements.

During stable conditions, storage fluxes and advection become important, especially for flux measurements over tall canopies and complex terrains. This subject is often discussed as night flux error and is mostly related to an underestimation of CO_2 fluxes during low turbulent conditions which could lead to an overestimation of NEE at annual scales (Aubinet et al., 2000; Goulden et al., 2006; Aubinet et al., 2012). The two processes mentioned above must be considered separately, as they have different effects on the measured fluxes. Storage

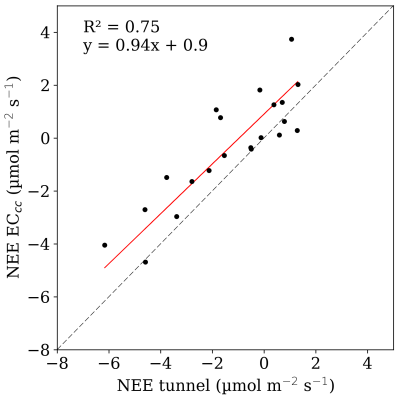

Figure 3.3.3: *NEE measured with a minimum-disturbance chamber (tunnel) vs. observed NEE from the clearcut EC station. Points represent daily averaged NEE. The red line is the reduced major axis (Webster, 1997). The scattered black line is the 1:1 line.*

fluxes have a minor influence on long-term carbon balances, since the stored CO_2 is detected at the measurement sensor with a time delay when the turbulence reappears. However, this is not the case for advection processes, in which accumulated CO_2 are removed beneath the measurement system and not recorded at all. While the first mentioned problem can be solved by including a storage flux correction, the second case requires a selection of the affected nighttime data, which is mostly done with an u_* filtering procedure (Aubinet et al., 2012). Since the tower at the forest site is situated on a gentle slope, it is possible that along the topographic gradient cold air drainage flows may occur under stable stratification. Although u* filtering has been applied and resulting gaps were filled, it is possible that annual sums of carbon fluxes might be slightly biased.

3.3.3 Diurnal, seasonal and interannual changes in carbon fluxes of forest and clearcut before and after deforestation

The open-path self-heating correction (Sect. 3.2.2) has a negligible small effect on single half-hourly NEE fluxes but gains importance when considering long-term budgets. For this reason and for the sake of clarity, we also show annual totals with this correction in brackets. Figure 3.3.4 shows gap-filled half-hourly values of NEE for the forest (top panel) and deforested area (lower panel). Positive values indicate a release from the ecosystem to the atmosphere and negative values the reverse. At the forest site, the maximum amplitude between CO_2 uptake (blue color in the daytime) and release (red color during the night) was higher (40.5 µmol m^{-2} s^{-1}) than in the deforested area (21 µmol m^{-2} s^{-1}). The deforested area was a clear carbon source with positive NEE fluxes in the first year after deforestation. In the following growing seasons, fluxes during the day became increasingly negative caused by regrowth of vegetation.

7-day running means for forest NEE fluxes in Figure 3.3.5 were mostly negative, even during most of the winter periods, indicating a strong sink for CO_2. Clearcut NEE was mostly positive (0 to 5 µmol m^{-2} s^{-1}) during the first year after the deforestation. In the fol-

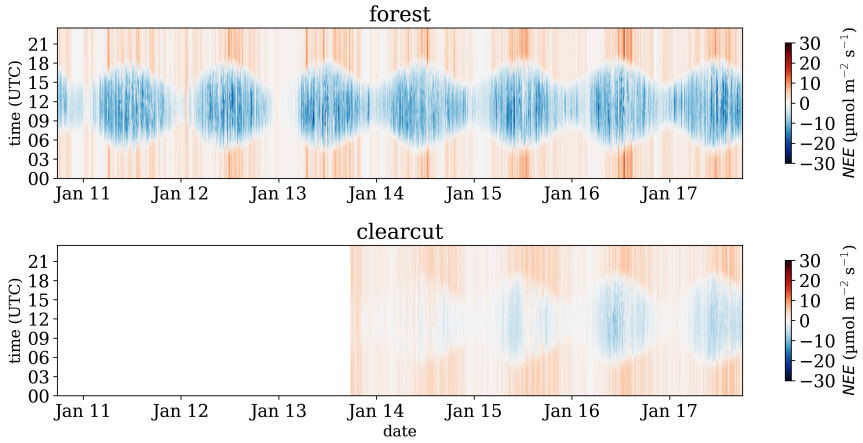

Figure 3.3.4: *Net ecosystem exchange (NEE) (30-min values, with gap-filling after Lasslop et al., 2010). Top panel shows the values of the forest EC station from 1 October 2010 until 30 September 2017 and the lower panel shows the clearcut from 1 October 2013 until 30 September 2017.*

lowing years, negative values were reached for short periods during each growing season (-1.0 µmol m^{-2} s^{-1} in 2015 and -2.5 µmol m^{-2} s^{-1} in 2016). Comparing the intra-annual trends of both areas, the period of CO_2 uptake in the forest began earlier and persisted longer than on the clearcut area.

During the first year after clear-cutting, strongly reduced photosynthetic uptake is indicated by low fluxes of inferred GPP (2.5 µmol m^{-2} s^{-1}), which approximately tripled in the third year (7.5 µmol m^{-2} $^{-1}$) and remained at this level during the fourth. The level of GPP in the clearcut never exceeded the one in the forest, which ranged in all observed years between 0.5 and 11.0 µmol m^{-2} s^{-1} in winter and summer, respectively. Under sufficient radiation conditions, spruce is still able to assimilate CO_2 even during frost down to -7 °C (Schmidt-Vogt, 1989).

7-day averaged fluxes of R_{eco} in the clearcut area were small in the first year (0.5 to 5.0 µmol m^{-2} s^{-1}) and increased slightly until the last year (0.8 to 7.0 µmol m^{-2} s^{-1}). In the first two years after clear-cutting, R_{eco} remained on the same maximum level throughout the seasons and peaked more distinctly in midsummer thereafter, due to proceeding seasonal grass and tree development. The interannual course and amplitude of R_{eco} at the forest site remained relatively stable.

3.3.4 Annual carbon fluxes of forest and clearcut before and after deforestation

A small interannual variability was observed in the annual sums of NEE, GPP and R_{eco} in the forest (Tab. 3.3.2). Throughout the seven-year observation period, the mean annual carbon flux of the forested area was -663±78 (-535±72) g C m^{-2} for NEE, 1680±103 (1755±249) g C m^{-2} for GPP and 1020±106 (1219±232) g C m^{-2} for R_{eco}. These values correspond to the order of magnitude reported for a spruce forest in Eastern Germany (Grünwald and Bernhofer, 2007), whereby uncorrected NEE was higher at our study site. Four years after

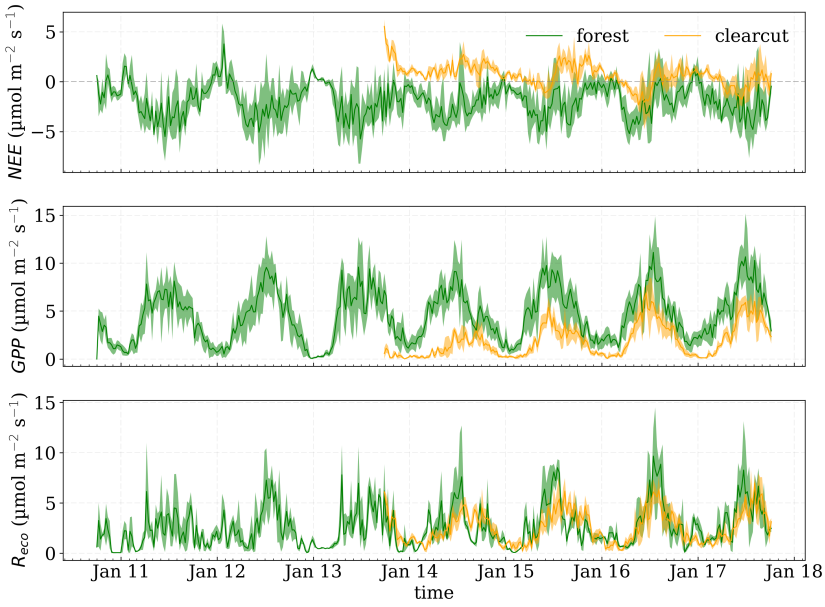

Figure 3.3.5: *Carbon fluxes of net ecosystem exchange (NEE), gross primary production (GPP) and ecosystem respiration (R_{eco}) as 7-day averages for the forested (green) and deforested (yellow) area. Shaded areas mark the minima and maxima during the respective 7 days.*

clear-cutting, the deforested area remained a source for CO_2 with a NEE of 83 (236) g C m^{-2}. NEE and GPP changed dynamically in the first three years, followed by a stagnation in the fourth year. While NEE decreased between year 1 and year 2, and GPP increased over the same period, NEE decreased only negligible from the third to the fourth year. At the beginning of the growing period (May and June) 2017, a decline in GPP (Fig. 3.3.6) could be observed in analogy to decreased air temperature (Fig. 3.3.1), 42 % less P and lower mean PAR (spring 2016: 361 µmol m^{-2} s^{-1} compared to spring 2017: 322 µmol m^{-2} s^{-1}), which probably have reduced the growth rate of vegetation on the clearcut area. On the contrary, the annual total GPP in the forest, showed an increased sum in 2017 despite the unfavorable weather conditions in spring and early summer. This indicates, that the evergreen spruce forest had a higher resilience towards shifting weather conditions within the vegetation phase than the grass dominated clearcut.

However, stagnation induced by natural fluctuations of the recovery phase of disturbed forest ecosystem is also conceivable. In studies with different types of post-disturbance land management, the shift of NEE from a carbon source to a sink was not linear and showed interannual fluctuations (Humphreys et al., 2005; Lindauer et al., 2014; Aguilos et al., 2014).

In the clearcut, R_{eco} increased slightly from 906 (995) g C m^{-2} in the first year to 1018 (1303) g C m^{-2} in the third year, which is contrary to observations made in a clearcut with new plantation (Takagi et al., 2009; Paul-Limoges et al., 2015) and a wind-throw disturbed spruce forest (Lindauer et al., 2014), where R_{eco} gained higher values rapidly within the first

Table 3.3.2: *Net ecosystem exchange (NEE), gross primary production (GPP) and ecosystem respiration (R_{eco}) from October 2010 for the forested region and from October 2013 for the clearcut until September 2017. Each observation year (y) starts at 1st October. Fluxes determined after correction for self-heating of open-path IRGA (Burba et al., 2008) are declared with CB.*

Annual total carbon flux forested area							
(g C m^{-2})	y1	y2	y3	y4	y5	y6	y7
NEE	-587	-664	-680	-761	-759	-658	-530
NEE_{CB}	*-481*	*-490*	*-592*	*-594*	*-425*	*-518*	*-648*
GPP	1515	1622	1569	1738	1816	1738	1760
GPP_{CB}	*1496*	*1288*	*1732*	*1980*	*1959*	*1862*	*1966*
R_{eco}	928	958	889	997	1057	1080	1230
$R_{eco,CB}$	*1015*	*798*	*1139*	*1386*	*1533*	*1343*	*1317*
Annual total carbon flux deforested area							
NEE	-	-	-	521	283	95	83
NEE_{CB}	-	-	-	*548*	*374*	*242*	*236*
GPP	-	-	-	385	670	923	892
GPP_{CB}	-	-	-	*447*	*763*	*1062*	*1036*
R_{eco}	-	-	-	906	953	1018	975
$R_{eco,CB}$	-	-	-	*995*	*1137*	*1303*	*1272*

year of forest succession. In the first years after harvesting, R_{eco} mainly results from wood debris decomposition (Noormets et al., 2012). At our study site, only 3 % of the previous aboveground biomass remained in the field (cf. Section 3.2.1), which could have suppressed carbon release from decomposition processes. Along with the recovery of the vegetation in the following years, R_{eco} increased simultaneously with increasing GPP. We assume, that above- and below-ground autotrophic respiration act as main contributors to the increase of R_{eco} and decomposition remained comparatively stable. Compared to the forest, the annual total of R_{eco} in the deforested area was lower and always exceeded clearcut GPP.

Compared to changes in evapotranspiration, which was initially reduced by approximately 50 % on the clearcut and returned rapidly towards forest-level values within the first years (Wiekenkamp et al., 2016a), changes in CO_2 fluxes were more profound and long-lasting. After four years, the deforested area still acted as a source for CO_2 on an annual basis, although growing biomass led to a fast increasing uptake through the years.

The ecosystem carbon compensation point, where a regenerating ecosystem changes from source to sink, varies between studies from 3 to 20 years covering a variety of climate conditions, forest ecosystems, stand age and post-disturbance land management (Takagi et al., 2009). Estimations including different chronosequence studies (mainly boreal forests) indicated a compensation point within 20 years after the clear-cutting, with a maximum at 10 years (Aguilos et al., 2014). In a next step, Aguilos et al. (2014) calculated the duration until a forest ecosystem completely recovers all the carbon emitted into the atmosphere after a disturbance. This duration, named payback period, was estimated by dividing the total amount of NEE during the period when the forest was a net source by the annual sum of NEE before disturbances. They concluded that most of the studied sites need at least the same time as they needed to become carbon neutral, and in general more than 20 years to recover all emitted CO_2 (Aguilos et al., 2014).

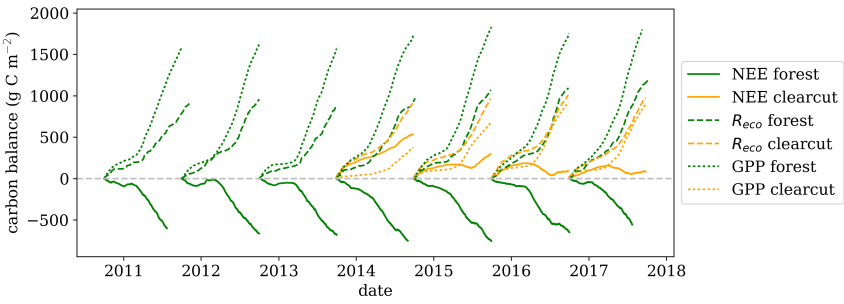

Figure 3.3.6: *Comparison of the cumulative net ecosystem exchange (NEE), gross primary productivity (GPP) and ecosystem respiration (R_{eco}) in g C m^{-2} (without correction for self-heating of open-path IRGA) from October 2010 for the forested region and October 2013 for the clearcut until September 2017. Each observation year starts at 1st October.*

3.3.5 Albedo effect

Table 3.3.3: *Annual mean values of albedo (α) for the forest and clearcut site, the difference of the cumulative net ecosystem exchange for forest and clearcut ($\Delta NEE_{f,cc}$ in g C m^{-2}, without correction for self-heating of open-path IRGA), the global radiative forcing of albedo (ΔRF_{α}) and the radiative forcing of CO_2 (ΔRF_{NEE}) in 10^{14} W m^{-2} (global) m^{-2} (treated surface) and the sum $\sum_{Forcing}$ of the former for the years after clear-cutting.*

	y4	y5	y6	y7
α_{forest}	0.07	0.07	0.07	0.07
$\alpha_{clearcut}$	0.16	0.22	0.25	0.21
$\Delta NEE_{f,cc}$	1282	1042	753	613
ΔRF_{α}	-2.10	-3.56	-4.19	-3.23
ΔRF_{NEE}	0.40	0.73	0.96	1.16
$\sum_{Forcing}$	-1.70	-2.83	-3.23	-2.08

Whereas the spruce forest showed a mean α of 7 %, α of the deforested area was clearly higher in all study years (Tab. 3.3.3). During the first three years after deforestation, α increased from 16 to 25 % presumably due to coverage of initially bare soil surface by grasses and shrubby vegetation. Likewise, the reduction in year 7 could be due to increasing abundance of darker-leaved rowan and broom vegetation (Sect. 3.2.1). The cooling effect ΔRF_{α} of this higher albedo outweighed the warming effect ΔRF_{NEE} throughout the study period, but due to cumulation of the latter over time, it becomes increasingly important (Rotenberg and Yakir, 2010). As a possible future scenario for the net effect of the study site on global warming, continuing failure to match the high net CO_2 uptake of the adjacent spruce forest throughout the next years, accompanied by a decreasing α as woody vegetation grows on, could turn the present net cooling effect of the deforestation into a warming effect in the medium term. However, α of the eventually expected deciduous natural forest will remain higher than that of spruce forest (various authors after Matthies and Valsta, 2016). Therefore, if ever the cumulative CO_2 sink strength of the new forest compared to spruce reaches a payback point (Aguilos et al., 2014), the point where the net effect of the land cover change is cooling will be reached even earlier due to the albedo effect.

As can be seen from Tab. 3.3.2, the application of self-heating correction adjusted the

annual totals towards a larger carbon loss. Reverter et al. (2011) studied the magnitude of this correction using EC data from different ecosystems spanning climate zones from Mediterranean temperate to cool alpine and found that annual corrections of NEE varied between 129 and 190 g C m^{-2} y^{-1}. Thus, they hypothesized that annual carbon balances obtained from measurements using the LI-7500 open-path systems may be biased without applying self-heating correction.

3.3.6 Comparison of soil respiration and its contribution to ecosystem respiration

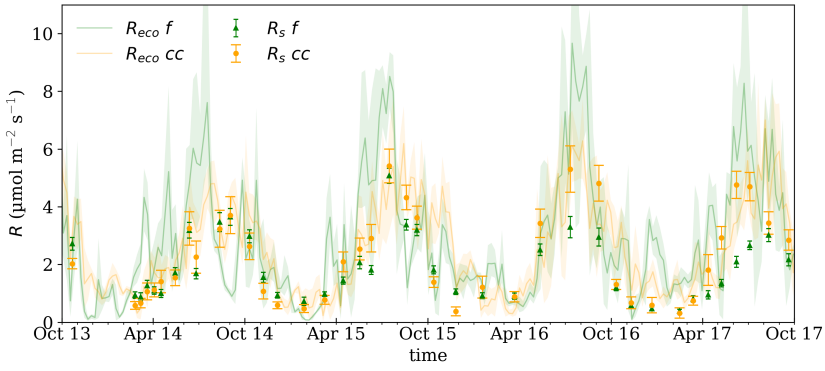

Figure 3.3.7: *Soil respiration (R_s) averaged over all measurement points for the forest (f) and the clearcut (cc) site. For comparison, total ecosystem respiration (R_{eco}) as also shown in Figure 3.3.5. Error bars indicate the 95 % confidence intervals of the mean values of R_s.*

R_s of forests accounts for about 30 to 80 % of R_{eco} (Davidson et al., 2006; Acosta et al., 2013) and should therefore be taken into account when studying ecosystem carbon balances. R_s varied in space and time in the forest and deforested area. The area-averaged R_s in forest and clearcut varied monthly and followed a typical seasonal pattern (Fig. 3.3.7). In the first year after cutting, maximum respiration rate was reached from late summer to early autumn (forest: 3.6 µmol m^{-2} s^{-1} and clearcut: 3.7 µmol m^{-2} s^{-1}) and the minimum during winter (forest: 0.9 µmol m^{-2} s^{-1}, clearcut: 0.6 µmol m^{-2} s^{-1}). In the following years, R_s peaked in summer (forest: 5.1 µmol m^{-2} s^{-1}, clearcut: 5.4 µmol m^{-2} s^{-1}), while the smallest values were measured in the winter months. The peak in R_s measured in the clearcut increased in the second and third year and stagnated in the last observation year 2017, which is consistent with the observed decreasing R_{eco} in Section 3.3.4. An increase of R_s in the second and third year after clear-cutting was also observed in a 100-year-old Norway spruce forest, Finland (Kulmala et al., 2014).

In the last two years, the annual range was approximately 1.5 times higher in the clearcut than in the forest. Forest R_s showed approximately the same behavior throughout all observation years for intra-annual minima and maxima. Here, heterotrophic respiration was the dominant component (Fig. 3.3.8) during April 2011 until July 2013 with a total average of all measurement points of 59 %, while autotrophic respiration for the various measurement points ranged between 19 and 54 %. These values are consistent with those observed in

previous years at the same study site (Dwersteg, 2012). The analysis of one measurement day in March 2014 shortly after deforestation, showed that autotrophic respiration in the clearcut accounted for 16 % of R_s. However, the significance of this single value is limited.

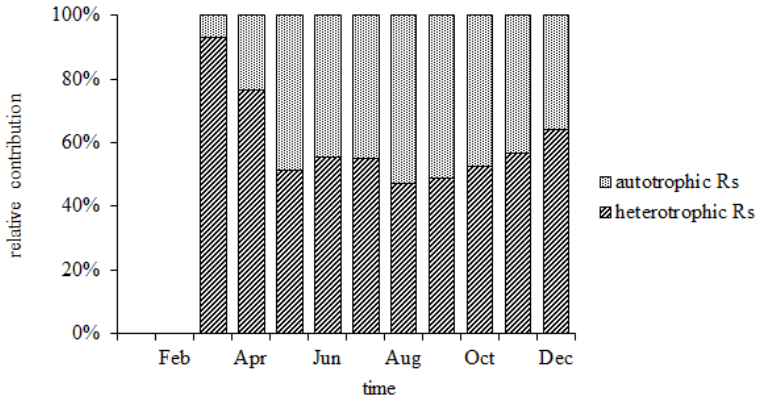

Figure 3.3.8: *Relative contribution of heterotrophic and autotrophic respiration at the forest site as monthly averages from April 2011 until July 2013. For January and February were no data available.*

R_s from both sites followed the seasonal pattern of R_{eco} (Fig. 3.3.7), but were less in the forest than in the clearcut, especially during the summer months. The difference of the monthly measured area-averages of R_s between forest and clearcut was not always statistically significant. During winter times and the first two years after cutting, the error bars overlap, indicating no appreciable differences of R_s in the forest and clearcut. In the last two growing seasons, R_s was significantly higher in the clearcut than in the forest, which is probably due to the increased root respiration. Molchanov et al. (2017) studied the effect of clear-cutting on soil CO_2 emission in a spruce forest and reported, that besides soil temperature also the thickness of the litter layer, the degree of damage of the upper soil layer and logging residue on the soil surface have influenced the rate of R_s. They showed that in general R_s was higher in undisturbed soil and plots with litter fall and accumulated logging residues, and was lower in plots with disturbed humus horizons. At our site, the soil surface was protected against heavy logging machines by padding with spruce branches and the extent of soil damage can be assumed to be relatively small. We conclude that in the deforested area, temperature and regenerating vegetation played the most important role in controlling temporal patterns of R_s.

The fraction of R_{eco} originated from R_s was estimated by dividing the spatial average of R_s by R_{eco}, inferred for the respective time stamp from the EC measurements (Section 3.3.3). Across the year, the clearcut fractions of R_s/R_{eco} in Figure 3.3.9 were in general higher (0.5) than for the forest (0.4) due to less above-ground biomass which could respire. Slightly higher fractions around 0.6 were found for example after harvesting of Douglas-fir forests (Paul-Limoges et al., 2015), which is possibly an indication that autotrophic respiration was more prominent in our clearcut area. The highest R_s/R_{eco} were found in spring and summer months in the deforested area, because of the higher proportion of R_s caused by higher temperatures of the soil surface. In autumn, the forest showed higher fractions, due

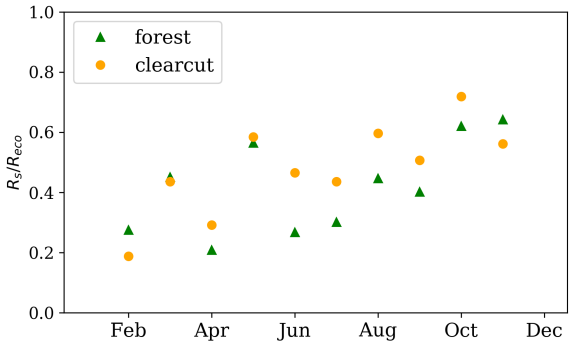

Figure 3.3.9: *Fraction between monthly soil respiration (R_s) measured by the manual chambers and the corresponding ecosystem respiration (R_{eco}) estimated after Lasslop et al. (2010), calculated as fraction for forest (triangles) and clearcut (circles) and averaged over all observation years after cutting. Fractions for January and December were rejected since the evaluable sample size was less than two measurements.*

to the ongoing plant and root activities and possibly dampened and delayed soil cooling. This behavior can also be seen in the comparison of the contributions by heterotrophic and autotrophic respiration to R_s (Fig. 3.3.8), where the autotrophic component in autumn is still clearly higher than in the spring months. The trend of R_s/R_{eco} in the forest is comparable with those evaluated for a spruce dominated forest, where the minimum fraction was observed in early spring, followed by increasing values until autumn (Davidson et al., 2006).

3.4 Summary and conclusion

We presented seven years of CO_2 flux measurements within a spruce forest catchment in the Eifel National Park, which was partly deforested three years after measurements started and was allowed to regenerate naturally. A second EC system was installed in the deforested area and operated simultaneously with the forest tower. During the seven years of observation, the spruce forest was a strong sink for CO_2 with net annual uptakes ranging between -530 (-425) and -761 (-594) g C m^{-2}. Gross primary production and ecosystem respiration showed typical annual cumulated values for a temperate central European spruce forest of 1680 (1755) and 1020 (1219) g C m^{-2}, respectively. According to chamber measurements, about 40 % of R_{eco} were due to soil respiration. Within the first year after deforestation, a strong reduction in photosynthetic uptake of CO_2 transformed the clearcut area from a previous sink into a large source for CO_2 with a net annual carbon emission of 521 (548) g C m^{-2}. In the following years, the annual net CO_2 release from the clearcut decreased continuously to 83 (236) g C m^{-2}, while GPP increased from 385 (447) to 832 (1036) g C m^{-2}, indicating that the area regenerated rapidly. R_s increased continuously year by year and was 1.5 times higher in the last two years than forest R_s. The contribution of R_s to R_{eco} on the clearcut was about 50 %.

The albedo of the clearcut area increased from 0.16 to 0.25 % in the third year after cutting and was thus up to 3.5 times higher than the forest albedo. While in the first years anaylzed

here, the cooling effect of ΔRF_{α} outweighs the warming effect ΔRF_{NEE} of the increased NEE release, a decreasing albedo due to a higher proportion of woody vegetation will weaken the cooling effect in the future. Assuming that the albedo of the regenerated deciduous forest remains below that of the spruce forest, however, its effect can be expected to cause an earlier occurrence of compensation and payback points when CO_2 and albedo effects are considered in combination. Existing information about the carbon compensation point and the duration of the payback time (Aguilos et al., 2014) of disturbed forest ecosystems base largely on assumptions made from chronosequence studies or are derived from ecosystem model estimations. With regard to the interaction between land management and climate change, it is important to continue studies such as the one presented here for at least several decades. It has been suggested that the frequency and intensity of natural forest disturbance regimes have increased in the context of climate change (Seidl et al., 2014; Hicke et al., 2012), such that forest management becomes an increasingly important part of climate change mitigation strategies (Canadell and Raupach, 2008; Matthews et al., 2017).

4 The carbon budget of a 3-year crop rotation: using three different non-linear regression CO_2 flux partitioning approaches [§]

4.1 Introduction

In 2015, 11 % of the earth's surface (24 % of Europe and 34 % of Germany) was covered by agricultural land (FAO, 2015). The ability of agroecosystems to sequester carbon but also to release CO_2 through management practices (e.g. cultivation activities), gives them an important role in the global and local carbon balance (West and Marland, 2002). The agricultural sector is crucial for the stabilization of CO_2 concentrations in the atmosphere to due to its large potential for mitigating climate change (Ravindranath and Ostwald, 2008). There is an increasing number of studies, which presents longterm measurements of biosphere fluxes and emissions of greenhouse gases on croplands. Their focus is on studying and evaluating the impact of different crops and management practices in order to identify the main factors that contribute to the carbon balance of arable land (Kutsch et al., 2010). Ceschia et al. (2010) presented the annual greenhouse gas budgets of 15 European crop sites along a large climatic gradient, considering the effect of different management practices. Some studies consider only one species, as for example for sugar beet Moureaux et al. (2006) or winter wheat crop Anthoni et al. (2004b); Dufranne et al. (2011); Schmidt et al. (2012). However, a larger proportion are investigating crop rotations (Aubinet et al., 2009; Béziat et al., 2009; Kutsch et al., 2010; Ceschia et al., 2010; Buysse et al., 2017), as they are an important component of agricultural management. Problems can arise for calculating annual carbon budgets during analyzing of single crops, which are usually also embedded in a rotation, since these are partly influenced by previous and subsequent crops.

All these studies have in common that they require daily, seasonal or annual cumulated sums of the measured net ecosystem exchange (NEE) and estimations of its components gross primary production (GPP) and total ecosystem respiration (R_{eco}) to estimate the overall carbon balance or budgets of the agricultural land. The most practiced technique to disentangle GPP and R_{eco} from NEE is the non-linear regression (NLR) method (Sect. 4.2.6). The method makes use of parameterized non-linear functions, which express semi-empirical relationships between NEE and environmental variables like temperature and solar radiation (Aubinet et al., 2012). The use of different NLR can lead in some cases to either an over- or underestimation of the two opposite components. For example, Wohlfahrt et al. (2005) stated, that using a nighttime based estimation of R_{eco} of a mountain meadow led

[§]This chapter is in preperation for submission as: Ney, P., Graf, A., Schmidt, M. and Vereecken, H. (2018): CO_2 fluxes of a 3-year crop rotation: using three different non-linear regression partitioning approaches.

to an overestimation of daytime respiration and hence to an overestimation of GPP. Also Isaac et al. (2017) reported that daytime approaches produced 20–57 % smaller values of R_{eco} at different Australian OzFlux sites compared to the nocturnal methods. These facts cannot be ignored since differences in the resulting annual values impede the interpretation of carbon flux measurements and total carbon budgets.
The aim of this study was:
1. to quantify the evolution of CO_2 exchange of a 3-year crop rotation cycle in an agricultural region in Western Germany using continuous eddy-covariance (EC) flux measurements and to compare the carbon budget of different crops,
2. to highlight and discuss the differences in the annual cycle and cumulated sums of NEE, GPP and R_{eco} when using a source-partitioning approach which relies on the temperature response function of measured nighttime NEE fluxes or a so-called daytime partitioning method, where a light response function is fitted to daytime NEE values and
3. to introduce an own algorithm which uses NLR functions to a full NEE dataset without previously separation into day- and nighttime observations.

4.2 Methods

4.2.1 Study site

The measurements were carried out at the TERENO research site Selhausen, located in the southern part of the Lower Rhine Embayment in Germany (50°52'09"N, 6°27'01"E, 104.5 m a.s.l., Fig. 4.2.1), in a region largely dominated by agriculture. The test field is completely surrounded by other croplands. The next inhabited settlement is located 500 m to the east. In 2011, the field was equipped with instruments for micrometeorological measurements for long-term monitoring of energy and carbon exchange. Since 2015, the station has been extended in accordance with ICOS standards for Level 1 sites (ICOS site code DE-RuS), whereby the old instrumentation is still in parallel operation and was used as a source of data in this study. As is common practice in the area, the field was cultivated with a 3-year crop rotation cycle. The crop rotation prior to the observation period consisted of sugar beet/potatoes/winter wheat/oil seed radish (catch-crop)/sugar beet rotation. Information on crop management during the observation period is provided in Sect. 4.2.2 and Tab. 4.2.1. In general, the land surface is flat (slopes $< 4°$) at the study site. A loess layer of about 1 m thickness lies on Quaternary sediments, which consist mainly of fluvial deposits of the Rur river system (Schmidt et al., 2012). The overlying soil is an Orthic Luvisol and the texture is silt loam (approx. 14 % clay, 73 % silt and 13 % sand) according to the USDA classification.
The climate at the study site is classified as temperate maritime with an annual mean air temperature of 10.3 °C and an annual mean precipitation of 718 mm (reference period 1981–2010, data taken from the DWD climate station of the Forschungszentrum Jülich at a distance of 5.3 km from the test site).

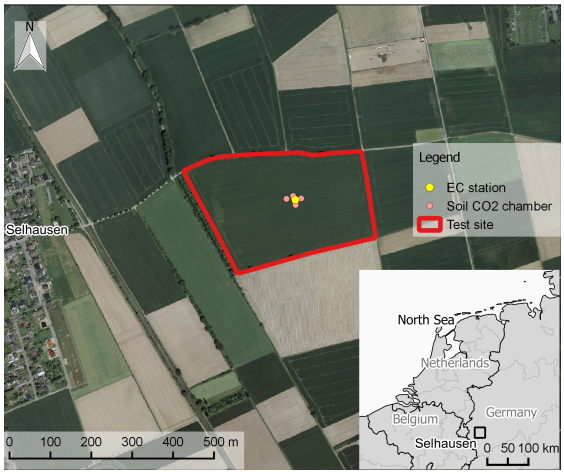

Figure 4.2.1: *Aerial view of the TERENO site Selhausen and of the different measurement systems.*

4.2.2 Crop management

Table 4.2.1 summarizes the main management activities during three cropping seasons. Before the rotation cycle started with sowing of winter wheat (*Triticum aestivum L.; variety Premio*) on 25 October 2014, residues of the previous harvest of sugar beet were left on the site and the soil was plowed one week before seeding. The field was fertilized in March, April and May 2015 (91.8, 51.3 and 65.8 kg ha^{-1} mineral N) at intervals of six weeks. Winter wheat was harvested on 2 August 2015 with straw as residues, which were removed the following day.

Subsequently, the field was prepared for the next crop by cultivating twice and deep plowing, then winter barley (*Hordeumvulgare L.*; variety Henriette) was seeded on 29 September 2015. Mineral nitrogen was applied in March (74.4 kg N ha^{-1}, April (49.9 kg N ha^{-1}) and May 2016 (50.7 kg N ha^{-1}). After harvesting barley on 10 July 2016, remaining straw was chopped and the field was fertilized two times in mid-July (5.2 kg ha^{-1} N, 2.7 kg ha^{-1} P_2O_5, 16.7 kg ha^{-1} K_2O, 1373 kg ha^{-1} CaO, 61 kg ha^{-1} P_2O_5, 51 kg ha^{-1} MgO, 18 kg ha^{-1} S). Soil was managed three times by cultivation until sowing of a catch-crop mixture (*Vicia sativa L., Pisum sativum L., Avena strigosa Schreb., Raphanus sativus L., Trifolium alexandrinum L., Phacelia tanacetifolia Benth., Guizotia abyssinica (L.f.) Cass.*) on 20 August 2016. Two days after seeding, 10.8 kg ha^{-1} mineral N was applied and the crop was not treated until the cut for mulching on 21 December 2016 (one half) and 6 January 2017 (other half).

Sugar beet (*Beta vulgaris L.*; variety Adrianna) was sown on 31 March 2017. Fertilizer was applied one week before sowing (104 kg N ha^{-1}) and in May 2017 (39.1 kg ha^{-1}). Harvesting took place on 25 October, leaving sugar beet leaves on the field. The 3-year crop rotation ended with plowing, harrowing and sowing of winter wheat on 25 October 2017. During the whole crop rotation, the crops (excluding catch-crops) were treated with fungicides, herbicides, insecticides and growth regulator. More details are given in Table 4.2.1. The 3-year crop rotation has never been irrigated.

Table 4.2.1: *Management activities during 3-years crop rotation cycle.*

date	management	product
25 Oct 2014	seeding	**winter wheat**(Premio)
11 Mar 2015	fertilization	91.8 kg N ha^{-1}
9 Apr 2015	fungizide treatment	220 g ha^{-1} Broadway,
	growth regulator treatment	0.4 l ha^{-1} CCC
22 April 2015	fertilization	51.3 kg N ha^{-1}
23 April 2015	fungizide treatment	1.6 l ha^{-1} Capalo,
	growth regulator treatment	0.4 l ha^{-1} CCC
21 May 2015	fungizide treatment	0.5 l ha^{-1} Diamant
	fungizide treatment	1.5 l ha^{-1} Adexar
27 May 2015	fertilization	65.8 kg N ha^{-1}
2 Aug 2015	harvesting	winter wheat, 105 dt ha^{-1}
5 Aug 2015	cultivation	
9 Sep 2015	cultivation	
29 Sep 2015	deep plowing, cultivation,	
	seeding	**winter barley** (Henriette)
27 Oct 2015	herbicide treatment	1.0 l ha^{-1} Arelon
	herbicide treatment	1.0 l ha^{-1} Bacara
	herbicide treatment	150 mm ha^{-1} Cyclone
12 Mar 2016	fertilization	74.4 kg N ha^{-1}
10 Apr 2016	fungizide treatment	0.9 l ha^{-1} Input Classic
	growth regulator treatment	0.5 l ha^{-1} Moddus
14 Apr 2016	fertilization	49.9 kg N ha^{-1}
2 May 2016	insectizide treatment	1.0 l ha^{-1} Credo
	herbicide treatment	1.5 l ha^{-1} Bontima
4 May 2016	fertilization	50.7 kg N ha^{-1}
5 Jul 2016	deinstallation soil sensors	
10 Jul 2016	harvesting	winter barley, 79.7 dt ha^{-1}
15 Jul 2016	fertilization	5.2 kg N ha^{-1}, P_2O_5, K_2O
16 Jul 2016	cultivation	
19 Jul 2016	fertilization	CaO, P_2O_5, MgO, S
30 Jul 2016	cultivation	
20 Aug 2016	cultivation,	
	seeding	**catch-crop** (greening mix)
22 Aug 2016	fertilization	10.8 kg N ha^{-1}
21 Dec 2016	cutting catch-crop for mulch seed	
6 Jan 2017	cutting catch-crop for mulch seed	
16 Mar 2017	fertilization	104 kg N ha^{-1}
24 Mar 2017	herbicide treatment	4.0 l ha^{-1} Glyphosat
	herbicide treatment	0.3 l ha^{-1} Kantor
30 Mar 2017	cultivation	
31 Mar 2017	cultivation, crumbling roller,	
	sowing	**sugar beet** (Lisanna)
6 May 2017	herbicide treatment	
10 May 2017	fertilization	39,1 kg N ha^{-1}
15 May 2017	herbicide treatment	2.0 l ha^{-1} Goltix Titan
	herbicide treatment	2.0 l ha^{-1} Betasana Trio
22 May 2017	herbicide treatment	0.8 l ha^{-1} Agils
30 May 2017	herbicide treatment	2.0 l ha^{-1} Goltix Titan
	herbicide treatment	2.0 l ha^{-1} Betasana Trio
28 Jul 2017	herbicide treatment	1.0 l ha^{-1} Juwel
5 Oct 2017	harvesting	sugar beet, 832 dt ha^{-1}
25 Oct 2017	plowing, harrow,	
	seeding	winter wheat (Premio)

4.2.3 Eddy-covariance measurements and flux data treatment

A permanently running eddy-covariance (EC) system operated in the middle of the field (Fig. 4.2.1) with a three-dimensional sonic anemometer (Model CSAT-3, Campbell Scientific, Inc., Logan, Utah, USA) and an open path infrared gas analyzer (Model LI- 7500, Li-Cor, Inc., Biosciences, Lincoln, Nebraska, USA), which were mounted 2.5 m above surface. The measurement height was selected to ensure measurements above the zero plane-displacement height, which corresponds to approximately 2/3 of the canopy height (Foken, 2006). In addition, the aim was to make sure that the fetch contained fluxes originating within the study area and that the influence of neighboring agricultural areas was minimized. Fluxes of NEE were sampled in a 20 Hz mode.

30-min averages of NEE were calculated using the "TK3.11" software package from the University Bayreuth which includes post-processing correction methods (Mauder and Foken 2011) and quality assurance / quality control (QA/QC) after Mauder et al. (2013). Here, only data of the highest and moderate quality (flag 0 and flag 1) were used. Gaps in the calculated turbulent fluxes were filled with the marginal distribution sampling (MDS) method after Reichstein et al. (2005), which is implemented in the REddyProc software package (REddyProc Team, 2014).

In general, measured NEE is composed of the CO_2 flux and the CO_2 storage flux (F_s) in the air column below the EC system. F_s plays particularly a role in tall canopies. Here it was estimated from a single point CO_2 measurement as suggested by Hollinger et al. (2004). However, additional profile measurements were carried out sporadically and a storage term was calculated. Details of the set-up and procedure are given in Ney and Graf (2018).

Fluxes of CO_2 measured in conditions with low turbulent mixing (especially under stable stratification at night) tend to be underestimated (Van Gorsel et al., 2007; Aubinet et al., 2000). To overcome this problem, values of NEE measured under the above mentioned conditions were filtered using the friction velocity (u_*)-filtering. We used the moving point method after Papale et al. (2006) (implemented in REddyProc) to estimate u_* thresholds. To take into account the changing surface roughness of the test site during one year, which can also influence the u_*–NEE relationship (Wutzler et al., 2018), we re-estimated the u_*-threshold at different times of the year, depending on periods with vegetation cover and periods of bare soil. To check the plausibility of the EC measurements, the test on energy balance closure (EBC) after Wilson et al. (2002) was used:

$$Q - B = H + \lambda E \tag{4.2.1}$$

where Q is net radiation, B is ground heat flux (the storage term of soil heat flux SHF was calculated according to Campbell Scientific (2003) and added to the measured values), H and λE are eddy-covariance fluxes for sensible and latent heat, respectively. To determine the EBC, a linear regression between the available energy ($Q-B$) and the energy fluxes ($H+\lambda E$) was applied.

Although the measurement height was chosen as low as possible and the EC system was set up as far as possible from the field edges, under certain situations fraction of measured NEE fluxes could still originate from surrounding fields. In order to dispose of these values, an analytical footprint model based on Kormann and Meixner (2001) was used. Here, as suggested in Schmidt et al. (2012), 30-min NEE fluxes were discarded in cases where the cumulative source distribution fell below 70 % during daytime and 50 % at night.

In the following, half-hourly fluxes of CO_2 are expressed as µmol m^{-2} s^{-1}, daily averages in g C m^{-2} d^{-1} and annual cumulated sums in g C m^{-2} y^{-1}.

4.2.4 Ancillary micrometeorological measurements

Meteorological variables like air temperature (T_{air}, HMP45C, Vaisala Inc., Helsinki, Finland) and precipitation (P, Thies Clima type tipping bucket, distributed by Ecotech, Bonn, Germany) were measured at 2.105 m and 1.0 m a.g.l., respectively. Values of net (Q) and global radiation ($S\downarrow$) were sampled by thermal sensors (NR01, Hukseflux, Delft, Netherlands). Up to four self-calibrating soil heat-flux plates (HFP01, Hukseflux Thermal Sensors, Delft, Netherlands) were installed at a depth of 0.08 m. Soil water content (SWC, CS616, Campbell Scientific, Inc., Logan, USA) and soil temperature (T_{soil}, TCAV, Campbell Scientific, Inc., Logan, USA) were sampled in the layer above the heat flux plates. Both measurements were performed in the immediate vicinity of the EC station in representatively managed soil to determine the soil heat flux (SHF) for the energy balance closure according to the calometric method (Campbell Scientific, 2003).
Data gaps in meteorological variables of T_{air}, humidity and $S\downarrow$ were filled with an interpolation method based on empirical orthogonal functions (Beckers and Rixen, 2003; Graf, 2017). This method uses linear relations to the same variables derived from up to 19 other TERENO stations within a radius of 50 km.
Soil respiration (R_s) was observed with an automated soil CO_2 gas flux system (Li-8100, Li-Cor Inc., Lincoln, Nebraska, USA), connected to at least three and up to four long-term soil flux chambers. The chambers were installed close to the EC-station (Fig. 4.2.1) on soil collars with a diameter of 0.2 m. The total collar height was 0.07 m, from which 0.05 m was in the soil. The closing interval for each chamber was 30 min and they were closed for 90 s for each flux measurement. The sampling rate of the CO_2 and water vapor concentration, as well as chamber head space temperature were 1 Hz. The CO_2 concentration was corrected for changes in air density and water vapor dilution. R_s was calculated by adjusting only the last 60 s before reopening against the corrected CO_2 concentrations by linear regression.

4.2.5 Biometric measurements

To obtain information about the crop development and growing stages, biometric measurements were carried out over the plant growing seasons in intervals of four weeks. The canopy height was measured nearly every week. In order to determine dry matter (DM) and vegetation area indices, plants from sections of 1 m length were harvested over five rows at each of five sampling locations and subsequently analyzed in the lab. Belowground biomass was not collected for winter barley and therefore also the root biomass for other crops is not considered in this study, with the exception of sugar beet.
The biomass samples of each sampling location were separated into living (green) and senescent (brown/yellow) leaves, stems and ears (including grain, glume and rest of the ear). Sugar beet was separated into green/brown leaves and stems, as well as into portions of beet above and below the ground. Plant area index (PAI), which comprised green and senescent leaves and stems, was determined destructively with a Area Meter (Li-3000C, Li-Cor Biosciences, Lincoln, NE, USA).
DM was analyzed by weighing the separated samples before and after they had been dried in a drying cabinet at a temperature of 65 °C for sugar beet and between 65 and 105 °C for

the other crops. Drying duration ranged from 24 to 96 hours.

4.2.6 CO_2 flux source-partitioning: Non-linear regression approaches

EC measurements usually provide half-hourly values of the net exchange of CO_2 (NEE) between an ecosystem and the atmosphere. For a better understanding of land-atmosphere interactions it is necessary to obtain additional information about the componentss GPP and R_{eco}, which are derived from the directly measured NEE, where NEE=R_{eco}-GPP. The most practiced technique to disentangle GPP and R_{eco} from NEE is the non-linear regression method (NLR). NLR is based on parameterized non-linear functions, which express semi-empirical relationships between net ecosystem fluxes and environmental variables (Fig. 4.2.2), commonly temperature (T_{air} or T_{soil}) and light (R_g or $PPFD$). Many different models have been implemented (Falge et al., 2001a; Barr et al., 2004; Reichstein et al., 2005; Richardson et al., 2006; Noormets et al., 2007; Lasslop et al., 2010), which basically differ in the form of the functions, the choice of meteorological driving variables, parameter time dependencies, time window length, and the use of measures and tests for goodness of fit (Moffat et al., 2007; Desai et al., 2008). Each implementation needs one regression equation for R_{eco} (mainly estimated from nighttime data) and one regression equation for the light response of the ecosystem (GPP, estimated from daytime data).

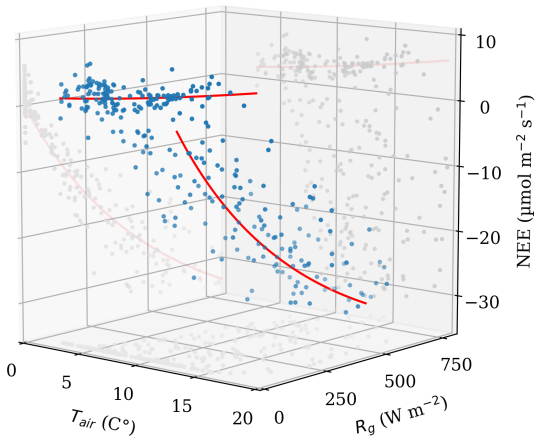

Figure 4.2.2: *Geometric illustration of the relationship between net ecosystem exchange (NEE) and the environmental variables air temperature (T_{air}) and global radiation (R_g) in a three dimensional Cartesian coordinate system. It shows the data of a 12-day period, where the regression lines were estimated according to the non-linear functional equations for ecosystem respiration (R_{eco}, cf. Eq. 4.2.2) and gross primary production (GPP, cf. Eq. 4.2.5).*

For our study, we chose the most widely used applications from a nighttime data-based method after Reichstein et al. (2005) (hereinafter NT) and an application that fits a light reponse curve to daytime NEE data, considering the effects of radiation and vapour pressure deficite on GPP, and the effects of temperature on R_{eco} after Lasslop et al. (2010) (hereinafter DT). In addition, we introduce a method (hereinafter own), which uses a data set of NEE for the regression analyses without a prevously separation into day- and nighttime observations.

Nighttime data-based flux partitioning after Reichstein et al. (2005)

The regression parameters in NLR may be kept constant over a certain period of time. The adjustment of these parameters is usually depending on seasons or bimonthly periods (Falge et al., 2001b). In this context, Reichstein et al. (2005) observed, that the temperature-respiration (R_{eco}) relationship, derived from long-term (annual) data sets, does not reflect the short-term conditions. The application of a long-term parametrization to estimate the daytime respiration from nighttime data from summer active ecosystems leads to an overestimation of R_{eco} over 25 % for an annual budget. This in turn also influences the estimation of GPP. To avoid this bias, an algorithm has been introduced which defines a short-term temperature response of R_{eco} (Reichstein et al. 2005).
For flux partitioning, Reichstein et al. (2005) use in their software REddyProc (REddyProc Team, 2014) a nighttime based NLR function according to the Lloyd and Taylor (1994) relationship, which was extended by using an algorithm that defines a short-term temperature sensitivity (E_0) of R_{eco}:

$$R_{eco} = R_b \exp\left(E_0 \left(\frac{1}{T_{ref} - T_0} - \frac{1}{T - T_0}\right)\right) \tag{4.2.2}$$

where T_0 is the activation temperature and kept constant at 277.13 K, R_b (µmol m^{-2} s^{-1}) is the ecosystem respiration at the reference temperature T_{ref}= 288.15 K (15 °C), T (K) is the air or soil temperature and E_0 (K) is an activation-energy parameter that describes the temperature sensitivity of R_{eco}.
For the parameterization, only original (i.e. no gap-filled) data is used for the flux partitioning and all data sampled under non-turbulent conditions are rejected by the u_*-threshold criterion (Sect. 4.2.3). To define R_{eco}, the measured NEE at nighttime (global radiation $S\downarrow$<10 W m^{-2}) is selected and split into consecutive intervals of 15 days. If there are more than six data points within each interval and the temperature range is more than 5 °C, the regression equation 4.2.2 is fitted to the scatter of R_{eco} and the temperature (Wutzler et al., 2018). After fitting the model, only intervals with a standard error of the estimates of E_0 less than 50 % and estimates within realistic bounds (40 to 450 K) are accepted. The three estimates of E_0 with the smallest standard error are averaged in an E_0-average value and represents the annual temperature sensitivity of the respiration (Reichstein et al., 2005). Subsequently, R_b is re-estimated in a time window of 7 days for consecutive intervals of 4 days using Equation 4.2.2, where E_0 is the E_0-average value. The calculated R_b is then set to the central time-point of the 4 day interval and linearly interpolated between them. Then, with R_b, E_0 and T, the ecosystem respiration for each half hour during daytime and nighttime can be estimated. In the last step, GPP was determined by subtracting R_{eco} from NEE during daytime (Wutzler et al., 2018). Missing NEE values were determined prior to source-partitioning via marginal distribution sampling (MDS) after Reichstein et al. (2005). MDS is a gap-filling technique and based on the look up table and mean diurnal variation principle. This technique utilizes the covariation of fluxes with meteorological drivers and their temporal auto-correlation.

Daytime data-based flux partitioning after Lasslop et al. (2010)

Because of the nighttime flux problem (underestimation of NEE) (Aubinet et al., 2000; Falge et al., 2001a; Gu et al., 2004), the measured nocturnal NEE flux requires a particlar

treatment (e.g. u_*-filtering in Sect. 4.2.3). This can lead to a high loss of nighttime data and hence to unreliable parameterization using a nighttime data-based estimation. For some EC sites the daytime data-based NLR can be more appropriate. For daytime data, the response of fluxes to $PPFD$ or R_g is modelled using the rectangular hyperbola light-response function equation by Michaelis and Menten (1913). Lasslop et al. (2010) provide a NLR model based on this function, which includes the temperature dependency of respiration and a water vapor pressure deficit (VPD) limitation of photosynthesis:

$$NEE = \frac{\alpha\, S\downarrow GPP_{sat}}{\alpha\, S\downarrow + GPP_{sat}} + \gamma, \tag{4.2.3}$$

where α (µmol C J^{-1}) is the canopy light use efficiency and defines the initial slope of the light-response curve (LRC), $S\downarrow$ is the global radiation (W m^{-2}), GPP_{sat} (µmol C m^{-2} s^{-1}) is the maximum CO_2 uptake rate of the canopy at light saturation and γ (µmol C m^{-2} s^{-1}) is R_{eco} (Eq. 4.2.2).
To consider the limitation of photosynthesis at higher VPD values, the constant parameter GPP_{sat} in Eq. 4.2.3 is replaced by an exponential decreasing function:

$$GPP_{sat} = \begin{cases} GPP_{sat,0} \exp\left(-k\left(VDP - VDP_o\right)\right) & if\, VDP > 10hPa \\ GPP_{sat,0} & otherwise \end{cases}, \tag{4.2.4}$$

where VPD is the vapour pressure deficit in the atmosphere, VDP_0 is set to a threshold of 10 hPa and parameter k determines the strength of the decrease (Lasslop et al., 2010).
As in the nighttime data-based estimation, T_0 in Eq. 4.2.2 was fixed. For each window, R_b was set to the median T within the window. E_0 was estimated using nighttime data ($S\downarrow$<10 W m^{-2}) with a window shift of two days. Then, R_b for T_{ref}=15 °C is re-estimated from nighttime data with E_0 for each window. Parameters α, $GPP_{sat,0}$, k, and $R_{eco,ref}$ of the LRC are fitted for each window using only daytime data and the previously estimated E_0. In the last step, GPP and R_{eco} are calculated with the linearly interpolated parameters of the adjacent valid windows (Wutzler et al., 2018). Contrary to the nighttime-based flux partitioning, GPP and R_{eco} estimated by the daytime-based approach are modelled values and do not add up exactly to observed NEE (Wutzler et al., 2018).

Data-based flux partitioning without separating into day- and nighttime

In the following, a source-partitioning approach is described, which uses a dataset of NEE to compute R_{eco} and GPP, without separating into day- and nighttime values. The used algorithm, illustrated schematically in Figure 4.2.3, was designed to disentangle NEE in a conservative and robust way by slicing out data within a defined time window dynamically through the whole time series. The window size was set to a range of seven days, wherein R_{eco} and GPP were partitioned and modelled using a NLR for the respiration (Eq. 4.2.2) and a LRC function step by step. For estimating GPP, we adopted the *Michaelis-Menten* type LRC used in the method after Lasslop et al. (2010) (Eq. 4.2.4):

$$GPP = \frac{\alpha\, S\downarrow GPP_{sat}}{\alpha\, S\downarrow + GPP_{sat}}, \tag{4.2.5}$$

where again α (µmol C J^{-1}) is the canopy light utilization efficiency, $S\downarrow$ is the global radiation (W m^{-2}) and GPP_{sat} (µmol C m^{-2} s^{-1}) is the gross primary productivity of the

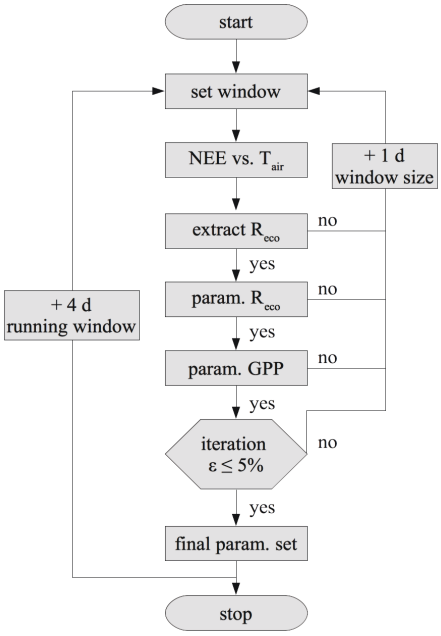

Figure 4.2.3: *General scheme of the procedure used in the own source-partitioning approach*

canopy at light saturation.

In the first step, NEE data were filtered by the estimated u_*-thresholds in Section 4.3.3. Then, the raw data were selected within the default window size (seven days), starting at the beginning of the time series. To extract T_{air} dependent respiration R_{eco} from NEE data points, a binning algorithm was implemented. Figure 4.2.4 shows the principle of the data point selection. First, a temperature bin within the 7-day window length were defined with a bin width of 5 °C, starting at the minimum temperature within the window. NEE data inside of these temperature bin were then binned to 1.0 µmol m^{-2} s^{-1} increments. Since nighttime NEE are of purely respiratory origin and also have a lower variability than daytime values, the NEE bin with the maximum number of NEE was used to select the respiration-dominated values from the point cloud (Fig. 4.2.4a). In the last step, a median of NEE values within the selected NEE bin was build. This procedure was repeated for each new temperature bin within the whole temperature range of the window. The temperature bin step width was set to 2.5 °C to ensure sufficient data overlap.

In the next step, R_{eco} was modelled using Equation 4.2.2 by fitting the function onto the medians of the binned data points (Fig. 4.2.4b) using the *curve fit* tool of the *scipy* package in Python, which uses the Levenberg-Marquardt algorithm to minimize non-linear least squares. If there were less than 3 data points (N_{NEE} in 4.2.2), the time window of the procedure described above was increased by one day. The obtained parameters E_0 and R_b during this process are checked for consistency with the limits shown in Tab. 4.2.2. If the parameters were outside the specified limits, the check fails and the algorithm reverted back to the window size setting point, increased the window size by one day and repeated the previous steps as long as no plausible parameters were found. However, if they met the

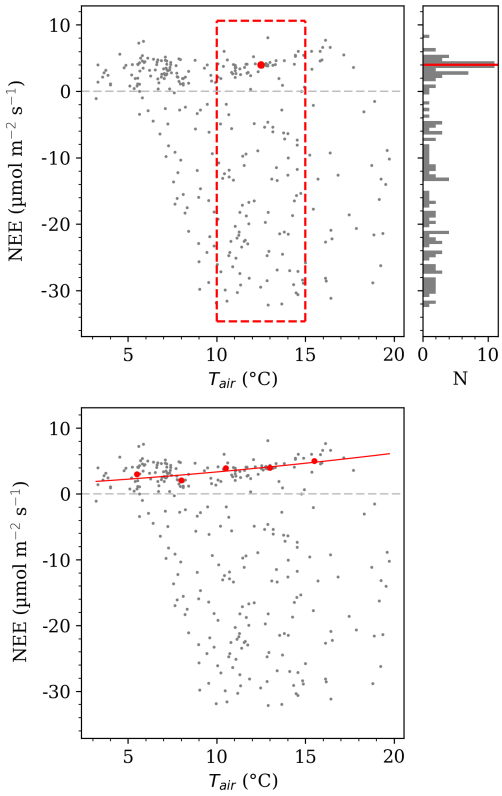

Figure 4.2.4: *Illustrated principle of the data point selection for fitting the respiration function in Eq. 4.2.2 to the scatter of net ecosystem exchange (NEE) versus air temperature (T_{air}). Plot a) shows the scatter of a 7-day period (left) and the distribution of NEE values, which lay within the 5 °C temperature (red rectangular) bin (right). NEE bin size is in this case 1.0 µmol m^{-2} s^{-1}. The NEE bin with the maximum number (N) of values was then selected to build a median (red dot). b) This procedure was done for all possible temperature bins within the whole temperature range of the considered time window, with an overlap of 2.5 °C. Thereafter, the respiration function was fitted to the previously determined medians (red line).*

requirements, GPP was calculated in the following step by subtracting the modelled R_{eco} from NEE. GPP was then used to fit the LRC function (Eq. 4.2.5) to obtain the quality checked parameters GPP_{sat} and α (Tab. 4.2.2). The window size increased by another day if the check failed at this point. In the final step, GPP was modelled using the derived parameters and subtracted from the original NEE data to calculate another estimate of R_{eco}. The algorithm reverted back to the LRC curve fitting and repeated all steps in an iterative process until all parameters converted against stable values within a 5 % range of the parameters obtained from a previous iteration step. If a certain amount of iterations (N_{iter}) did not lead to a stable set of parameters, the window size increased again by one day. After a successful set of iterations, the window size was reset to its initial size and moved 4 days further in time, where the whole process began again. Fitted parameters were assigned to the date in the middle of the data window and interpolated linearly to a complete half-hourly time series. As in the DT data-based flux partitioning method also

Table 4.2.2: *Settings for the variables and parameter used in the estimation procedure and limits for checking consistency for the algorithm shown in Fig. 4.2.3.*

variable	limits	initial guess	if not fulfilled
E_0	50 – 400	270	window width extended by one day
R_b	>0	/	/
α	≥0,<0.3	0.01	window width extended by one day
GPP_{sat}	≥0,<100	0.5 quantile of NEE	window width extended by one day
N_{NEE}	≥3	/	window width extended by one day
N_{iter}	≤20	1	window width extended by one day

here GPP and R_{eco} are modelled values and do not add up exactly to observed NEE.

4.2.7 Crop carbon budget calculations

Crop carbon budgets for each crop period and the whole 3-year crop rotation were determined as net ecosystem carbon budget (NECB) and total greenhouse gas carbon budget (GHGB) in g C m^{-2} in adapted form according to Ceschia et al. (2010). NECB is expressed as the change in carbon stocks of an ecosystem due to natural or athropogenic disturbances:

$$NECB = NEE + C_{imp} + C_{exp}, \tag{4.2.6}$$

where C_{imp} (counted negative) is the carbon import to the field by sowing and application of organic fertilizer (which was not applied to the test site). C_{exp} is the carbon export via harvest (biomass such as grains, tuber or straw). To estimate the total GHGB, additional greenhouse gas emissions from field operations (EFO) were added to the NECB (Ceschia et al., 2010; Buysse et al., 2017):

$$GHGB = NECB + EFO. \tag{4.2.7}$$

C_{imp} and C_{exp} were determined by a combination of information provided by the farm manager of the test site according to seed volumes and harvest yields (as dry mass) and from biometric measurements of the last plant sample before harvesting. Carbon content of plant parts (seeds, grains, stems and leaves) were calculated with carbon fractions given in Penning de Vries et al. (1989). Emissions from field operations were categorized into primary, secondary and tertiary C sources according to Gifford (1984) and Ceschia et al. (2010), where primary sources comprise direct emissions from burned full of farm machinery. Secondary and tertiary greenhouse gas sources have been converted to carbon equivalents and include the production, transportation and storage of fertilizers, pesticides and N_2O emissions of fertilizers as well as the manufacturing and maintenance of agricultural machinery. Emission factors of mineral fertilizers and estimates of primary and tertiary emissions as C equivalent for a range of field operations and for production, transportation, storage and transfer of pesticides were taken from tables listed in Ceschia et al. (2010).
The calculation of NECB and GHGB for a crop period started with sowing and ended with the last field management before sowing the following crop, ensuring that the harvest of the respective fruit was always included.

4.3 Results and discussion

4.3.1 Site meteorology

All years during the full crop rotation were characterized by higher annual mean T_{air} compared to the long-term average, where in particular the spring and summer months in 2015 and 2016 were 0.5 to 1.5 °C warmer (Tab. 4.3.1 and Fig. 4.3.1a). The annual course of T_{soil} in 0.03 m depth followed closely the course of T_{air} and remained on a slightly lower level.

Table 4.3.1: *Annual statistics of meteorological parameters at the research station in Selhausen during 3-years crop rotation. Each year refers to the period from 25 October to 26 October of the following year.*

variable	year 1	year 2	year 3
T_{air} (°C)	10.7	11.7	11.2
T_{soil} (°C)	10.6	11.7	11.1
P (mm)	628	646	501
$S\downarrow$ (W m^{-2})	130	126	130
VPD (hPa)	6.1	5.7	5.4
SWC (vol. %)	30	30	22

The annual precipitation during the observation years (Tab. 4.3.1) was lower than the long-term average, whereas the third year had 22 % less P than the other two years. The number of days with snow cover was limited to the month of December and January, with only five, three and seven days registered in winters 2014/1015, 2015/2016 and 2016/2017, respectively. The annual distribution of P (Fig. 4.3.1c) is reflected in the annual course of SWC (Fig. 4.3.1e) in 0.02 m depth, with higher values in the summer half-year 2015 compared to those in the summer half-year 2016. In the driest year 2017, the annual mean of SWC (22 vol.%) was on average 27% lower than in previous years (30 vol.%).
Daily means of global radiation ($S\downarrow$, Fig. 4.3.1b) varied from 5 W m^{-2} in winter to a maximum of about 355 W m^{-2} in summer. Annual averaged $S\downarrow$ (Tab. 4.3.1) was around 130 W m^{-2} in 2015 and 2017 and was slightly lower (126 W m^{-2}) in 2016 due to the reduced daily averages in the summer months. The mean vapour pressure deficit of the air (Fig. 4.3.1f) ranged between 0 to 5 hPa in the winter half-year and 10 to 20 hPa in the summer months. Daily maxima of VDP ($VDP \geq 20$ hPa) occurred mainly between May and September of each year, with smaller deficits in 2016. The presence of high VPD values is correlated to phases of high air temperatures, high $S\downarrow$ values and conditions with lower SWC.

4.3.2 Crop development

Figure 4.3.2 shows the crop development with the measurement of canopy height, PAI and biomass. The observed crop properties followed the typical annual cycle. Values of PAI (Fig. 4.3.2a) were highest in the second half of May for winter wheat (6.7 m^2 m^{-2}) and winter barley (6.0 m^2 m^{-2}) and in end of July for sugar beet (5.6). Despite the limiting climatic conditions during the winter half-year, a PAI of 3.9 m^2 m^{-2} could still be observed for the catch-crops in mid-November.
Total DM, represented by the sum of green and brown biomass and storage organs, was highest for winter wheat (2.55 kg m^{-2}), followed by sugar beet (2.24 kg m^{-2}) and winter

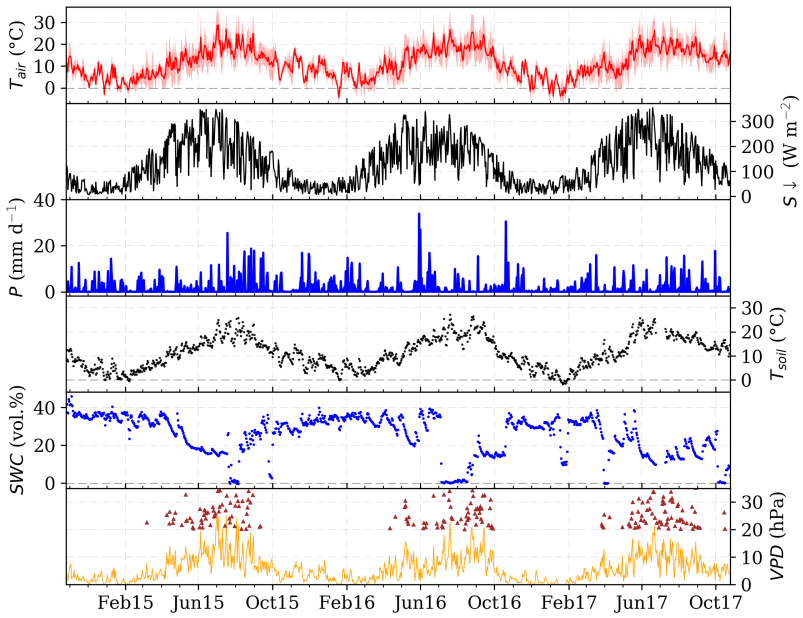

Figure 4.3.1: *Meteorological parameters at the TERENO site Selhausen during the measurement period from October 2014 until October 2017. Daily means of (a) air temperature (T_{air}, shaded area marks the minimum and maximum range), (b) global radiation ($S\downarrow$), daily sums of (c) precipitation (P), daily means of (d) soil temperature (T_{soil}), (e) soil water content (SWC) and (f) daytime vapour pressure deficit (VPD, curve) and daily maxima $\geq$ 20 hPa (triangles).*

barley (1.6 kg m^{-2}). Lowest DM was associated with the catch-crop with 0.22 kg m^{-2}. DM of the storage organs (Fig. 4.3.2b) contained ears for cereals and taproots for sugar beet. Winter wheat and sugar beet showed the highest DM values for storage organs with 1.6 kg m^{-2} and 1.5 kg m^{-2}, respectively. The biomass values for winter wheat are comparable with the observations made some years earlier in an adjacent field (Schmidt et al., 2012).

First brown biomass (Fig. 4.3.2b) occurred for winter wheat and winter barley in March, while the overall transformation from green to brown biomass reached a maximum for winter barley approximately two weeks earlier (beginning of June) than for winter wheat. For catch-crop and sugar beet, DM of brown biomass was negligibly small.

The yield (Tab. 4.2.1) for winter wheat was 105 dt ha^{-1} (grains), for winter barley 79 dt ha^{-1} (grains) and for sugar beet 832 dt ha^{-1} (taproot). The duration of the crop seasons (from seeding to harvest) was 281 days for winter wheat, 285 days for winter barley, 139 days for catch-crop and 188 days for sugar beet.

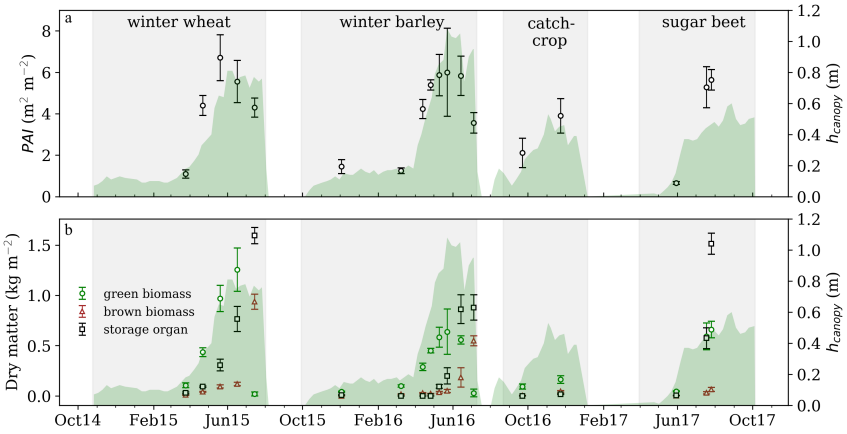

Figure 4.3.2: *Plant development and vegetation parameters of winter wheat, winter barley, catch-crop and sugar beet between 25 October 2014 and 25 October 2017. Green shaded area marks the evolution of canopy height (m). Also (a) plant area index (PAI) in and (b) storage organs (biomass of ears and taproot), aboveground green biomass (living leaves and stems) and aboveground brown biomass (senescent leaves and stems) as dry matter are shown. Error bars refer to one standard deviation.*

4.3.3 Flux measurement availability and quality

In order to be able to calculate reasonable annual balances of EC measured NEE, a high data coverage is indispensable. The data availability (Fig. 4.3.3) after the calculation of half-hourly mean fluxes of NEE for each crop season was between 61 and 65 % (or rather 35 and 39 % missing records). Here, data rejection is mainly the result of quality control (see Sect. 4.2.3) and instrument failure of the measuring system. Most common are short gaps with lengths less than one day (Fig. 4.3.3a). Half-hourly gaps occurred most frequently, followed by gaps that were between 2 hours and 1 day long. The proportion of gaps greater than one day was less than 1.5 % for each crop season. Two larger periods with missing data occurred in April 2015 and June 2017 with a total gap length of 5 days and 16 days, respectively (4.3.3c).

Estimated u_*-thresholds (Sect. 4.2.3) varied between 0.04 and 0.11 m s^{-1}, depending on underlaying vegetation cover. The footprint analysis gave a fetch of at least 120 m and up to 210 m in the prevailing west-south-west wind direction. After discarding records according to the u_*-threshold and footprint analysis, the total gap lengths increased to 40.4 – 44 % and the maximum proportion of gap length shifted from 0.5 to 2 hours and 1 day (Fig. 4.3.3b). The reason for this shift is that the exclusion of data mainly concerned fluxes measured at night, which occurred during stable atmospheric stratification and often last for several hours.

The test for energy balance closure (Eq. 4.2.1) of the EC measurements ranged between 0.83 and 0.86 for each crop season. These closures coincide with the balance ratio of 0.86 observed at the same test field by Eder et al. (2015).

Sporadic tests with a lift system to determine vertical concentration profiles (Ney and Graf, 2018) revealed that the magnitude of the storage term was very low during the daytime (< 1 % of the EC flux) and reached more than 10 % of the EC flux during night and times of

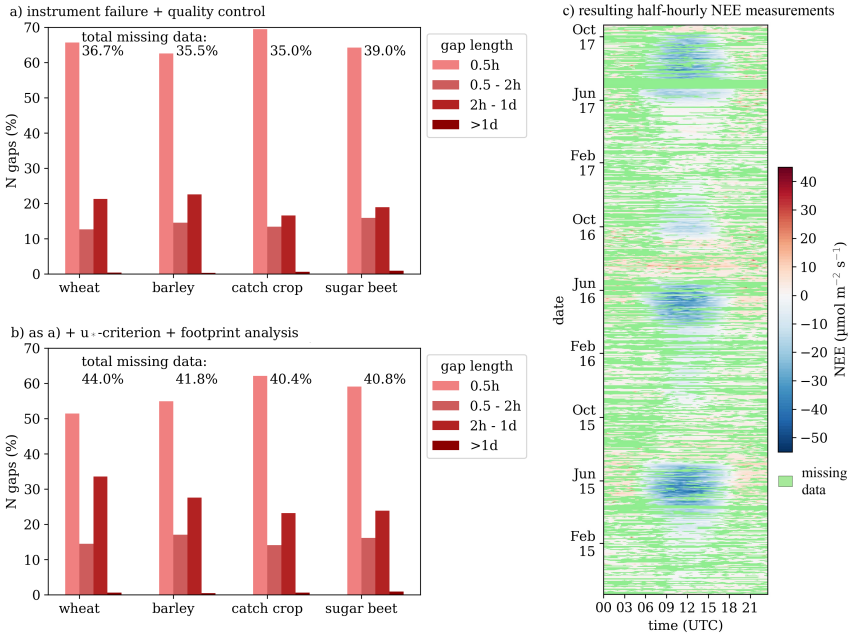

Figure 4.3.3: *Histograms of the fraction of gap length by duration to total gap length for fluxes of net ecosystem exchange: a) missing data including instrument failure and quality control, b)includes additionally data rejection after the u_*-criterion and data rejection due to large footprint. Percentages written in the diagram represent resulting missing data within the total data set for each crop. c) resulting half-hourly values of NEE, missing data points are marked green.*

twilight. The difference compared to the single point method after Hollinger et al. (2004) was with 0.7 % small. Based on the high availability of data and performed quality controls, it can be concluded that a good quality of the EC measured NEE fluxes exists for the test site and the considered time period.

4.3.4 Inter-annual variability of CO_2-fluxes

In this Section and Sect. 4.3.5, resulting CO_2 fluxes are described and discussed independently of the used source-partitioning method. For this purpose, the cumulated values from the own application are shown with the respective values for the NT and DT method in brackets. A comparison of the methods follows in Sect. 4.3.6 .In the following figures, tables and discussions the results are presented with the usual micrometeorological sign convention, the positive sign indicating fluxes from the surface to the atmosphere and the negative sign indicating downward fluxes. For better practicality, GPP is considered as absolute values. Daily integrated fluxes of NEE, GPP and R_{eco} in Figure 4.3.4a, b, c show a typical annual course and seasonal variability. Daily values of NEE (Fig. 4.3.4a) ranged during the 3-years crop rotation between 10 and -14 g C m^{-2}. It was strongly negative (net carbon uptake) during the spring and summer month, slightly positive during the winter months and after harvest, and reached maximum emission after ripening of winter wheat and winter barley. Maximum daily net carbon uptake was found for winter wheat between May and

July (-14 g C m^{-2}), for winter barley in early May (-13 g C m^{-2}), for catch-crop in end of September (-5 g C m^{-2}) and in sugar beet between July and September (-12 g C m^{-2}). These values are in the same order of magnitude as reported in other crop studies. Maximum observed mean daily fluxes were -12 g C m^{-2} in winter wheat and -10 g C m^{-2} in winter barley in Denmark (Soegaard et al., 2003), about -12 g C m^{-2} in Germany (Anthoni et al., 2004b) and between -10 and -13 g C m^{-2} in winter wheat in the same region (Schmidt et al., 2012). In sugar beet crop, Moureaux et al. (2006) noted maximum daily integrated fluxes of -11 g C m^{-2}.

Maximum values of GPP (Fig. 4.3.4b) were reached during the summer months with 25 g C m^{-2} d^{-1} in winter wheat, 20 g C m^{-2} in winter barley and 17 g C m^{-2} in sugar beet. Catch-crop vegetation reached a maximum daily GPP of 9 g C m^{-2} in end of September. Remarkable are the high day-to-day fluctuations during the growing seasons, especially in winter barley as well in winter wheat and attenuated also in sugar beet. Schmidt et al. (2012) stated out, that 62 % of this variation can be explained by fluctuating radiation supply. Daily R_{eco} (Fig. 4.3.4c) was high during the vegetation periods and low between growing seasons, especially during the winter months.

The amplitude of R_{eco} was highest in winter wheat (1 to 12 g C m^{-2}) and winter barley (1 to 10 g C m^{-2}) and lower in catch-crop (1 to 8 g C m^{-2}) and in sugar beet (3 to 8 g C m^{-2}). After the harvest of winter barley (mid-July 2016), high R_{eco} occurred, which was not observed after the harvest of winter wheat, although at both times regrowth of weeds and grain residues was observed. However, some studies (Anthoni et al., 2004a; Aubinet et al., 2009; Buysse et al., 2017) report that carbon emissions from soil after ploughing are very limited in quantity and duration. Al-Kaisi and Yin (2005) stated, that tillage causes an increase in decomposition rate, due to an increase in physical degradation of organic matter, which provides a higher availability for microorganisms. Therefore, another possibility might be that crop residues in the field combined with cultivation and higher T_{soil} (4.3.1a) resulted in an increase of R_s. Unfortunately, at that time no R_s measurements were available to check the determined R_{eco} for plausibility. However, this is contradicted by the fact that the base respiration at 15 °C (R_b, Fig. 4.3.6) and the temperature sensitivities (E_0, not shown) differed for wheat and barley, including the post-harvest period. For winter wheat, slightly higher half-hourly values of R_b (maximum 9.0 µmol m^{-2} s^{-1}) were estimated than for winter barley (maximum 8.0 µmol m^{-2} s^{-1}). Shortly after harvest, R_b was almost twice as high in barley (6 µmol m^{-2} s^{-1}) as in wheat (3.0 µmol m^{-2} s^{-1}) for a period of 3 weeks. In contrast, E_0 was lower in barley (160 K) than in wheat (265 K) at this time. In the following phase of regrowth of weed and crop volunteers, R_b equaled to a value of 3.5 µmol m^{-2} s^{-1}. We therefore assume that T_{air} was not causing the higher R_{eco} in winter barley and that the main factors relate to the type of crop, the previous crop or other environmental variables such as soil moisture.

Daily integrated R_s (Fig 4.3.4c) followed in general the annual course of R_{eco}. Notable differences in the course of R_s existed between winter wheat and winter barley. In general, R_s in winter barley was higher than for winter wheat. For the latter, R_s rate increased with the start of plant growth until mid-April and remained at the same level until mid-May. This was followed by a slight decline with relatively constant values of 2.5 g C m^{-2} until maturity and another maximum (5 g C m^{-2}) shortly before the harvest in August. Excluding the maxima of soil respiration, R_{eco} exceeded R_s by up to 10 g C m^{-2} on average. For winter barley, on the other hand, R_s increases continuously during the growing period and

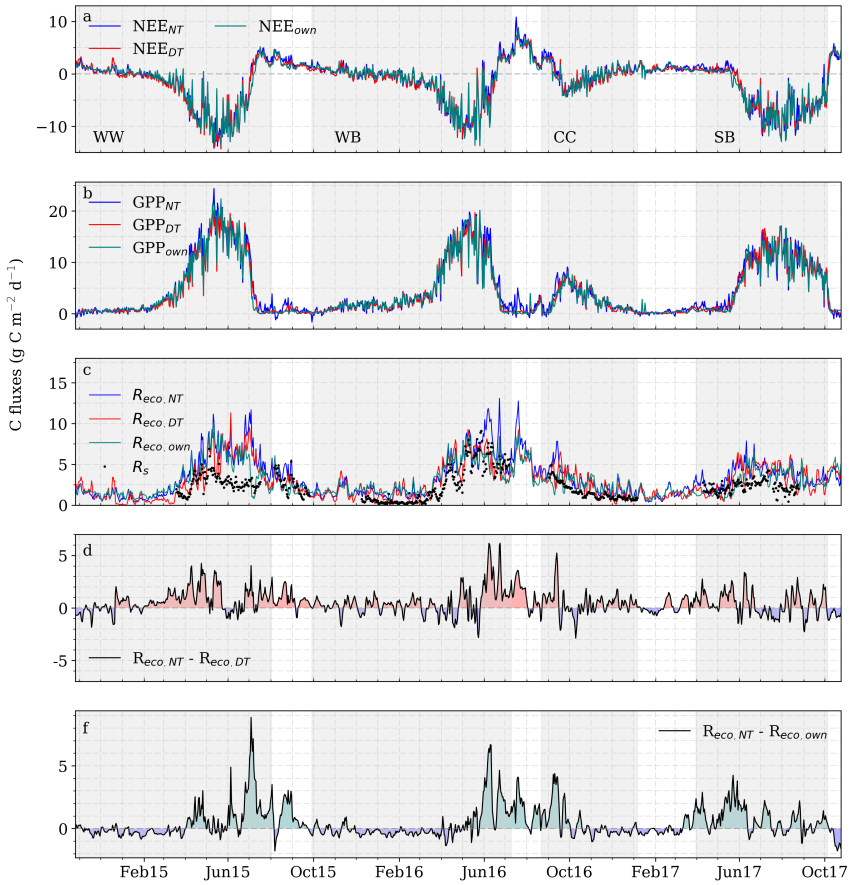

Figure 4.3.4: *Comparison of daily integrated values of a) NEE , b) GPP and c) R_{eco} for each tested source-partitioning methods after Reichstein et al. (2005) (NT), Lasslop et al. (2010) (DT) and our own approach. c) daily integrated measurements of soil respiration (R_s). Due to the harvesting and cultivation activities caused deinstallation of the soil CO_2 flux chambers, no R_s was available between October and November 2015, between July and September 2016 and between January and April 2017. d) and f) present the differences of R_{eco} between NT - DT and NT - own. Gray shaded areas mark the vegetation periods of each cultivated crop from seeding to harvest.*

decreases in the ripening phase. The difference to R_{eco} was smaller and amounted about 2 g C m^{-2} on average.

4.3.5 Cumulated CO_2-fluxes

In the following, the cumulated fluxes of NEE, GPP and R_{eco} are presented, whereby a crop season is calculated from the seeding to the seeding of the following crop. Cumulated NEE for the complete 3-year rotation was -1494 (NT: -1371, DT: -1639) g C m^{-2} and ranged, depending on the crop season, between -769 (NT: -696, DT: -740) g C m^{-2} (sugar beet) and 109 (NT: 77, DT: 44) g C m^{-2} (catch-crop). Compared to winter barley, winter wheat had a 40 % higher CO_2 uptake, related to the higher proportion of green biomass (Fig. 4.3.2b) and

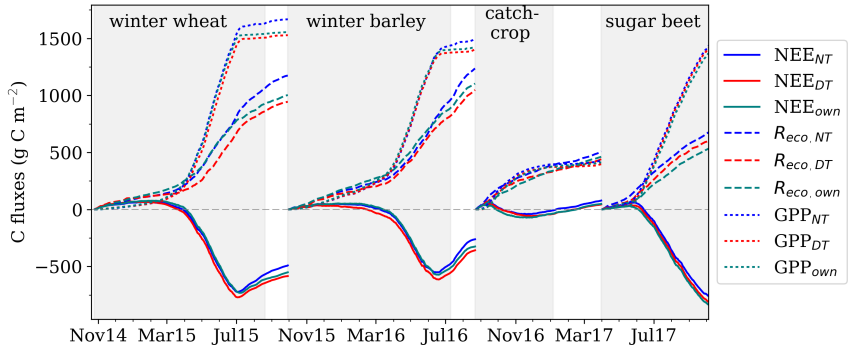

Figure 4.3.5: *Comparison of cumulative sums of NEE (line), R_{eco} (dashed line) and GPP (dotted line) for each tested source-partitioning method after Reichstein et al. (2005) (NT), Lasslop et al. (2010) (DT) and our own approach. Values are cumulated over each crop season from seeding to seeding of successive crop. Gray shaded areas mark the vegetation periods of each cultivated crop from seeding to harvest.*

larger GPP. Cumulated NEE, GPP and R_{eco} in Figure 4.3.5 show a typical temporal course. During winter, there was a small release of CO_2 through ongoing ecosystem respiration. An exception was the period with catch-crop between October and December 2016 with a small uptake caused by photosynthetically activities. However, catch-crop was a source for CO_2, although the CO_2 emissions were assumed to be lower than they would have been on bare soil during the same period. For all other crop cycles, the beginning of the growth period was indicated by a negative NEE (downward slope of cumulated curve in Fig. 4.3.5). The net carbon uptake started for winter wheat and winter barley in March, while sugar beet started later in May. GPP (dotted line in Fig. 4.3.5) increased continuously until the maturity phase of winter wheat and winter barley and subsequently dropped to zero. At the same time, the NEE reversed and the ecosystem lost carbon. Sugar beet, on the other hand, remained a sink until the harvest.

The order of magnitude of NEE, GPP and R_{eco} coincides mostly with observations of crop and crop rotations at other locations within Central Europe. NEE values of winter wheat at the agricultural site of Lonzée (Belgium) were -630 and -730 g C m^{-2} (GPP: 1580/1680 g C m^{-2} and R_{eco}: 950/950 g C m^{-2} referring to a seasonal year from November until August (Aubinet et al., 2009). Within an equal observation timespan, a field nearby the Selhausen test site showed -445/-502 g C m^{-2} for NEE, 1338/1120 g C m^{-2} for GPP and 836/674 g C m^{-2} for R_{eco} (Schmidt et al., 2012). Moureaux et al. (2006) found for a sugar beet crop at Lonzée an annual sequestration of -610 g C m^{-2}. For the same site and year, but different observation period (21 April to 29 September), Aubinet et al. (2009) reported a value of -800 g C m^{-2}, which is comparable to our findings (Tab. 3.3.2). The cumulated CO_2 fluxes shown above only contain values of the vertical CO_2 exchange (NEE). For an overall carbon budget of the test field, organic and inorganic carbon import (organic fertilizer) and export (harvest), as well as emissions from field operations have to be taken into account (Ceschia et al., 2010). Values of C_{imp}, C_{exp}, NECB, EFO and total GHGB for each crop and the complete crop rotation are given in Tab. 4.3.2. C_{imp} through seeding was generally small with a maximum of only -7 g C m^{-2}. C_{exp} is composed of the harvested grains,tubers and straw, and reached a maximum of 776 g C m^{-2} for winter crop and

Table 4.3.2: *Cumulative net ecosystem exchange (NEE), gross primary production (GPP), ecosystem respiration (R_{eco}), carbon import (C_{imp}) and export (C_{exp}), net ecosystem carbon budget (NECB), emissions from field operations (EOF) and GHG budget (GHGB) of the 3-year rotation cycle (explanation of the different terms see Sect. 4.2.7). Values were calculated in g C m^{-2} over each crop season from seeding to seeding of adjutant crop (see Tab. 4.2.1) for each applied source-partitioning method: nighttime (NT) and daytime (DT) data-based NLR, and own approach.*

	wheat	barley	catch-crop	sugar beet	3-year cycle
NEE_{NT}	-491	-261	77	-696	-1371
GPP_{NT}	1665	1497	432	1440	5034
$R_{eco,NT}$	1174	1236	509	744	3663
NEE_{DT}	-585	-358	44	-740	-1639
GPP_{DT}	1529	1406	397	1426	4758
$R_{eco,DT}$	944	1048	441	686	3119
NEE_{own}	-553	-381	109	-769	-1494
GPP_{own}	1555	1689	154	1389	4787
$R_{eco,own}$	1002	1308	263	620	3193
C_{imp}	-7.0	-6.4	-0.3	-0.4	-14.0
C_{exp}	776	552	0	874	2201
$NECB_{NT}$	278	284	77	178	816
$NECB_{DT}$	184	187	44	134	548
$NECB_{own}$	216	264	109	105	693
EFO	60	46	33	47	185
$GHGB_{NT}$	337	330	109	225	1002
$GHGB_{DT}$	330	233	76	181	734
$GHGB_{own}$	275	310	141	152	879

874 g C m^{-2} for sugar beet. Since catch-crop was not harvested, its plant residues (and thus the carbon) remained in the field. Over the 3-year crop cycle, 2201 g C m^{-2} was exported. EFO ranged between 33 and 60 g C m^{-2} with an additional release of 185 g C m^{-2} over the entire observation period. Considering only NEE, the Selhausen site represented a sink for CO_2 during the 3-year crop rotation cycle. However, the total GHGB indicates a source with values between 141 (NT: 109, DT: 76) g C m^{-2} for catch-crop and 310 (NT: 330, DT: 233) g C m^{-2} for winter barley. Over the 3-year crop rotation, the total GHGB adds up to 879 (NT: 1002, DT: 734) g C m^{-2}. Different studies about rotation cycles in European croplands, which combine measurements of NEE with lateral C flux inventories, have also shown that agroecosystems are a source for carbon (Anthoni et al., 2004b; Ceschia et al., 2010; Béziat et al., 2009; Aubinet et al., 2009; Buysse et al., 2017; Kutsch et al., 2010).

4.3.6 Comparison of flux-partitioning tools

In general, the results from the three source-partitioning methods (Sect. 4.2.6) show notable differences in GPP and R_{eco} and thus also in the modelled NEE of the daytime and own approach. In this context it should be noted that the choice of the source-partitioning model also has an influence on the gap filling of NEE. In some models, the measured NEE is completely replaced by the difference between the modelled GPP and R_{eco} (DT and own),

while the NT approach used here fills the gaps in the time series of NEE independently of the source-partitioning with the gap filling method MDS (Reichstein et al., 2005). Over the 3-year crop rotation, the differences in the integrated sums (Tab. 3.3.2 and Fig. 4.3.5) between NT and DT were 276 g C m^2 (6 %) in GPP and 544 g C m^2 (15 %) in R_{eco}. The modelled absolute sum of NEE_{DT} was 268 g C m^2 (16 %) higher than NEE_{NT}. Smaller discrepancies arose between NT and own as well as between DT and own. The differences between NT and own were 247 g C m^2 (5 %) in GPP, 470 g C m^2 (13 %) in R_{eco} and 123 g C m^2 (9 %) in NEE (NEE_{own} modelled). The discrepancies between the source-partitioning methods also varied between the crop seasons. For example, in winter wheat GPP_{NT} and GPP_{own} were about the same magnitude but differed in R_{eco}. In sugar beet, on the other hand, GPP_{NT} and GPP_{own} differed only slightly. Also here, a larger difference in R_{eco} existed. In winter barley and the patterns in differences were similar: higher values in GPP_{NT} and $R_{eco,NT}$, followed by GPP_{own} and $R_{eco,own}$ and then by GPP_{DT} and $R_{eco,DT}$.
Discrepancies between the three methods in the daily integrated fluxes (Fig. 4.3.4) are mainly visible in R_{eco}. Figure 4.3.4 d and e show the differences between $R_{eco,NT}$ and $R_{eco,DT}$ as well as $R_{eco,NT}$ and $R_{eco,own}$. $R_{eco,NT}$ usually exceeds $R_{eco,DT}$, particularly during the growing seasons. The positive deviation was maximum 4 g C m^{-2} d^{-1} in winter wheat and reached over 5 g C m^{-2} d^{-1} in winter barley. Occasionally, $R_{eco,DT}$ was higher with maximum values of 2 g C m^{-2} d^{-1}. Most negative deviations occurred in sugar beet. $R_{eco,own}$ showed a large positive difference (up to 8 g C m^{-2} d^{-1}) compared to $R_{eco,NT}$ in winter wheat. Despite this, the overall differences between $R_{eco,NT}$ and $R_{eco,own}$ over the entire observation period were smaller than between $R_{eco,NT}$ and $R_{eco,DT}$. The

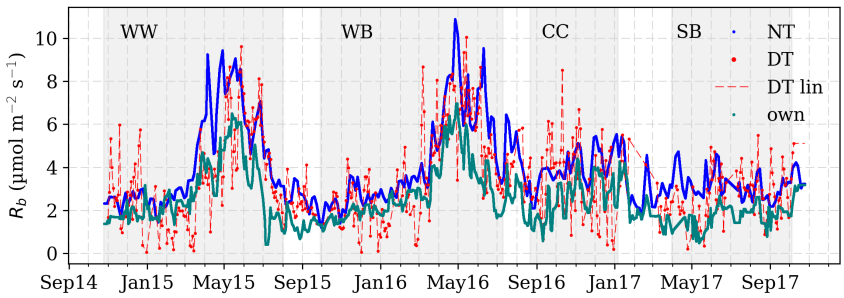

Figure 4.3.6: *Comparison of estimated base respiration R_b (or reference respiration) at 15 °C in the source-partitioning methods after Reichstein et al. (2005) (NT), Lasslop et al. (2010) (DT), and our own approach. Gray shaded areas mark the vegetation periods of each cultivated crop from seeding to harvest. Note that NT and own show every half-hourly value of R_b, while DT, however, displays only one estimated value of a time window. For better visualization, DT lin (dashed red line) represents a subsequent linear interpolation (which is also used in the DT method to estimate a complete dataset of R_{eco} but is not given in the resulting file of REddyProc).*

discrepancy of $R_{eco,NT}$ compared to $R_{eco,DT}$ and $R_{eco,own}$ is based on the estimated base (or reference) respirations R_b (Fig. 4.3.6). The respiration at 15°C was highest for NT in winter wheat (9 µmol m^{-2} s^{-1}) and winter barley (11 µmol m^{-2} s^{-1}), and was lower in catch-crop (5.5 µmol m^{-2} s^{-1}) and sugar beet (5 µmol m^{-2} s^{-1}). Even the inter-annual fluctuations are similar between R_b NT and R_b own, the determined R_b own was smaller with maximum 2.5 µmol m^{-2} s^{-1} in winter wheat, 5 µmol m^{-2} s^{-1} in winter barley, 0.5 µmol m^{-2} s^{-1}

in catch-crop and 4 µmol m^{-2} s^{-1} in sugar beet. For comparison, Moureaux et al. (2006) observed a R_b of 3.3 µmol m^{-2} s^{-1} in sugar beet crop, or Anthoni et al. (2004b) reported a value of 6.1 µmol m^{-2} s^{-1} for winter wheat during May and June.

Figure 4.3.7 shows the comparison of daily sums of NEE, GPP and R_{eco} partitioned after the

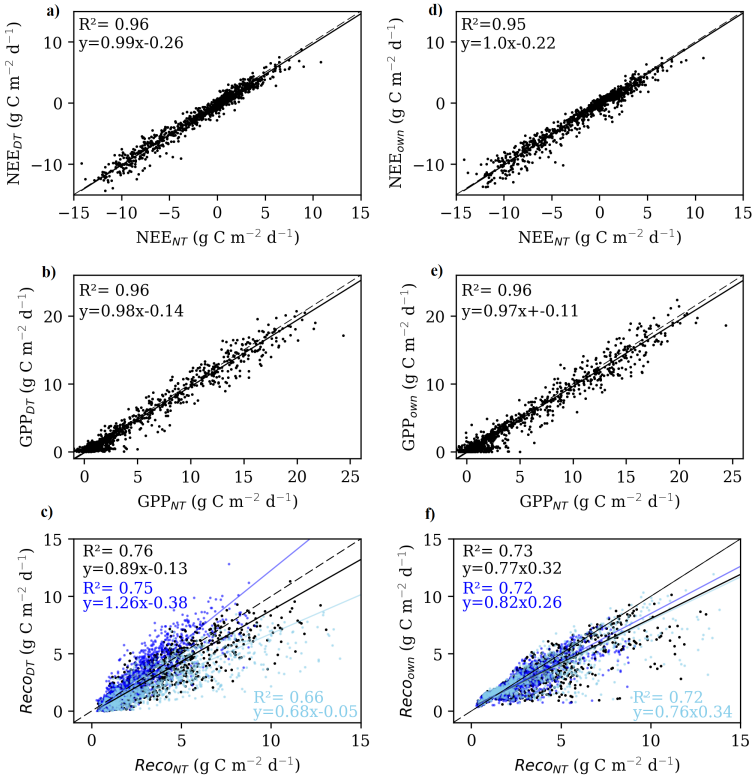

Figure 4.3.7: *Comparison of NEE, GPP and R_{eco} partitioned by the nighttime method a) to c) after Reichstein et al. (2005) (NT) vs. daytime method Lasslop et al. (2010) (DT) and our own approach (d to f). Daytime (light blue) and nighttime (darkblue) values are considered separately for R_{eco} (c and f). The dashed black line is the 1:1 line, the solid line is the reduced major axis (Webster, 1997).*

NT method versus DT and own approach. The coefficients of determination (R^2) indicate a good agreement ($R^2 \geq 0.95$) between all methods for NEE and GPP (4.3.7a,b,d and e) with a small underestimation of NEE and GPP DT and own compared to NT. Larger differences exist in the comparison of R_{eco} (DT: R^2=0.76 and own: R^2=0.73, Fig. 4.3.7c and f). While the nocturnal DT overestimates R_{eco} compared to NT and underestimates daytime respiration, only a slightly underestimation of both day and nighttime R_{eco} of the own source-partitioning application was observed. This comparison underlines the differences between the used methods and partitioned components described above.

In order to check the regression performance of the DT method and the own approach, daily sums of NEE residuals (NEE measured − NEE modelled) were tested for VPD, T_{air} and $S\downarrow$ dependency (Fig. 4.3.8). There are no clear dependencies in the residuals in the DT approach, although there are larger differences in the highest VPD, temperature and

radiation bins. This result is not surprising, since the DT method considers the temperature sensitivity of respiration and the VPD limitation of photosynthesis in the modeling (Lasslop et al., 2010). Slightly larger dependencies of NEE residuals on T_{air} (maximum +2 g C m^{-2}) are shown in the higher bins for the own partitioning tool. An elimination of the this residual dependency could also reduce the dependency on VPD and $S\downarrow$.

The above comparison showed that the use of different approaches can lead to differences

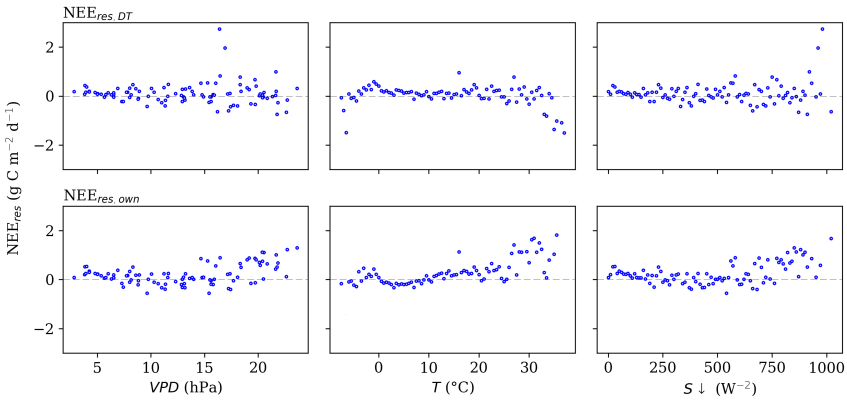

Figure 4.3.8: *Daily cumulated sums of NEE residuals tested for each source-partitioning methods after Reichstein et al. (2005) (NT), Lasslop et al. (2010) (DT) and our own approach. NEE residuals are assembled into of 0.2 hP for VPD, 0.5 °C for T_{air} and 10 W m^2 for $S\downarrow$.*

in NEE and its estimated components GPP and R_{eco}. Jérôme et al. (2010) found for a mixed forest in the Belgian Ardennes that the nighttime and daytime approach gave disagreeing results in R_{eco}. Stoy et al. (2006) tested different flux partitioning models by their information content and recommended the use of methods that use daytime NEE data for estimating R_{eco} and GPP. The reasons for the differences are not yet well understood. In the early 2000s it was observed that irradiation plays an important role in the partitioning of GPP and R_{eco}, as irradiation inhibits leaf respiration and can result in a 25 % to 100 % reduction in the respiration rate at leaf level (Heskel et al., 2013). This effect is called the Kok effect (Atkin et al., 1997). In some studies, alternative methods for estimating daytime R_{eco} were introduced. All of them were based on the principles of the Kok-method and considered R_{eco} at leaf level (Bruhn et al., 2011; Heskel et al., 2013; Wohlfahrt et al., 2005). Wohlfahrt et al. (2005) analyzed for a two year dataset of mountain meadow a reduction of GPP by 11-13 % and 13-17 %, for a low and high estimate of the maximum reduction of dark respiration at leaf level. Their findings correspond with a reduction of 15 % for a forest ecosystems (Janssens et al., 2001). In summary, night-based approaches can overestimate daytime R_{eco} caused by a reduction in leaf respiration in light. As a result, the relationship derived from nighttime data could overestimate daytime respiration and vice versa for daytime data-based estimation (Lasslop et al., 2010; Atkin et al., 1997). But also other factors can lead to differences between the approaches. Isaac et al. (2017) introduced a tool for processing flux data for Australien OzFlux sites. They stated, that daytime approaches by OzFlux, REddyProc and FLUXNET produced 20-57 % (median 37 %) smaller values of R_{eco} compared to nighttime data based methods. They assume that the use of different parameters (e.g. E_0) and u_*-thresholds led to the observed differences.

Using the same u_*-threshold for all tested sites reduced the mean difference to 22 % for R_{eco}. The underestimation of R_{eco} therefore led to an overestimation of NEE.
Our own approach, which does not separate day- and nighttime data for the partitioning, also underestimates R_{eco} compared to the used NT method. We agree with the statement given by Isaac et al. (2017), that the main focus for further work should be to reduce the differences in cumulated sums of NEE, GPP and R_{eco} given by using different source-partitioning applications.

4.4 Conclusion

We evaluated the annual net exchange of CO_2 and its components GPP and R_{eco}, as well as the total carbon budget by a 3-year winter wheat/winter barley/catch-crop/sugar beet rotation cycle of an agricultural ecosystem in Selhausen (Germany) by using EC, meteorological and biometric measurements. The second focus was on the partitioning of NEE. We used two common non-linear regression approaches for flux source-partitioning: one nighttime data-based estimation of R_{eco} and GPP and a so-called daytime data-based estimation. In addition, an own algorithm was applied. In most cases, the partitioned components of the own source-partitioning approach were between those of the other two methods and showed a overall good performance.
The cumulated NEE for the entire crop rotation was -1494 (NT:-1371, DT:-1639) g C m^{-2} and differed between the crop season from a weak source of CO_2 in catch-crop 109 (NT:77, DT:44) g C m^{-2} and strong sink in sugar beet -769 (NT:-696, DT:-740) g C m^{-2}. An overall carbon budget (including carbon import and export by fertilization, harvest and field management) of the study site turn the crop rotation cycle into a net source of 879 (NT:1002,DT:734) g C m^{-2}, as also shown in other studies dealing with various crop rotation cycles in Europe (Anthoni et al., 2004b; Ceschia et al., 2010; Béziat et al., 2009; Aubinet et al., 2009; Buysse et al., 2017; Kutsch et al., 2010). The inter-annual variability of carbon fluxes mainly depend on the climatic conditions and the crop species. Daily integrated values of NEE ranged during the 3-year crop rotation between +10 and -14 g C m^{-2} d^{-1}, with high uptake rates during the vegetation period of winter wheat and high emission rates after harvest of winter barley, due to increasing soil respiration. The observed values compare well to data from other crop studies throughout Europe.
The comparison of the source-partitioning approaches showed differences in the cumulative sums for the 3-year crop rotation. The discrepancy of annual sums between the night- (NT) and daytime (DT) based NLR was 16 % for NEE, 6 % for GPP and 15 % for R_{eco}. Even slighter differences were found in the comparison of NT versus the own approach. Here, differences in the cumulated sums varied between 5 % and 13 %. In general, R_{eco} was lower for DT and own compared to NT, resulting in higher sums of modelled NEE for DT and own.
This study showed that the use of various source-partitioning methods can lead to differences in results, especially in cumulative sums over seasons or years. For this reason, further work is needed in the future to identify the reasons of discrepancies and to explore new approaches, in order to ensure a reliable and consistent method for CO_2-flux partitioning.

5 Overall conclusions and outlook

Chapter 2 presents a prototype of an elevator based device, which measures high resolution vertical profiles of CO_2 and H_2O mole fractions, temperature and wind speed within and above dense crop canopies. In contrast to existing profile measurement techniques with a limited number of measurement heights, this system measures continuously over the entire profile height and thus allows a closer insight into the locations of scalar sources and sinks within a plant canopy until close to the soil surface. Profiles of several field campaigns were evaluated for different crops and growth stages, including 24-hour measurements that allow interesting findings on the temporal evolution of the source and sink processes. Fluxes of sensible and latent heat, CO_2 and momentum derived with the help of MOST from profile measurements with a single source/sink near the surface (mainly above bare soil) show a strong correlation to the fluxes obtained from the nearby EC station and underlines the validity of our measurement system.

A big advantage of the system is the mobility and the low weight which allows it to be set up and initialized by two people within an hour. In future studies, high resolution profile measurements could be used to validate soil-vegetation-atmosphere-exchange models that require information of different quantities, e.g. at leaf level, and thus improve their performance.

With regard to source-partitioning applications, the next step would be to quantify the measured vertical concentration profiles of CO_2 and H_2O mole fractions into their source and sink strengths, i.e. in their components NPP, R_{above} and R_s as well as in evaporation and transpiration. In the past, attempts have already been made to invert vertical concentration profiles from measurements with a finite number of measurement levels within sparse and medium-high vegetation canopies into flux densities using the inverse form of Lagrangian dispersion analysis (Raupach, 1989b; Leuning, 2000; Santos et al., 2011). Using concentrations with high vertical resolution could potentially improve the applicability and robustness of these approaches, especially in low dense plant canopies. First own tests to estimate source profiles and flux distributions were made using inversions (Warland and Thurtell, 2000; Santos et al., 2011; Cava et al., 2006). In contrast to the methods used in the literature, we apply a simplex optimization method (Nelder and Mead, 1965) to fit four parameters to the profile: soil source, total canopy source and two shape parameters of a beta distribution that describes the vertical source distribution within the canopy. Preliminary results show similar correlations between profile- and EC-derived net fluxes, while systematic deviations (regression slope < 0.8) indicate a lower robustness of their parameters compared to MOST-derived fluxes.

We discuss in section 2.4 technical possibilities and limitations of the modification of our profile system to high vegetation. Under nocturnal stable conditions, especially in tall vegetation like forests, respiratory CO_2 accumulates in the absence of turbulence and is not

transported vertically, with the result that measured NEE fluxes at EC station height is not representative anymore (Gu et al., 2004; Falge et al., 2001a). Profile measurements can be carried out, additionally to determine storage terms and thus to correct the flux measurements.

In Chapter 3, a re-naturalization project from a spruce monoculture to a deciduous forest was investigated with regard to the ecosystem atmosphere exchange of CO_2. Compared to agroecosystems, the change from a source to a sink of CO_2 in a disturbed forest ecosystem occurs significantly slower. Undisturbed forests in the middle latitude have the capability to assimilate and store large amounts of carbon, and thus contribute an important part to the global carbon cycle (Luyssaert et al., 2010). A seven year EC dataset of the forest was used, including three-years before and four years after the partial deforestation, and a four year EC dataset from the deforested site (clearcut). Measured time series of NEE were partitioned into GPP and R_{eco} using a daytimes data-driven NLR approach. In addition, R_s chamber measurements were carried out.
As expected, the undisturbed part of the forest was a strong sink for CO_2 with annual carbon uptake rates ranging between -530 (-425) and -761 (-594) g C m^{-2}. GPP and R_{eco}, of which 40 % is due to R_s, showed typical annual cumulated sums for a temperate central European spruce forest (Grünwald and Bernhofer, 2007). The deforested area was in the first year after the harvest a big source for CO_2 (net annual carbon emission of 521 (548) g C m^{-2} and returned slowly to a near neutral state 83 (236) g C m^{-2} within four years, indicating a fast regeneration of the area. Furthermore, the climate effect due to changing CO_2 sequestration was compared to the biophysical effect of changed canopy albedo. Estimates of ΔRF_α and ΔRF_{NEE} showed that the cooling effect of albedo predominates the warming effect of NEE, however, this condition will be attenuated by an increase in darker wooden plant parts. Considering CO_2 and albedo effects in combination will result in an earlier occurrence of compensation and payback points.
The dynamics of the carbon balance after disturbance, e.g., loggings, wind throws or forest fires, are often modelled or evaluated in so called chronosequence studies, with the majority of the studies referring to boreal forests. A more precise quantification of the effects of clearcutting on the above- and below-ground carbon dynamics is still lacking (Howard et al., 2004; Noormets et al., 2012; Aguilos et al., 2014). For an in-depth analysis, however, even longer measurement time series and information on paths and storage of non-CO_2-C are required.
Long-term time series will be necessary to observe and evaluate the interactions between land management and climate change. Studies have shown that natural disturbances in forest ecosystems will increase in intensity and frequency in context of climate change (Seidl et al., 2014; Hicke et al., 2012). Heat and droughts, as observed in the spring and summer of the year 2018 in Central and Northern Europe, may occur more frequently in future as a consequence of climate change (Miralles et al., 2018). Lessons learned from observations can be beneficial as a basis for decision-making on climate change mitigation strategies (Canadell and Raupach, 2008; Matthews et al., 2017).

Chapter 4 focuses again on the CO_2- flux exchange in an agroecosystem. The carbon balance of a 3-year crop rotation cycle, which is a well-established cultivation practice, was investigated. Particular interest was given to EC measured NEE and its two opposing

components GPP and R_{eco}, as well as micrometeorological and biometric measurements. The crop rotation showed typical seasonal and interannual patterns, the seasonal and daily integrated sums of NEE, GPP and R_{eco} correspond in the same order of magnitude to the values seen in the literature. The net CO_2 exchange over the whole crop rotation ranged, depending on the source-partitioning model, between -1.3 and -1.6 kg m^{-2}. This magnitude was also observed for other crop rotations, e.g. a 4 year-crop rotation of sugar beet/winter wheat/seed potato/winter wheat in Belgium (Aubinet et al., 2009). However, if in addition to the pure CO_2 exchange, the carbon import and export through seeding, harvesting and the emissions of field operations are included in the calculation of the total GHG carbon budget, the arable land in our study became a source between 0.7 and 1,0 kg m^{-2} (depending on the used source-partitioning model), which corresponds with findings of other studies (Anthoni et al., 2004b; Ceschia et al., 2010; Béziat et al., 2009; Aubinet et al., 2009; Buysse et al., 2017; Kutsch et al., 2010). A mitigation strategy applied at the Selhausen site was the cultivation of catch-crops. Our analysis showed that the catch-crop can partly absorb CO_2 until the winter during the daytime (5 g C m^{-2} d^{-1}). If other factors such as the albedo effect (as used in Chapter 3) were considered, the cultivation of catch-crops could have an additional mitigating effect on climate change, due to its higher albedo compared to bare soil.

The study in Chapter 4 also showed differences in the estimations of non-linear regression functions, which led to different cumulated sums of NEE, GPP and R_{eco}. Since the two large opposite fluxes, GPP and R_{eco}, cannot be measured directly, they can only be approximated from NEE using source-partitioning applications. According to recent studies, the bias in the estimations amount to approximately 25 % (Keenan, 2017; Jérôme et al., 2010; Isaac et al., 2017). A frequently mentioned reason for the bias in estimations is the inhibition of leaf respiration in light (Kok effect) (Heskel et al., 2013; Wohlfahrt et al., 2005; Keenan, 2017; Janssens et al., 2001). Here the use of the high resolution profile lift (Chapter 2) could help to achieve a better insight into the processes at leaf level and to understand when and how sources or sinks occur. Each of the presented source-partitioning approaches include different advantages and disadvantages. The presently used techniques are subject to constant modification and are not final (Aubinet et al., 2012). Additional efforts to improve existing methods, to combine them or to develop new routines for carbon and water flux partitioning are still necessary.

Bibliography

Acosta M, Pavelka M, Montagnani L, Kutsch W, Lindroth A, Juszczak R, Janous D (2013) Soil surface CO_2 efflux measurements in Norway spruce forests: Comparison between four different sites across Europe - from boreal to alpine forest. Geoderma 192:295–303, DOI 10.1016/j.geoderma.2012.08.027

Aguilos M, Takagi K, Liang N, Ueyama M, Fukuzawa K, Nomura M, Kishida O, Fukazawa T, Takahashi H, Kotsuka C, Sakai R, Ito K, Watanabe Y, Fujinuma Y, Takahashi Y, Murayama T, Saigusa N, Sasa K (2014) Dynamics of ecosystem carbon balance recovering from a clear-cutting in a cool-temperate forest. Agricultural and Forest Meteorology 197:26–39, DOI 10.1016/j.agrformet.2014.06.002

Ahonen T, Aalto P, Rannik Ü, Kulmala M, Nilsson ED, Palmroth S, Ylitalo H, Hari P (1997) Variations and vertical profiles of trace gas and aerosol concentrations and CO_2 exchange in Eastern Lapland. Atmospheric Environment 31:3351–3362, DOI 10.1016/S1352-2310(97)00151-9

Al-Kaisi MM, Yin X (2005) Tillage and crop residue effects on soil carbon and carbon dioxide emission in corn–soybean rotations. Journal of Environmental Quality 34(2):437–445, DOI 110.2134/jeq2005.0437

Al-Saidi A, Fukuzawa Y, Furukawa N, Ueno M, Baba S, Kawamitsu Y (2009) A system for the measurement of vertical gradients of CO_2, H_2O and air temperature within and above the canopy of plant. Plant Production Science 12:139–149, DOI 10.1626/pps.12.139

Allen Jr L, Amthor J (1995) Biotic Feedbacks in the Global Climatic System: Will the Warming Increase the Warming?, Oxford Univ. Press, New York, chap Plant physiological responses to elevated CO_2, temperature, air pollution, and UV-B radiation, pp 51–84

Amiro B, Barr A, Black T, Iwashita H, Kljun N, McCaughey J, Morgenstern K, Murayama S, Nesic Z, Orchansky A, Saigusa N (2006) Carbon, energy and water fluxes at mature and disturbed forest sites, Saskatchewan, Canada. Agricultural and Forest Meteorology 136(3):237–251

Amiro BD, Barr AG, Barr J, Black TA, Bracho R, Brown M, Chen J, Clark K, Davis K, Desai A, Dore S, Engel V, Fuentes J, Goldstein A, Goulden M, Kolb T, Lavigne M, Law B, Margolis H, Martin T, McCaughey J, Misson L, Montes-Helu M, Noormets A, Randerson J, Starr G, Xiao J (2010) Ecosystem carbon dioxide fluxes after disturbance in forests of North America. Journal of Geophysical Research: Biogeosciences 115(G4), DOI 10.1029/2010JG001390

Anthoni PM, Freibauer A, Kolle O, Schulze ED (2004a) Winter wheat carbon exchange in Thuringia, Germany. Agricultural and Forest Meteorology 121(1-2):55–67, DOI 10.1016/S0168-1923(03)00162-X

Anthoni PM, Knohl A, Rebmann C, Freibauer A, Mund M, Ziegler W, Kolle O, Schulze ED (2004b) Forest and agricultural land-use-dependent CO_2 exchange in Thuringia, Germany. Global Change Biology 10(12):2005–2019, DOI 10.1111/j.1365-2486.2004.00863.x

Arya PS (2001) Introduction to micrometeorology. Academic Press, San Diego, 420 pp

Atkin OK, Westbeek MH, Cambridge ML, Lambers H, Pons TL (1997) Leaf respiration in light and darkness (a comparison of slow-and fast-growing Poa species). Plant Physiology 113(3):961–965, DOI 10.1104/pp.113.3.961

Aubinet M, Grelle A, Ibrom A, Rannik U, Moncrieff J, Foken T, Kowalski AS, Martin PH, Berbigier P, Bernhofer C, Clement R, Elbers J, Granier A, Gruenwald T, Morgenstern K, Pilegaard K, Rebmann C, Snijders W, Valentini R, Vesala T (2000) Estimates of the annual net carbon and water exchange of forests: The EUROFLUX methodology. Advances in Ecological Research 30:113–175, DOI 0.1016/S0065-2504(08)60018-5

Aubinet M, Berbigier P, Bernhofer C, Cescatti A, Feigenwinter C, Granier A, Gruenwald T, Havrankova K, Heinesch B, Longdoz B, et al. (2005) Comparing CO_2 storage and advection conditions at night at different CARBOEUROFLUX sites. Boundary-Layer Meteorology 116:63–93, DOI 10.1007/s10546-004-7091-8

Aubinet M, Moureaux C, Bodson B, Dufranne D, Heinesch B, Suleau M, Vancutsem F, Vilret A (2009) Carbon sequestration by a crop over a 4-year sugar beet/winter wheat/seed potato/winter wheat rotation cycle. Agricultural and Forest Meteorology 149(3-4):407–418, DOI 0.1016/j.agrformet.2008.09.003

Aubinet M, Vesala T, Papale D (2012) Eddy covariance: a practical guide to measurement and data analysis. Springer, Dordrecht, 438 pp

Baatz R, Bogena H, Hendricks Franssen H, Huisman J, Montzka C, Vereecken H (2015) An empirical vegetation correction for soil water content quantification using cosmic ray probes. Water Resources Research 51:2030—2046, DOI 10.1002/2014WR016443

Baghi R, Durand P, Jambert C, Jarnot C, Delon C, Serça D, Striebig N, Ferlicoq M, Keravec P (2012) A new disjunct eddy-covariance system for BVOC flux measurements-validation on CO_2 and H_2O fluxes. Atmospheric Measurement Techniques 5:3119–3132, DOI 110.5194/amt-5-3119-2012

Baldocchi D (2014) Measuring fluxes of trace gases and energy between ecosystems and the atmosphere–the state and future of the eddy covariance method. Global Change Biology 20:3600–3609, DOI 110.1111/gcb.12649

Barr A, Richardson A, Hollinger D, Papale D, Arain M, Black T, Bohrer G, Dragoni D, Fischer M, Gu L, Law B, Margolis H, McCaughey J, Munger J, Oechel W, Schaeffer K (2013) Use of change-point detection for friction–velocity threshold evaluation in eddy-covariance studies. Agricultural and Forest Meteorology 171:31–45, DOI 10.1016/j.agrformet.2012.11.023

Barr AG, Black TA, Hogg EH, Kljun N, Morgenstern K, Nesic Z (2004) Inter-annual variability in the leaf area index of a boreal aspen-hazelnut forest in relation to net ecosystem production. Agricultural and Forest Meteorology 126(3):237–255, DOI 0.1016/j.agrformet.2004.06.011

Beckers JM, Rixen M (2003) EOF calculations and data filling from incomplete oceanographic datasets. J Atmos Ocean Technol 20(12):1839–1856

Op de Beeck M, Gielen B, Merboldt L, co authors (2015) ICOS protocol soil-meteorological variables, final version v3. Internal report, ICOS Ecosystem Thematic Centre, 48 pp

Betts R (2000) Offset of the potential carbon sink from boreal forestation by decreases in surface albedo. Nature 408(6809):187–190, DOI 10.1038/35041545

Béziat P, Ceschia E, Dedieu G (2009) Carbon balance of a three crop succession over two cropland sites in South West France. Agricultural and Forest Meteorology 149(10):1628–1645, DOI 10.1016/j.agrformet.2009.05.004

Billesbach DP (2011) Estimating uncertainties in individual eddy covariance flux measurements: a comparison of methods and a proposed new method. Agricultural and Forest Meteorology 151:394–405, DOI 10.1016/j.agrformet.2010.12.001

Bloom AJ, Mooney HA, Björkman O, Berry J (1980) Materials and methods for carbon dioxide and water exchange analysis. Plant, Cell & Environment 3:371–376, DOI 10.1111/1365-3040.ep11581885

Bogena H, Bol R, Borchard N, Brüggemann N, Diekkrüger B, Drüe C, Groh J, Gottselig N, Huisman JA, Lücke A, Missong A, Neuwirth B, Pütz T, Schmidt M, Stockinger M, Tappe W, Weihermüller L, Wiekenkamp I, Vereecken H (2015) A terrestrial observatory approach for the integrated investigation of the effects of deforestation on water, energy, and matter fluxes. Science China Earth Sciences 58:61–75, DOI 10.1007/s11430-014-4911-7

Bogena HR, Herbst M, Huisman JA, Rosenbaum U, Weuthen A, Vereecken H (2010) Potential of wireless sensor networks for measuring soil water content variability. Vadose Zone Journal 9:1002–1013, DOI 10.2136/vzj2009.0173

Bowling DR, Tans PP, Monson RK (2001) Partitioning net ecosystem carbon exchange with isotopic fluxes of CO_2. Global Change Biology 7(2):127–145, DOI 10.1046/j.1365-2486.2001.00400.x

Braswell BH, Sacks WJ, Linder E, Schimel DS (2005) Estimating diurnal to annual ecosystem parameters by synthesis of a carbon flux model with eddy covariance net ecosystem exchange observations. Global Change Biology 11(2):335–355, DOI 10.1111/j.1365-2486.2005.00897.x, URL `http://dx.doi.org/10.1111/j.1365-2486.2005.00897.x`

Brooks JR, Flanagan LB, Varney GT, Ehleringer JR (1997) Vertical gradients in photosynthetic gas exchange characteristics and refixation of respired CO_2 within boreal forest canopies. Tree Physiology 17:1–12, DOI 10.1093/treephys/17.1.1

Brosy C, Krampf K, Zeeman M, Wolf B, Junkermann W, Schäfer K, Emeis S, Kunstmann H (2017) Simultaneous multicopter-based air sampling and sensing of meteorological variables. Atmospheric Measurement Techniques 10(8):2773, DOI 10.5194/amt-10-2773-2017

Bruhn D, Mikkelsen TN, Herbst M, Kutsch WL, Ball MC, Pilegaard K (2011) Estimating daytime ecosystem respiration from eddy-flux data. Biosystems 103(2):309–313, DOI 10.1016/j.biosystems.2010.10.007

Buchmann N, Ehleringer JR (1998) CO_2 concentration profiles, and carbon and oxygen isotopes in C_3 and C_4 crop canopies. Agricultural and Forest Meteorology 89:45–58, DOI 10.1016/S0168-1923(97)00059-2

Burba GG, McDermitt DK, Grelle A, Anderson DJ, Xu L (2008) Addressing the influence of instrument surface heat exchange on the measurements of CO_2 flux from open-path gas analyzers. Global Change Biology 14(8):1854–1876, DOI 10.1111/j.1365-2486.2008.01606.x

Businger JA, Oncley SP (1990) Flux measurement with conditional sampling. Journal of Atmospheric and Oceanic Technology 7:349–352, DOI 10.1175/1520-0426(1990)007<0349:FMWCS>2.0.CO;2

Businger JA, Wyngaard JC, I Y, Bradley EF (1971) Flux-profile relationships in the atmospheric surface layer. Journal of the Atmospheric Sciences 28:181–189, DOI 10.1175/1520-0469(1971)028<0181:FPRITA>2.0.CO;2

Buysse P, Bodson B, Debacq A, De Ligne A, Heinesch B, Manise T, Moureaux C, Aubinet M (2017) Carbon budget measurement over 12 years at a crop production site in the silty-loam region in Belgium. Agricultural and Forest Meteorology 246:241–255, DOI 10.1016/j.agrformet.2017.07.004

Campbell Scientific (2003) HTF3 soil heat flux plate. Campbell Scientific, Inc., Logan, USA

Canadell JG, Raupach MR (2008) Managing forests for climate change mitigation. Science 320(5882):1456–1457, DOI 10.1126/science.1155458

Cava D, Katul GG, Scrimieri A, Poggi D, Cescatti A, Giostra U (2006) Buoyancy and the sensible heat flux budget within dense canopies. Boundary-Layer Meteorology 118(1):217–240, DOI 10.1007/s10546-005-4736-1

Ceschia E, Béziat P, Dejoux JF, Aubinet M, Bernhofer C, Bodson B, Buchmann N, Carrara A, Cellier P, Di Tommasi P, et al. (2010) Management effects on net ecosystem carbon and GHG budgets at European crop sites. Agriculture, Ecosystems & Environment 139(3):363–383, DOI 10.1016/j.agee.2010.09.020

Clark KL, Gholz HL, Castro MS (2004) Carbon dynamics along a chronosequence of Slash Pine plantations in North Florida. Ecological Applications 14(4):1154–1171, DOI 10.1890/02-5391

Darenova E, Pavelka M, Acosta M (2014) Diurnal deviations in the relationship between CO_2 efflux and temperature: A case study. Catena 123:263–269, DOI 10.1016/j.catena.2014.08.008

Davidson EA, Richardson AD, Savage KE, Hollinger DY (2006) A distinct seasonal pattern of the ratio of soil respiration to total ecosystem respiration in a spruce-dominated forest. Global Change Biology 12(2):230–239, DOI 10.1111/j.1365-2486.2005.01062.x

Denmead OT, Bradley EF (1985) Flux-gradient relationships in a forest canopy. In: The forest-atmosphere interaction, Springer, pp 421–442

Desai AR, Bolstad PV, Cook BD, Davis KJ, Carey EV (2005) Comparing net ecosystem exchange of carbon dioxide between an old-growth and mature forest in the upper Midwest, USA. Agricultural and Forest Meteorology 128(1):33–55, DOI 10.1016/j.agrformet.2004.09.005

Desai AR, Richardson AD, Moffat AM, Kattge J, Hollinger DY, Barr A, Falge E, Noormets A, Papale D, Reichstein M, et al. (2008) Cross-site evaluation of eddy covariance gpp and re decomposition techniques. Agricultural and Forest Meteorology 148:821–838, DOI 10.1016/j.agrformet.2007.11.012

Dessler AE, Sherwood SC (2009) A matter of humidity. Science 323(5917):1020–1021, DOI 10.1126/science.1171264

Detto M, Katul GG, Siqueira M, Juang JY, Stoy P (2008) The structure of turbulence near a tall forest edge: The backward-facing step flow analogy revisited. Ecological Applications 18(6):1420–1435

Dore S, Montes-Helu M, Hart SC, Hungate BA, Koch GW, Moon JB, Finkral AJ, Kolb TE (2012) Recovery of ponderosa pine ecosystem carbon and water fluxes from thinning and stand-replacing fire. Global Change Biology 18(10):3171–3185, DOI 10.1111/j.1365-2486.2012.02775.x

Drüe C (1996) Aufbau einer Profil-Messstation im Pflanzenbestand. Master's thesis, Meteorologisches Institut Universität Bonn, Auf dem Hügel 20, 53121 Bonn, Germany

Dufranne D, Moureaux C, Vancutsem F, Bodson B, Aubinet M (2011) Comparison of carbon fluxes, growth and productivity of a winter wheat crop in three contrasting growing seasons. Agriculture, Ecosystems & Environment 141(1-2):133–142, DOI 10.1016/j.agee.2011.02.023

Dwersteg D (2012) Spatial and temporal variability of soil CO_2 efflux in a spruce-dominated forest in the Eifel National Park, Germany. PhD thesis, Rheinischen Friedrich-Wilhelms-Universität Bonn

Eder F, Schmidt M, Damian T, Träumner K, Mauder M (2015) Mesoscale eddies affect near-surface turbulent exchange: evidence from lidar and tower measurements. Journal of Applied Meteorology and Climatology 54:189–206, DOI 10.1175/JAMC-D-14-0140.1

Erb KH, Kastner T, Plutzar C, Bais ALS, Carvalhais N, Fetzel T, Gingrich S, Haberl H, Lauk C, Iedertscheider MN, Pongratz J, Thurner M, Luyssaert S (2018) Unexpectedly large impact of forest management and grazing on global vegetation biomass. Nature 553(7686):73+, DOI 10.1038/nature25138

Etmann M (2009) Dendrologische Aufnahmen im Wassereinzugsgebiet Oberer Wüstebach anhand Verschiedener Mess- und Schätzverfahren. Master's thesis, Westfälische Wilhelms-Universität, Münster, Germany

Euser T, Luxemburg W, Everson C, Mengistu M, Clulow A, Bastiaanssen W (2014) A new method to measure Bowen ratios using high-resolution vertical dry and wet bulb temperature profiles. Hydrology and Earth System Sciences 18:2021–2032, DOI 10.5194/hess-18-2021-2014

Evrendilek F (2013) Quantifying biosphere–atmosphere exchange of CO_2 using eddy covariance, wavelet denoising, neural networks, and multiple regression models. Agricultural and Forest Meteorology 171:1–8, DOI 10.1016/j.agrformet.2012.11.002

Falge E, Baldocchi D, Olson R, Anthoni P, Aubinet M, Bernhofer C, Burba G, Ceulemans R, Clement R, Dolman H, Granier A, Gross P, Grünwald T, Hollinger D, Jensen NO, Katul G, Keronen P, Kowalski A, Lai CT, Law BE, Meyers T, Moncrieff J, Moors E, Munger J, Pilegaard K, Rannik Ü, Rebmann C, Suyker A, Tenhunen J, Tu K, Verma S, Vesala T, Wilson K, Wofsy S (2001a) Gap filling strategies for defensible annual sums of net ecosystem exchange. Agricultural and Forest Meteorology 107(1):43–69, DOI 10.1016/S0168-1923(00)00225-2

Falge E, Baldocchi D, Olson R, Anthoni P, Aubinet M, Bernhofer C, Burba G, Ceulemans R, Clement R, Dolman H, et al. (2001b) Gap filling strategies for long term energy flux data sets. Agricultural and Forest Meteorology 107(1):71–77, DOI 10.1016/S0168-1923(00)00235-5

FAO (2015) Statistical database. URL `http://www.fao.org/faostat/en/`, [Accessed 25 January 2019]

Finkelstein PL, Sims PF (2001) Sampling error in eddy correlation flux measurements. Journal of Geophysical Research: Atmospheres 106:3503–3509, DOI 10.1029/2000JD900731

Foken T (2006) Angewandte Meteorologie. Mikrometeorologische Methoden, 2nd edn. Springer, Berlin, 344 pp

Fotiadi AK, Lohou F, Druilhet A, Serça D, Brunet Y, Delmas R (2005a) Methodological development of the conditional sampling method. part I: Sensitivity to statistical and technical characteristics. Boundary-Layer Meteorology 114(3):615–640, DOI 10.1007/s10546-004-1080-9

Fotiadi AK, Lohou F, Druilhet A, Serça D, Said F, Laville P, Brut A (2005b) Methodological development of the conditional sampling method. part II: Quality control criteria of relaxed eddy accumulation flux measurements. Boundary-Layer Meteorology 117(3):577–603, DOI 10.1007/s10546-005-4497-x

Gifford R (1984) Energy in different agricultural systems: renewable and nonrenewable sources. In: Energy and agriculture, Springer, pp 84–112, DOI 10.1007/978-3-642-69784-5_5

Gottselig N, Wiekenkamp I, Weihermüller L, Brüggemann N, Berns A, Bogena H, Borchard N, Klumpp E, Lücke A, Missong A, Pütz T, Vereecken H, Huisman JA, Bol R (2017) A three-dimensional view on soil biogeochemistry: A dataset for a forested headwater catchment. Journal of Environmental Quality 46(1):210–218, DOI 10.2134/jeq2016.07.0276

Gough C, Vogel CS, Harrold KH, George K, Curtis PS (2007) The legacy of harvest and fire on ecosystem carbon storage in a north temperate forest. Global Change Biology 13(9):1935–1949, DOI 10.1111/j.1365-2486.2007.01406.x

Goulden ML, Miller SD, Da Rocha HR (2006) Nocturnal cold air drainage and pooling in a tropical forest. Journal of Geophysical Research: Atmospheres 111(D8), DOI 10.1029/2005JD006037

Gove J, Hollinger D (2006) Application of a dual unscented Kalman filter for simultaneous state and parameter estimation in problems of surface-atmosphere exchange. Journal of Geophysical Research: Atmospheres 111(D8), DOI 10.1029/2005JD006021

Graf A (2017) Gap-filling meteorological variables with Empirical Orthogonal Functions. EGU 2017 General Assembly, Vienna (Austria), 23 Apr 2017 - 28 Apr 2017, URL `https://juser.fz-juelich.de/record/829701`, [Accessed 25 January 2019]

Graf A, Weihermüller L, Huisman JA, Herbst M, Bauer J, Vereecken H (2008) Measurement depth effects on the apparent temperature sensitivity of soil respiration in field studies. Biogeosciences 5:1175–1188, DOI 10.5194/bg-5-1175-2008

Graf A, Schüttemeyer D, Geiß H, Knaps A, Möllmann-Coers M, Schween JH, Kollet S, Neininger B, Herbst M, Vereecken H (2010) Boundedness of turbulent temperature probability distributions, and their relation to the vertical profile in the convective boundary layer. Boundary-Layer Meteorology 134(3):459–486, DOI 10.1007/s10546-009-9444-9

Graf A, Herbst M, Weihermüller L, Huisman JA, Prolingheuer N, Bornemann L, Vereecken H (2012) Analyzing spatiotemporal variability of heterotrophic soil respiration at the field scale using orthogonal functions. Geoderma 181:91–101, DOI 10.1016/j.geoderma.2012.02.016

Graf A, Werner J, Langensiepen M, van de Boer A, Schmidt M, Kupisch M, Vereecken H (2013) Validation of a minimum microclimate disturbance chamber for net ecosystem flux measurements. Agricultural and Forest Meteorology 174:1–14, DOI 10.1016/j.agrformet.2013.02.001

Graf A, Bogena HR, Drüe C, Hardelauf H, Pütz T, Heinemann G, Vereecken H (2014) Spatiotemporal relations between water budget components and soil water content in a forested tributary catchment. Water Resources Research 50:4837–4857, DOI 10.1002/2013WR014516

Grant R, Barr A, Black T, Margolis H, McCaughey J, Trofymow J (2010) Net ecosystem productivity of temperate and boreal forests after clearcutting—a Fluxnet-Canada measurement and modelling synthesis. Tellus B 62(5):475–496, DOI 10.1111/j.1600-0889.2010.00500.x

Grünwald T, Bernhofer C (2007) A decade of carbon, water and energy flux measurements of an old spruce forest at the Anchor Station Tharandt. Tellus B 59(3):387–396, DOI 10.1111/j.1600-0889.2007.00259.x

Gryning SE, Batchvarova E, De Bruin HAR (2001) Energy balance of a sparse coniferous high-latitude forest under winter conditions. Boundary-Layer Meteorology 99:465–488, DOI 10.1023/A:1018939329915

Gu L, Falge E, Boden T, Baldocchi D, Black T, Saleska SR, Suni T, Verma SB, Vesala T (2004) Objective threshold determination for nighttime eddy flux filtering. Agricultural and Forest Meteorology 128:179–197, DOI 10.1016/j.agrformet.2004.11.006

Haverd V, Cuntz M, Griffith D, Keitel C, Tadros C, Twining J (2011) Measured deuterium in water vapour concentration does not improve the constraint on the partitioning of evapotranspiration in a tall forest canopy, as estimated using a soil vegetation atmosphere transfer model. Agricultural and Forest Meteorology 151:645–654, DOI 10.1016/j.agrformet.2011.02.005

Heskel MA, Atkin OK, Turnbull MH, Griffin KL (2013) Bringing the Kok effect to light: a review on the integration of daytime respiration and net ecosystem exchange. Ecosphere 4(8):1–14, DOI 10.1890/ES13-00120.1

Hicke JA, Allen CD, Desai AR, Dietze MC, Hall RJ, Hogg ETH, Kashian DM, Moore D, Raffa KF, Sturrock RN, Vogelmann J (2012) Effects of biotic disturbances on forest carbon cycling in the United States and Canada. Global Change Biology 18(1):7–34, DOI 10.1111/j.1365-2486.2011.02543.x

Högström U (1988) Non-dimensional wind and temperature profiles in the atmospheric surface layer: A re-evaluation. Boundary-Layer Meteorology 42:55–78, DOI 10.1007/978-94-009-2935-7_6

Hollinger DY, Aber J, Dail B, Davidson EA, Goltz SM, Hughes H, Leclerc MY, Lee JT, Richardson AD, Rodrigues C, Scott NA, Achuatavarier D, Walsh J (2004) Spatial and temporal variability in forest–atmosphere CO_2 exchange. Global Change Biology 10(10):1689–1706, DOI 10.1111/j.1365-2486.2004.00847.x

Houghton RA, Skole DL, Nobre CA, Hackler JL, Lawrence KT, Chomentowski WH (2000) Annual fluxes of carbon from deforestation and regrowth in the Brazilian Amazon. Nature 403(6767):301, DOI 10.1038/35002062

Howard EA, Gower ST, Foley JA, Kucharik CJ (2004) Effects of logging on carbon dynamics of a jack pine forest in Saskatchewan, Canada. Global Change Biology 10(8):1267–1284, DOI 10.1111/j.1529-8817.2003.00804.x

Humphreys ER, Andrew Black T, Morgenstern K, Li Z, Nesic Z (2005) Net ecosystem production of a Douglas-fir stand for 3 years following clearcut harvesting. Global Change Biology 11(3):450–464, DOI 10.1111/j.1365-2486.2005.00914.x

Humphreys ER, Black TA, Morgenstern K, Cai T, Drewitt GB, Nesic Z, Trofymow JA (2006) Carbon dioxide fluxes in coastal Douglas-fir stands at different stages of development after clearcut harvesting. Agricultural and Forest Meteorology 140(1):6–22, DOI 10.1016/j.agrformet.2006.03.018

Ibrom A, Dellwik E, Flyvbjerg H, Jensen NO, Pilegaard K (2007) Strong low-pass filtering effects on water vapour flux measurements with closed-path eddy correlation systems. Agricultural and Forest Meteorology 147:140–156, DOI 10.1016/j.agrformet.2007.07.007

Isaac P, Cleverly J, McHugh I, Gorsel Ev, Ewenz C, Beringer J (2017) OzFlux Data: Network integration from collection to curation. Biogeosciences 14(12):2903–2928, DOI 10.5194/bg-14-2903-2017

Jacobs A, Van Boxel J, El-Kilani R (1994) Nighttime free convection characteristics within a plant canopy. Boundary-Layer Meteorology 71:375–391, DOI 10.1007/BF00712176

Jäggi M, Ammann C, Neftel A, Fuhrer J (2006) Environmental control of profiles of ozone concentration in a grassland canopy. Atmospheric Environment 40:5496–5507, DOI 10.1016/j.atmosenv.2006.01.025

Janssens IA, Lankreijer H, Matteucci G, Kowalski AS, Buchmann N, Epron D, Pilegaard K, Kutsch W, Longdoz B, Grünwald T, et al. (2001) Productivity overshadows temperature in determining soil and ecosystem respiration across European forests. Global Change Biology 7(3):269–278, DOI 10.1046/j.1365-2486.2001.00412.x

Järvi L, Mammarella I, Eugster W, Ibrom A, Siivola E, Dellwik E, Keronen P, Burba G, Vesala T (2009) Comparison of net CO_2 fluxes measured with open-and closed-path infrared gas analyzers in an urban complex environment. Boreal Environment Research 14:499–514

Jérôme E, Aubinet M, Heinesch B (2010) Long term carbon dioxide exchange above a mixed forest in the Belgian Ardennes: evaluation of different approaches to deduce total ecosystem respiration from Eddy covariance measurements. EGU 2010 General Assembly, Vienna (Austria), 23 Apr 2017 - 28 Apr 2017

Kaimal JC, Finnigan JJ (1994) Atmospheric boundary layer flows: their structure and measurement. Oxford University Press, New York, 289 pp

Keane JB, Ineson P (2017) Technical note: Differences in the diurnal pattern of soil respiration under adjacent miscanthus giganteus and barley crops reveal potential flaws in accepted sampling strategies. Biogeosciences 14:1181

Keenan TF (2017) Widespread inhibition of day-time ecosystem respiration and implications for eddy-covariance flux partitioning. AGU Fall Meeting 2017, New Orleans (USA), 11 Dec 2017 - 16 Dec 2017

Keenan TF, Prentice IC, Canadell JG, Williams CA, Wang H, Raupach M, Collatz GJ (2016) Recent pause in the growth rate of atmospheric CO_2 due to enhanced terrestrial carbon uptake. Nature Communications 7:13428, DOI 10.1038/ncomms13428

Kessomkiat W, Franssen HJH, Graf A, Vereecken H (2013) Estimating random errors of eddy covariance data: An extended two-tower approach. Agricultural and Forest Meteorology 171:203–219, DOI 10.1016/j.agrformet.2012.11.019

Kimball B, Mauney J, Nakayama F, Idso S (1993) Effects of increasing atmospheric CO_2 on vegetation. Vegetatio 104/105:65–76, DOI 10.1007/978-94-011-1797-5_5

Kittler F, Eugster W, Foken T, Heimann M, Kolle O, Göckede M (2017) High-quality eddy-covariance CO_2 budgets under cold climate conditions. Journal of Geophysical Research: Biogeosciences 122(8):2064–2084, DOI 10.1002/2017JG003830

Klosterhalfen A, Herbst M, Weihermüller L, Graf A, Schmidt M, Stadler A, Schneider K, Subke JA, Huisman JA, Vereecken H (2017) Multi-site calibration and validation of a net ecosystem carbon exchange model for croplands. Ecological Modelling 363:137–156, DOI 10.1016/j.ecolmodel.2017.07.028

Knohl A, Kolle O, Minayeva TY, Milyukova IM, Vygodskaya NN, Foken T, Schulze ED (2002) Carbon dioxide exchange of a russian boreal forest after disturbance by wind throw. Global Change Biology 8(3):231–246, DOI 10.1046/j.1365-2486.2002.00475.x

Knorr W, Kattge J (2005) Inversion of terrestrial ecosystem model parameter values against eddy covariance measurements by Monte Carlo sampling. Global Change Biology 11(8):1333–1351, DOI 10.1111/j.1365-2486.2005.00977.x

Kolari P, Pumpanen J, Rannik Ü, Ilvesniemi H, Hari P, Berninger F (2004) Carbon balance of different aged Scots pine forests in Southern Finland. Global Change Biology 10(7):1106–1119, DOI 10.1111/j.1529-8817.2003.00797.x

Kormann R, Meixner FX (2001) An analytical footprint model for non-neutral stratification. Boundary-Layer Meteorology 99:207–224, DOI 10.1023/A:1018991015119

Kowalski AS, Loustau D, Berbigier P, Manca G, Tedeschi V, Borghetti M, Valentini R, Kolari P, Berninger F, Rannik Ü, Hari P, Rayment M, Mencuccini M, Moncrieff J, Grace J (2004) Paired comparisons of carbon exchange between undisturbed and regenerating stands in four managed forests in Europe. Global Change Biology 10(10):1707–1723, DOI 10.1111/j.1365-2486.2004.00846.x

Kowalski S, Sartore M, Burlett R, Berbigier P, Loustau D (2003) The annual carbon budget of a French pine forest (Pinus pinaster) following harvest. Global Change Biology 9(7):1051–1065, DOI 10.1046/j.1365-2486.2003.00627.x

Kulmala L, Aaltonen H, Berninger F, Kieloaho AJ, Levula J, B/"ack J, Hari P, Kolari P, Korhonen JF, Kulmala M, Nikinmaa E, Pihlatie M, Vesala T, Pumpanen J (2014) Changes in biogeochemistry and carbon fluxes in a boreal forest after the clear-cutting and partial burning of slash. Agricultural and Forest Meteorology 188:33–44, DOI 10.1016/j.agrformet.2013.12.003

Kutsch W, Aubinet M, Buchmann N, Smith P, Osborne B, Eugster W, Wattenbach M, Schrumpf M, Schulze E, Tomelleri E, Ceschia E, Bernhofer C, Carrara A, Di Tommasi P, Grünwald T, Jones M, Magliulo V, Ziegler W (2010) The net biome production of full crop rotations in Europe. Agriculture, Ecosystems & Environment 139(3):336–345, DOI 10.1016/j.agee.2010.07.016

Kuzyakov Y, Gavrichkova O (2010) REVIEW: Time lag between photosynthesis and carbon dioxide efflux from soil: a review of mechanisms and controls. Global Change Biology 16(12):3386–3406, DOI 10.1111/j.1365-2486.2010.02179.x

Lasslop G, Reichstein M, Papale D, Richardson AD, Arneth A, Barr A, Stoy P, Wohlfahrt G (2010) Separation of net ecosystem exchange into assimilation and respiration using a light response curve approach: critical issues and global evaluation. Global Change Biology 16(1):187–208, DOI 10.1111/j.1365-2486.2009.02041.x

Lehmkuhl F, Loibl D, Borchardt H (2010) Geomorphological map of the Wüstebach (Nationalpark Eifel, Germany) - an example of human impact on mid-European mountain areas. Journal of Maps 6:520–530, DOI 10.4113/jom.2010.1118

Lenschow DH, Mann J, Kristensen L (1994) How long is long enough when measuring fluxes and other turbulence statistics? Journal of Atmospheric and Oceanic Technology 11:661–673, DOI 10.1175/1520-0426(1994)011<0661:HLILEW>2.0.CO;2

Leuning R (2000) Estimation of scalar source/sink distributions in plant canopies using Lagrangian dispersion analysis: corrections for atmospheric stability and comparison with a multilayer canopy model. Boundary-Layer Meteorology 96:293–314, DOI 10.1023/A:1002449700617

Lindauer M, Schmid HP, Grote R, Mauder M, Steinbrecher R, Wolpert B (2014) Net ecosystem exchange over a non-cleared wind-throw-disturbed upland spruce forest—Measurements and simulations. Agricultural and Forest Meteorology 197:219–234, DOI 10.1016/j.agrformet.2014.07.005

Lindroth A, Lagergren F, Grelle A, Klemedtsson L, Langvall O, Weslien P, Tuulik J (2009) Storms can cause Europe-wide reduction in forest carbon sink. Global Change Biology 15(2):346–355, DOI 10.1111/j.1365-2486.2008.01719.x

Liu S, Xu H, Ding J, Chen HYH, Wang J, Xu Z, Ruan H, Chen Y (2016) CO_2 emission increases with damage severity in moso bamboo forests following a winter storm in Southern China. Scientific reports 6:30351, DOI 10.1038/srep30351

Lloyd J, Taylor JA (1994) On the temperature dependence of soil respiration. Functional Ecology pp 315–323, DOI 10.2307/2389824

Lothon M, Lohou F, Pino D, Couvreux F, Pardyjak E, Reuder J, Vilà-Guerau De Arellano J, Durand P, Hartogensis O, Legain D, et al. (2014) The BLLAST field experiment: Boundary-layer late afternoon and sunset turbulence. Atmospheric Chemistry and Physics 14:10931–10960, DOI 10.5194/acp-14-10931-2014

Luyssaert S, Schulze ED, Boerner A, Knohl A, Hessenmoeller D, Law BE, Ciais P, Grace J (2008) Old-growth forests as global carbon sinks. Nature 455(7210):213–215, DOI 10.1038/nature07276

Luyssaert S, Ciais P, Piao S, Schulze ED, Jung M, Zaehle S, Schelhaas M, Reichstein M, Churkina G, Papale D, et al. (2010) The European carbon balance. Part 3: forests. Global Change Biology 16(5):1429–14500, DOI 10.1111/j.1365-2486.2009.02056.x

Maitani T, Seo T (1986) A case study of temperature fluctuations within and above a wheat field before and after sunset. Boundary-Layer Meteorology 35:247–256, DOI 10.1007/BF00123643

Mammarella I, Launiainen S, Gronholm T, Keronen P, Pumpanen J, Rannik Ü, Vesala T (2009) Relative humidity effect on the high-frequency attenuation of water vapor flux measured by a closed-path eddy covariance system. Journal of Atmospheric and Oceanic Technology 26:1856–1866, DOI 10.1175/2009JTECHA1179.1

Matthews B, Mayer M, Katzensteiner K, Godbold DL, Schume H (2017) Turbulent energy and carbon dioxide exchange along an early-successional windthrow chronosequence in the European Alps. Agricultural and Forest Meteorology 232:576–594, DOI 10.1016/j.agrformet.2016.10.011

Matthies BD, Valsta LT (2016) Optimal forest species mixture with carbon storage and albedo effect for climate change mitigation. Ecological Economics 123:95–105, DOI 10.1016/j.ecolecon.2016.01.004

Mauder M, Foken T (2011) Documentation and instruction manual of the eddy-covariance software package TK3, vol 46. University of Bayreuth, Department of Micrometeorology

Mauder M, Cuntz M, Drüe C, Graf A, Rebmann C, Schmid HP, Schmidt M, Steinbrecher R (2013) A strategy for quality and uncertainty assessment of long-term eddy-covariance measurements. Agricultural and Forest Meteorology 169:122–135, DOI 10.1016/j.agrformet.2012.09.006

Mayer JC, Hens K, Rummel U, Meixner FX, Foken T (2009) Moving measurement platforms–specific challenges and corrections. Meteorologische Zeitschrift 18(5):477–488, DOI 10.1127/0941-2948/2009/0401

Mayer JC, Bargsten A, Rummel U, Meixner FX, Foken T (2011) Distributed modified bowen ratio method for surface layer fluxes of reactive and non-reactive trace gases. Agricultural and Forest Meteorology 151(6):655–668, DOI 10.1016/j.agrformet.2010.10.001

Michaelis L, Menten M (1913) Die Kinetik der Invertinwirkung. Biochemische Zeitschrift 49:352

Miralles DG, Gentine P, Seneviratne SI, Teuling AJ (2018) Land–atmospheric feedbacks during droughts and heatwaves: state of the science and current challenges. Annals of the New York Academy of Sciences pp 1–17, DOI 10.1111/nyas.13912

Miyata A, Leuning R, Denmead OT, Kim J, Harazono Y (2000) Carbon dioxide and methane fluxes from an intermittently flooded paddy field. Agricultural and Forest Meteorology 102:287–303, DOI 10.1016/S0168-1923(00)00092-7

Moderow U, Aubinet M, Feigenwinter C, Kolle O, Lindroth A, Mölder M, Montagnani L, Rebmann C, Bernhofer C (2009) Available energy and energy balance closure at four coniferous forest sites across Europe. Theoretical and applied climatology 98(3-4):397–412, DOI 10.1007/s00704-009-0175-0

Moene AF, Michels BI (2002) Estimation of the statistical error in large eddy simulation results. In: 15th Symposium on Boundary Layers and Turbulence, 15-19 July 2002, Wageningen, The Netherlands, pp 287–288

Moffat AM, Papale D, Reichstein M, Hollinger DY, Richardson AD, Barr AG, Beckstein C, Braswell BH, Churkina G, Desai AR, Falge E, Govec JH, Heimann M, Huij D, Jarvisk AJ, Kattgea J, Noormetsl A, Stauch VJ (2007) Comprehensive comparison of gap-filling techniques for eddy covariance net carbon fluxes. Agricultural and Forest Meteorology 147(3):209–232, DOI 10.1016/j.agrformet.2007.08.011

Moffat AM, Beckstein C, Churkina G, Mund M, Heimann M (2010) Characterization of ecosystem responses to climatic controls using artificial neural networks. Global change biology 16(10):2737–2749, DOI 10.1111/j.1365-2486.2010.02171.x

Molchanov AG, Kurbatova YA, Olchev AV (2017) Effect of clear-cutting on soil co_2 emission. Biology Bulletin 44(2):218–223, DOI 10.1134/S1062359016060121

Montagnani L, Manca G, Canepa E, Georgieva E, Acosta M, Feigenwinter C, Janous D, Kerschbaumer G, Lindroth A, Minach L, Minerbi S, Mölder M, Pavelka M, Seufert G, Zeri M, Ziegler W (2009) A new mass conservation approach to the study of co_2 advection in an alpine forest. Journal of Geophysical Research: Atmospheres 114(D7), DOI 10.1029/2008JD010650

Monteith J, Unsworth M (2013) Principles of environmental physics: plants, animals, and the atmosphere, 4th edn. Elsevier, Ltd., 423 pp

Moureaux C, Debacq A, Bodson B, Heinesch B, Aubinet M (2006) Annual net ecosystem carbon exchange by a sugar beet crop. Agricultural and Forest Meteorology 139(1-2):25–39, DOI 10.1016/j.agrformet.2006.05.009

Munger JW, Loescher HW, Luo H (2012) Measurement, tower, and site design considerations. In: Eddy Covariance, Springer, pp 21–58, DOI 10.1007/978-94-007-2351-1_2

Myhre G, Highwood EJ, Shine KP, Stordal F (1998) New estimates of radiative forcing due to well mixed greenhouse gases. Geophysical Research Letters 25(14):2715–2718, DOI 10.1029/98GL01908

Nelder JA, Mead R (1965) A simplex method for function minimization. The Computer Journal 7(4):308–313, DOI 10.1093/comjnl/7.4.308

Ney P, Graf A (2018) High-resolution vertical profile measurements for carbon dioxide and water vapour concentrations within and above crop canopies. Boundary-Layer Meteorology 166(3):449–473, DOI 10.1007/s10546-017-0316-4

Ney P, Schmidt M, Klosterhalfen A, Graf A (2017) A high-resolution measurement technique for vertical co_2 and h_2o profiles within and above crop canopies and its use for flux partitioning. EGU 2017 General Assembly, Vienna (Austria), 23 Apr 2017 - 28 Apr 2017, URL `https://juser.fz-juelich.de/record/829700/files/Poster.pdf`, [Accessed 25 January 2019]

Noone D, Risi C, Bailey A, Berkelhammer M, Brown D, Buenning N, Gregory S, Nusbaumer J, Schneider D, Sykes J, Vanderwende B, Wong J, Meillier Y, Wolfe D (2013) Determining water sources in the boundary layer from tall tower profiles of water vapor and surface water isotope

ratios after a snowstorm in Colorado. Atmospheric Chemistry and Physics 13:1607–1623, DOI 10.5194/acp-13-1607-2013

Noormets A, Chen J, Crow TR (2007) Age-dependent changes in ecosystem carbon fluxes in managed forests in northern Wisconsin, USA. Ecosystems 10(2):187–203, DOI 10.1007/s10021-007-9018-y

Noormets A, McNulty SG, Domec JC, Gavazzi G Mand Sun, King JS (2012) The role of harvest residue in rotation cycle carbon balance in loblolly pine plantations. respiration partitioning approach. Global Change Biology 18(10):3186–3201, DOI 10.1111/j.1365-2486.2012.02776.x

Nordbo A, Kekäläinen P, Siivola E, Lehto R, Vesala T, Timonen J (2013) Tube transport of water vapor with condensation and desorption. Applied Physics Letters 102:194101, DOI 10.1063/1.4804639

North GR, Pyle JA, Zhang F (2014) Encyclopedia of Atmospheric Sciences, vol 2, 2nd edn. Elsevier, 10pp

Panofsky HA, Dutton JA (1984) Atmospheric turbulence. Models and methods for engineering applications. John Wiley & Sons, Inc., New York, 397 pp

Papale D, Valentini R (2003) A new assessment of European forests carbon exchanges by eddy fluxes and artificial neural network spatialization. Global Change Biology 9(4):525–535, DOI 10.1046/j.1365-2486.2003.00609.x

Papale D, Reichstein M, Aubinet M, Canfora E, Bernhofer C, Kutsch W, Longdoz B, Rambal S, Valentini R, Vesala T, Yakir D (2006) Towards a standardized processing of Net Ecosystem Exchange measured with eddy covariance technique: algorithms and uncertainty estimation. Biogeosciences 3:571–583, DOI 10.5194/bg-3-571-2006

Paul-Limoges E, Black T, Christen A, Nesic Z, Jassal R (2015) Effect of clearcut harvesting on the carbon balance of a Douglas-fir forest. Agricultural and Forest Meteorology 203:30–42, DOI 10.1016/j.agrformet.2014.12.010

Pavelka M, Acosta M, Marek MV, Kutsch W, Janous D (2007) Dependence of the Q10 values on the depth of the soil temperature measuring point. Plant and Soil 292(1-2):171–179, DOI 10.1007/s11104-007-9213-9

Phillips CL, Nickerson N, Risk D, Bond BJ (2011) Interpreting diel hysteresis between soil respiration and temperature. Global Change Biology 17(1):515–527, DOI 10.1111/j.1365-2486.2010.02250.x

Rannik Ü, Altimir N, Raittila J, Suni T, Gaman A, Hussein T, Hölttä T, Lassila H, Latokartano M, Lauri A, Natsheh A, Petäjä T, Sorjamaa R, Ylä-Mella H, Keronen P, Berninger F, Vesala T, Hari P, Kulmala M (2002) Fluxes of carbon dioxide and water vapour over Scots pine forest and clearing. Agricultural and Forest Meteorology 111(3):187–202, DOI 10.1016/S0168-1923(02)00022-9

Raupach MR (1989a) Applying lagrangian fluid mechanics to infer scalar source distributions from concentration profiles in plant canopies. Agricultural and Forest Meteorology 47(2-4):85–108, DOI 10.1016/0168-1923(89)90089-0

Raupach MR (1989b) A practical Lagrangian method for relating scalar concentrations to source distributions in vegetation canopies. Quarterly Journal of the Royal Meteorological Society 115:609–632, DOI 10.1002/qj.49711548710

Ravindranath NH, Ostwald M (2008) Carbon Inventory Methods: Handbook for Greenhouse Gas Inventory, Carbon Mitigation and Roundwood Production Projects. Springer Netherlands, Dordrecht

REddyProc Team (2014) REddyProc: Data processing and plotting utilities of (half-) hourly eddy-covariance measurements. R package version 1.1.3. URL `https://www.bgc-jena.mpg.de/bgi/index.php/Services/REddyProcWebRPackage`, [Accessed 25 January 2019]

Reichstein M, Falge E, Baldocchi D, Papale D, Aubinet M, Berbigier P, Bernhofer C, Buchmann N, Gilmanov T, Granier A, Gruenwald T, Havrankova K, Janous D, Knohl A, Laurela T, Lohila A, Loustau D, Matteucci G, Meyers T, Miglietta F, Ourcival JM, Rambal S, Rotenberg E, Sanz M, Tenhunen J, Seufert G, Vaccari F, Vesala T, Yakir D (2005) On the separation of net ecosystem exchange into assimilation and ecosystem respiration: Review and improved algorithm. Global Change Biology 11:1424–1439, DOI 0.1111/j.1365-2486.2005.001002.x

Reverter BR, Carrara A, Fernández A, Gimeno C, Sanz M, Serrano-Ortiz P, Sánchez-Cañete E, Were A, Domingo F, Resco V, Burba G, Kowalski A (2011) Adjustment of annual NEE and ET for the open-path IRGA self-heating correction: Magnitude and approximation over a range of climate. Agricultural and Forest Meteorology 151(12):1856–1861, DOI 10.1016/j.agrformet.2011.06.001

Richardson AD, Hollinger DY (2007) A method to estimate the additional uncertainty in gap-filled nee resulting from long gaps in the CO_2 flux record. Agricultural and Forest Meteorology 147(3):199–208, DOI 10.1016/j.agrformet.2007.06.004

Richardson AD, Braswell BH, Hollinger DY, Burman P, Davidson EA, Evans RS, Flanagan LB, Munger JW, Savage K, Urbanski SP, et al. (2006) Comparing simple respiration models for eddy flux and dynamic chamber data. Agricultural and Forest Meteorology 141(2-4):219–234, DOI 10.1016/j.agrformet.2006.10.010

Rinne HJI, Guenther AB, Warneke C, De Gouw JA, Luxembourg SL (2001) Disjunct eddy covariance technique for trace gas flux measurements. Geophysical Research Letters 28(16), DOI 10.1029/2001GL012900

Rosenbaum U, Bogena HR, Herbst M, Huisman JA, Peterson TJ, Weuthen A, Western AW, Vereecken H (2012) Seasonal and event dynamics of spatial soil moisture patterns at the small catchment scale. Water Resources Research 48(10), DOI 10.1029/2011WR011518

Rotenberg E, Yakir D (2010) Contribution of semi-arid forests to the climate system. Science 327(5964):451–454, DOI 10.1126/science.1179998

Santos EA, Wagner-Riddle C, Warland JS, Brown S (2011) Applying a Lagrangian dispersion analysis to infer carbon dioxide and latent heat fluxes in a corn canopy. Agricultural and Forest Meteorology 151:620–632, DOI 10.1016/j.agrformet.2011.01.010

Scanlon TM, Kustas WP (2010) Partitioning carbon dioxide and water vapor fluxes using correlation analysis. Agricultural and Forest Meteorology 150(1):89–99, DOI 10.1016/j.agrformet.2009.09.005

Scanlon TM, Sahu P (2008) On the correlation structure of water vapor and carbon dioxide in the atmospheric surface layer: A basis for flux partitioning. Water Resources Research 44(10), DOI 10.1029/2008WR006932

Schmidt M, Reichenau TG, Fiener P, Schneider K (2012) The carbon budget of a winter wheat field: An eddy covariance analysis of seasonal and inter-annual variability. Agricultural and Forest Meteorology 165:114–126, DOI 10.1016/j.agrformet.2012.05.012

Schmidt-Vogt H (1989) Die Fichte: ein Handbuch in zwei Bänden. Band 2 Krankheiten, Schäden, Fichtensterben. Hamburg, Germany: Parey-Verlag

Seidl R, Rammer W, Jäger D, Lexer MJ (2008) Impact of bark beetle (Ips typographus L.) disturbance on timber production and carbon sequestration in different management strategies under climate change. Forest Ecology and Management 256(3):209–220, DOI 10.1016/j.foreco.2008.04.002

Seidl R, Schelhaas MJ, Rammer W, Verkerk PJ (2014) Increasing forest disturbances in Europe and their impact on carbon storage. Nature climate change 4(9):806, DOI 10.1038/nclimate2318

Soegaard H, Jensen NO, Boegh E, Hasager CB, Schelde K, Thomsen A (2003) Carbon dioxide exchange over agricultural landscape using eddy correlation and footprint modelling. Agricultural and Forest Meteorology 114(3-4):153–173, DOI 10.1016/S0168-1923(02)00177-6

Sogachev A, Leclerc M, Karipot A, Zhang G, Vesala T (2005) Effect of clearcuts on footprints and flux measurements above a forest canopy. Agricultural and Forest Meteorology 133:182–196, DOI 10.1016/j.agrformet.2005.09.008

Stauch VJ, Jarvis AJ (2006) A semi-parametric gap-filling model for eddy covariance CO_2 flux time series data. Global Change Biology 12(9):1707–1716, DOI 10.1111/j.1365-2486.2006.01227.x

Stocker T, Qin D, Plattner GK, Tignor M, Allen S, Boschung J, Nauels A, Xia Y, Bex V, Midgley P (2013) Climate change 2013: The physical science basis. working group I contribution to the fifth assessment report of the intergovernmental panel on climate change. Cambridge University Press

Stoy PC, Katul GG, Siqueira MBS, Juang JY, Novick KA, Uebelherr JM, Oren R (2006) An evaluation of models for partitioning eddy covariance-measured net ecosystem exchange into photosynthesis and respiration. Agricultural and Forest Meteorology 141(1):2–18, DOI 10.1016/j.agrformet.2006.09.001

Takagi K, Fukuzawa K, Liang N, Kayama M, Nomura M, Hojyo H, Sugata S, Shibata H, Fukazawa T, Takahashi Y, Nakaji T, Oguma H, Mano M, Akibayashi Y, Murayama T, Koike T, Sasa K, Fujinuma Y (2009) Change in CO_2 balance under a series of forestry activities in a cool-temperate mixed forest with dense undergrowth. Global Change Biology 15(5):1275–1288, DOI 10.1111/j.1365-2486.2008.01795.x

Thomas C, Martin JG, Goeckede M, Siqueira MB, Foken T, Law BE, Loescher HW, Katul G (2008) Estimating daytime subcanopy respiration from conditional sampling methods applied to multi-scalar high frequency turbulence time series. Agricultural and Forest Meteorology 148(8):1210–1229, DOI 10.1016/j.agrformet.2008.03.002

Thomas CK, Kennedy AM, Selker JS, Moretti A, Schroth MH, Smoot AR, Tufillaro NB, Zeeman MJ (2012) High-resolution fibre-optic temperature sensing: A new tool to study the two-dimensional structure of atmospheric surface-layer flow. Boundary-Layer Meteorology 142:177–192, DOI 10.1007/s10546-011-9672-7

Valentini R, Matteucci G, Dolman A, Schulze ED, Rebmann C, Moors E, Granier A, Gross P, Jensen N, Pilegaard K, Lindroth A, Grelle A, Bernhofer C, Grünwald T, Aubinet M, Ceulemans R, Kowalski AS, Vesala T, Rannik Ü, Berbigier P, Loustauand D, Guomundsson J, Thorgeirsson H, Ibrom A, Morgenstern K, Clement R, Moncrieff J, Montagnani L, Minerbi S, Jarvis PG (2000) Respiration as the main determinant of carbon balance in European forests. Nature 404(6780):861, DOI 10.1038/35009084

Van Dijk A, Moene AF, De Bruin HAR (2004) The principles of surface flux physics: theory, practice and description of the ECPACK library. Meteorology and Air Quality Group, Wageningen University, Wageningen, The Netherlands p 99 pp

Van Gorsel E, Leuning R, Cleugh HA, Keith H, Suni T (2007) Nocturnal carbon efflux: Reconciliation of eddy covariance and chamber measurements using an alternative to the u*-threshold filtering technique. Tellus B 59(3):397–403, DOI 10.1111/j.1600-0889.2007.00252.x

Penning de Vries F, Jensen D, ten Berge H, Bakema A (1989) Simulation of ecophysiological processes of growth in several annual crops, vol 29. IRRI, Los Banos

Wang W, Davis KJ (2008) A numerical study of the influence of a clearcut on eddy-covariance fluxes of CO_2 measured above a forest. Agricultural and Forest Meteorology 148(10):1488–1500, DOI 10.1016/j.agrformet.2008.05.009

Wang W, Xiao J, Ollinger SV, Desai AR, Chen J, Noormets A (2014) Quantifying the effects of harvesting on carbon fluxes and stocks in northern temperate forests. Biogeosciences 11(23):6667–6682, DOI 10.5194/bg-11-6667-2014

Warland JS, Thurtell GW (2000) A lagrangian solution to the relationship between a distributed source and concentration profile. Boundary-Layer Meteorology 96(3):453–471, DOI 10.1023/A:1002656907873

Waterhouse F (1955) Microclimatological profiles in grass cover in relation to biological problems. Quarterly Journal of the Royal Meteorological Society 81:63–71, DOI 10.1002/qj.49708134707

Webb E (1982) On the correction of flux measurements for effects of heat and water vapour transfer. Boundary-Layer Meteorology 23(2):251–254, DOI 10.1007/BF00123301

Webster R (1997) Regression and functional relations. European Journal of Soil Science 48:557–566

West T, Marland G (2002) Net carbon flux from agricultural ecosystems: methodology for full carbon cycle analyses. Environmental Pollution 116(3):439–444, DOI 10.1016/S0269-7491(01)00221-4

Wiekenkamp I, Huisman JA, Bogena HR, Graf A, Lin HS, Drüe C, Vereecken H (2016a) Changes in measured spatiotemporal patterns of hydrological response after partial deforestation in a headwater catchment. Journal of Hydrology 542:648–661, DOI 10.1016/j.jhydrol.2016.09.037

Wiekenkamp I, Huisman JA, Bogena HR, Lin HS, Vereecken H (2016b) Spatial and temporal occurrence of preferential flow in a forested headwater catchment. Journal of Hydrology 534:139–149, DOI 10.1016/j.jhydrol.2015.12.050

Wilson K, Goldstein A, Falge E, Aubinet M, Baldocchi D, Berbigier P, Bernhofer C, Ceulemans R, Dolman H, Field C, Grelle A, Ibrom A, Law B, Kowalski T A and; Meyers, Moncrieff J, Monson W Rand Oechel, Tenhunen J, Verma S, Valentini R (2002) Energy balance closure at FLUXNET sites. Agricultural and Forest Meteorology 113:223–243, DOI 10.1016/S0168-1923(02)00109-0

Wohlfahrt G, Bahn M, Haslwanter A, Newesely C, Cernusca A (2005) Estimation of daytime ecosystem respiration to determine gross primary production of a mountain meadow. Agricultural and Forest Meteorology 130(1-2):13–25, DOI 10.1016/j.agrformet.2005.02.001

Wu B, Wiekenkamp I, Sun Y, Fisher AS, Clough R, Gottselig N, Bogena H, Pütz T, Brüggemann N, Vereecken H, Bol R (2017) A dataset for three-dimensional distribution of 39 elements including plant nutrients and other metals and metalloids in the soils of a forested headwater catchment. Journal of Environmental Quality 46(6):1510–1518, DOI 10.2134/jeq2017.05.0193

Wutzler T, Lucas-Moffat A, Migliavacca M, Knauer J, Sickel K, Šigut L, Menzer O, Reichstein M (2018) Basic and extensible post-processing of eddy covariance flux data with REddyProc. Biogeosciences 15:5015–5030, DOI doi:10.5194/bg-15-5015-2018

Xu L, Matista AA, Hsiao TC (1999) A technique for measuring CO_2 and water vapor profiles within and above plant canopies over short periods. Agricultural and Forest Meteorology 94:1–12, DOI 10.1016/S0168-1923(99)00004-0

Yakir D, da Silveira Lobo Sternberg L (2000) The use of stable isotopes to study ecosystem gas exchange. Oecologia 123(3):297–311, DOI 10.1007/s004420051016

Yamanoi K, Mizoguchi Y, Utsugi H (2015) Effects of a windthrow disturbance on the carbon balance of a broadleaf deciduous forest in Hokkaido, Japan. Biogeosciences 12(23):6837–6851, DOI 10.5194/bg-12-6837-2015

Zacharias S, Bogena H, Samaniego L, Mauder M, Fuß R, Pütz T, Frenzel M, Schwank M, Baessler C, Butterbach-Bahl K, Bens O, Borg E, Brauer A, Dietrich P, Hajnsek I, Helle G, Kiese R, Kunstmann H, Klotz S, Munch JC, Papen H, Priesack W, Schmid HP, Steinbrecher R, Rosenbaum U, Teutsch G, Vereecken H (2011) A network of terrestrial environmental observatories in Germany. Vados Zone Journal 10:955–973, DOI 10.2136/vzj2010.0139

Zhang G, Thomas C, Leclerc MY, Karipot A, Gholz HL, Binford M, Foken T (2007) On the effect of clearcuts on turbulence structure above a forest canopy. Theoretical and Applied Climatology 88(1):133–137, DOI 10.1007/s00704-006-0250-8

Zhang Q, Katul GG, Oren R, Daly E, Manzoni S, Yang D (2015) The hysteresis response of soil CO_2 concentration and soil respiration to soil temperature. Journal of Geophysical Research-Biogeosciences 120(8):1605–1618, DOI 10.1002/2015JG003047

Appendix

Appendix A1

In 2015, the soil heat flux, temperature and moisture measurements (Sect. 2.2.2) were performed in a single location near the eddy-covariance station in representatively managed soil. In July 2016, this array was uninstalled due to cultivation, but installation of an ICOS-compliant (Op de Beeck et al., 2015) distributed array of five such locations was started. Until after repeated cultivation and seeding (September 2016), however, only the emergency plot of this array, directly next to the eddy-covariance station on unmanaged soil, was available. Heat flux plates were installed at a depth of 0.08 m in the pre-ICOS set-up and of 0.05 m in the ICOS-compliant set-up.

The two sampling tubes for the moving and the fixed χ_{CO_2} and χ_{H_2O} measurements (Sect. 2.2.3) are of the same length to assure identical time lags. However, this length was changed from 3 m to 4.5 m before 31 May 2016 to allow for a longer conduit for large canopy heights and a larger tolerance radius for setting up the analyzer. The extension ensured that the tube end dipped into the plant canopy at a horizontal distance of 0.3 m from all other installations and 1.1 m below the carriage, preventing the carriage itself from dipping into the canopy, and thus minimizing mechanical stress.

In 2016, the tubes were equipped with an optional heating system to prevent condensation of moist air on the inner surface of the tubing, particularly during nighttime conditions, with a 2.5-m long heating wire (bed heater for aquarium, Eco-Line ThermoTronic 5 Watt, Dennerle GmbH, Germany) wrapped helically around the first 1.2 m of both inlets tubes, insulated over the entire length of the tube by insulating hoses with an insulation thickness of 0.013 m, and covered by self-adhesive aluminum tape.

The signals of the wind sensors were logged on the same file as the gas concentrations via the auxiliary ports of the LI7000. The thermocouple temperatures were logged at intervals of 0.05 s to a logger (CR1000, Campbell Scientific, Inc., Logan, Utah, USA).

The final wind and temperature set-up, used in 2016, was the result of stepwise improvements to a preliminary set-up during 2015. Initially no fixed-height anemometer existed, and the moving thermocouple was operated in the open and without ventilation, shielded only by a wire mesh, which however failed to secure the delicate thermocouple junction for more than a few hours. As a result, temperature measurements during the first year are partly missing and were partly performed with an improvised repair, where the more rugged compensation lines of the thermocouple were directly connected to each other. These temperature data, however, were not used. Profiles of χ_{CO_2} and χ_{H_2O} are used during this time because they are not affected by missing temperature measurements. The most important changes to the set-up are indicated in Table 2.2.1.

Appendix A2

Flux derivation from surface-layer profiles is based on the integrated flux-profile relations for momentum, heat and mass:

$$\frac{u}{u_*} = \frac{1}{\kappa}\left[\ln\frac{z-d}{z_0} - \psi_m\left(\frac{z-d}{L}\right)\right], \tag{5.0.1}$$

$$\frac{\theta-\theta_0}{\theta_*} = \frac{1}{\kappa}\left[\ln\frac{z}{z_{0\theta}} - \psi_h\left(\frac{z-d}{L}\right)\right], \tag{5.0.2}$$

and

$$\frac{X-X_0}{X*} = \frac{1}{\kappa}\left[\ln\frac{z}{z_{0\theta}} - \psi_h\left(\frac{z-d}{L}\right)\right], \tag{5.0.3}$$

where u_* is the friction velocity, $\kappa = 0.4$ is the von Karman constant, z_0 and d are the aerodynamic roughness length and displacement height, $z_{0\theta}$ is the scalar roughness length, and L is the Obukhov length,

$$L = -\frac{u_*^3}{\kappa\,\frac{g}{\theta}\,\frac{H}{\rho_{air}\,c_p}}, \tag{5.0.4}$$

with the acceleration due to gravity g; θ is potential temperature, H is the sensible heat flux, ρ_{air} is the density of air and c_p is the specific heat at constant pressure. Potential temperature was computed by applying an adiabatic lapse rate, based on the 30-min mean temperature and pressure, such that the 2-m-a.s.l. level served as a reference. The largest deviations from air temperature, occurring thus at the surface, were 0.02 °C, and the effects on computed fluxes were $\leq$ 0.2 W m^{-2}. θ_0 and X_0 are the potential temperature or the fractional concentration by mass of the scalar X at $z-d = z_{0\theta}$; and θ_* and X_* are the scaling parameters for the temperature and a concentration X, expressed by

$$\theta_* = \frac{-H}{c_p\,\rho\,u_*}, \tag{5.0.5}$$

$$X_* = \frac{-F_X}{\rho\,u_*}. \tag{5.0.6}$$

The stability corrections required in Eq. 5.0.1 and 5.0.2 (integrated form universal functions) for momentum exchange ψ_m and the exchange of sensible heat ψ_h after Businger et al. (1971) are used in the modified version after Högström (1988). The universal function for the exchange of sensible heat ψ_h is also used in the profile equation 5.0.3 for the calculation of moisture exchange and for the exchange of trace gases like CO_2 (Panofsky and Dutton, 1984).

Appendix B

Manual chamber measurements have the advantage that robust spatial averages of soil respiration (R_s) can be estimated with few mobile instruments even for large areas. At the same time, however, they are time-consuming and provide only snapshots in time, typically at a fixed time of the day (late morning to noon in our case). While some of the representativity issues caused by this fact can be solved by relating instantaneous R_s area-averages to simultaneous R_{eco} estimates as in Figure 3.3.9, any hypothetical diurnal cycle of this fraction and its effect on conclusions gained from snapshot measurements of R_s will remain unknown. Keane and Ineson (2017) demonstrated for a comparison of R_s between barley and Miscanthus grown on adjacent fields that different diurnal cycles of R_s combined with solely manual measurements at a fixed time-of-day can lead to erroneous conclusions in such comparisons at least in extreme cases.

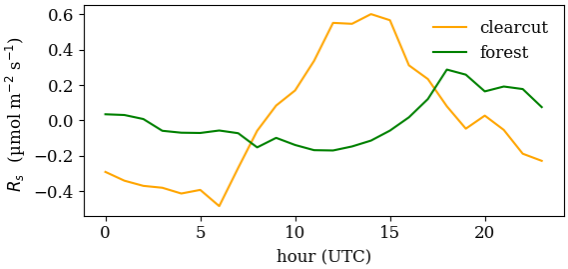

Figure 5.0.1: *Site comparison of the normalized mean diurnal cycle of R_s measured with the continuous chamber installation averaged over a period from 8 June until 19 September 2017.*

The mean diurnal cycle during the growing season 2017 of R_s is shown in Figure 5.0.1. Diurnal (and annual) cycles in R_s can result from cycles in surface temperature and heat transport into the soil, which act on total respiration via its temperature sensitivity, and from cycles in incoming photosynthetic active radiation, which can influence rhizospheric respiration through assimilate transport (Pavelka et al., 2007; Graf et al., 2008; Kuzyakov and Gavrichkova, 2010; Phillips et al., 2011; Darenova et al., 2014; Zhang et al., 2015). Both transport processes can be subject to similar delay and dampening effects, which may be expected to be larger under a high forest canopy. Consequently, the forest measurement shows a weaker diurnal cycle with a maximum shifted into the evening hours.
Since both curves reflect only a single measurement point in space and their average values (5.0 and 2.5 µmol m^{-2} s^{-1} for forest and clearcut, respectively) do not reflect the difference between both areas found with area-averaging of the manual measurements (Fig. 3.3.7), it remains uncertain whether the differences of up to 0.6 µmol m^{-2} s^{-1} found in the late morning (Fig. 5.0.1) should be used to correct the manually measured spatial averages. However, it becomes clear from the confidence intervals in Figure 3.3.7 that such a correction would not have changed the main finding of clearcut-forest differences that are insignificant during the first two growing seasons after the clearcut and significant during the last two on a 5 % error probability level.

Danksagung

This work was financed by the German Federal Ministry of Education and Research (BMBF) in the framework of the project "IDAS-GHG" (FKZ 01LN1313A). Some used ancillary hardware and its maintenance was supported by TERENO and the DFG Collaborative Research Centre 32 "Patterns in Soil-Vegetation-Atmsophere Systems".

An dieser Stelle möchte ich all den Leuten danken, die mich in den letzten dreieinhalb Jahren auf dem Weg zu dieser Doktorarbeit unterstützt und begleitet haben: Mein erster Dank gilt meinem Doktorvater, Herrn Prof. Dr. Harry Vereecken. Sie haben es mir überhaupt erst ermöglicht am Forschungszentrum Jülich im IBG-3 Agrosphäre promovieren zu können. Unsere Gespräche werden mir immer als ein bereichernder und konstruktiver Austausch in Erinnerung bleiben. Des Weiteren danke ich Herrn Prof. Dr. Clemens Simmer für die Bereitschaft der Übernahme des Zweitgutachtens. Ferner danke ich Herrn Prof. Dr. Bernd Diekkrüger und Herrn Prof. Dr. Cyrill Stachniss für die Teilnahme in der Promotionskommission.

Mein außerordentlicher Dank gilt einem besonderen Menschen: Dr. Alexander Graf. Ich danke dir für dein Vertrauen, dass ich als Doktorandin in deinem Projekt IDAS-GHG mitarbeiten durfte. Ohne deine unendliche Kompetenz, grenzenlose Geduld und feinfühliges Verständnis hätte ich den Arbeitsumfang niemals bewältigen können. Du hast mich motiviert wenn ich vor lauter Bäumen den Wald nicht mehr gesehen habe, ich konnte zu jeder Zeit mit Fragen zu dir kommen und du hast mir immer mit gutem Rat zur Seite gestanden. Mehr hätte ich mir gar nicht wünschen können. Vielen Dank dafür.

Ein großes Dankeschön geht an alle Mitarbeiterinnen und Mitarbeiter, die durch ihre Hilfe bei der Durchführung und Auswertung der mikrometeorologischen Messungen in Feld und Wald sowie der Wartung der Messsysteme in einem nicht geringen Umfang für das Gelingen dieser Arbeit beigetragen haben. Insbesondere seien genannt: Nicole Adels, Uwe Baltes, Daniel Dolfus, Odilia Esser, Norman Hermes, Katharina Pick, Marius Schmidt und Veronika Valler.

I would like to thank my colleagues and friends: Anne, Maria, Anneli, Phuong, Sean and Yajie for your help and stimulating discussions, for the long office days we were working together before deadlines, and for all the fun we had in the last years. I thank my dear friends Daniela, Oliver, Shirin and Veronika for their great support and encouragement. I wouldn't like to have missed you!

Ein herzliches Dankeschön geht an dich Friedel. Du konntest mich durch unsere Kunstaktionen auf wohltuende 'nicht-wissenschaftliche' kreative Gedanken bringen.

Ein ganz besonderer Dank geht an meine gesamte Familie und meinen Freund Alex. Ihr habt mich in all meinen Vorhaben unterstützt und mir durch eure Großzügigkeit mein Studium ermöglicht. Ihr habt immer hinter mir gestanden und mich in der schwierigsten Zeit, dem Verlust meiner Mutter, aufgefangen. Eure Liebe und Geborgenheit ist eine starkes Fundament für meine Motivation und meinen Antrieb es durch alle Unwägbarkeiten und Schwierigkeiten zu schaffen. Für all das empfinde ich tiefsten Dank.

Band / Volume 463
Simulation of Transport Processes through an Asymmetric Gas Separation Membrane
U. V. Unije (2019), xiv, 101 pp
ISBN: 978-3-95806-403-4

Band / Volume 464
Development, calibration and deployment of an airborne chemical ionization mass spectrometer for trace gas measurements
T. Khattatov (2019), 14, 125 pp
ISBN: 978-3-95806-404-1

Band / Volume 465
IEK-3 Report 2019
Maßgeschneiderte Energieumwandlung für nachhaltige Kraftstoffe
D. Stolten, B. Emonts (Eds.) (2019), 171 pp
ISBN: 978-3-95806-410-2

Band / Volume 466
Initialinfrastruktur für Wasserstoffmobilität auf Basis von Flotten
F. Grüger (2019), V, 209 pp
ISBN: 978-3-95806-413-3

Band / Volume 467
Techno-ökonomische Analyse alternativer Wasserstoffinfrastruktur
M. E. Reuß (2019), 205 pp
ISBN: 978-3-95806-414-0

Band / Volume 468
Study on a miniaturized satellite payload for atmospheric temperature measurements
J. Liu (2019), 153 pp
ISBN: 978-3-95806-415-7

Band / Volume 469
Partitioning Water Vapor Fluxes by the Use of Their Water Stable Isotopologues: From the Lab to the Field
M. E. Quade (2019), XVI, 113 pp
ISBN: 978-3-95806-417-1

Band / Volume 470
Entwicklung von Reparaturmethoden für Nickel-Superlegierungen mittels thermischer Spritzverfahren
T. Kalfhaus (2019), VI, 126, XXX pp
ISBN: 978-3-95806-418-8

Band / Volume 471
Entwicklung von korrosionsstabilen Schutzschichten für oxidische Faserverbundwerkstoffe
C. S. Gatzen (2019), II, 143 pp
ISBN: 978-3-95806-422-5

Band / Volume 472
Coatings for Metallic Bipolar Plates in High-Temperature Polymer Electrolyte Fuel Cells
R. Li (2019), II, 119 pp
ISBN: 978-3-95806-425-6

Band / Volume 473
Thermochemische Eigenschaften von kombinierten Katalysator- und Sauerstoffträgersystemen für die partielle Oxidation von Teeren aus der Biomassevergasung
M. Ma (2019), VII, 157 pp
ISBN: 978-3-95806-426-3

Band / Volume 474
Einfluss der klimatischen Fertigungsumgebung auf die Mechanik und Rissstrukturierung der elektrodenbeschichteten Membran einer PEM-Brennstoffzelle
B. Wienk-Borgert (2019), IV, 141 pp
ISBN: 978-3-95806-428-7

Band / Volume 475
Reversible wasserstoffbetriebene Festoxidzellensysteme
M. H. Frank (2019), 187 pp
ISBN: 978-3-95806-430-0

Band / Volume 476
Partitioning of carbon dioxide exchange in rapidly and slowly changing ecosystems
P. Ney (2019), xvi, 95 pp
ISBN: 978-3-95806-431-7

Energie & Umwelt / Energy & Environment
Band / Volume 476
ISBN 978-3-95806-431-7

Mitglied der Helmholtz-Gemeinschaft

JÜLICH
Forschungszentrum